



INGEGNERIA CIVILE  
DOTTORATO DI RICERCA IN


XXX  
CICLO DEL CORSO DI DOTTORATO

Seismic Assessment of Architectural Heritage  
using Discrete Element Method


Anna Mordanova  
Nome e Cognome del dottorando

  
firma

Gianmarco de Felice  
Docente Guida/Tutor: Prof.

  
firma

Gianmarco de Felice  
Coordinatore: Prof.

  
firma

Collana delle tesi di Dottorato di Ricerca  
In Ingegneria Civile  
Università degli Studi Roma Tre  
Tesi n° 71

*to my mom*





# Abstract

In the present dissertation seismic assessment of the architectural heritage is studied by means of numerical analyses with Discrete Element Method (DEM). There is a variety of historical structures ranging from ancient monuments to traditional buildings majority of which are made of stone masonry. The fundamentals of DEM are overviewed as it embodied in existing DE code, together with new implemented routines accounted for, firstly, realistic model representation and, secondly, performing of seismic analyses of the masonry structures according to quasistatic and dynamic approaches.

Applicability of the DEM for analyses of historical masonry is discussed on 3 case studies such as the Colosseum and the Aqueduct Claudio in Rome and the monastery of Beata Antonia in L'Aquila. All the monuments represent examples of the architectural heritage assets located in seismic prone zones. Seismic assessment is performed based on pushover, step pulse and seismic analyses after preliminary historical and structural surveys of the monuments.

The seismic analysis based on DEM provides reliable results on assessment of seismic capacity of historical masonry structures and representation of their expected collapse; the analysis also ensures evaluation of the past earthquakes intensity based on recognition of structural damage and provides effective estimation of the potential reinforcement measures of the architectural heritage.

## Sommario

Nella presente tesi la valutazione sismica del patrimonio architettonico è studiata mediante analisi numeriche con il metodo ad elementi distinti (DEM). Sotto il patrimonio architettonico si fa riferimento a una vasta gamma di strutture murarie in pietra storiche che vanno dai monumenti provenienti da antiche strutture agli edifici tradizionali. I principi fondamentali del DEM sono considerati come incorporati nel codice DE esistente, unitamente alle nuove routine implementate, in primo luogo, rappresentazione realistica della geometria del modello e, in secondo luogo, effettuazione di analisi sismiche delle strutture murarie secondo approcci quasistatici e dinamici.

L'applicabilità del DEM per l'analisi della muratura storica è discussa su 3 studi di casi come il Colosseo e l'Acquedotto Claudio a Roma e il monastero di Beata Antonia a L'Aquila. Tutti i monumenti rappresentano esempi delle risorse del patrimonio architettonico situate in zone sismiche. La valutazione sismica dei monumenti viene effettuata in base a pushover, impulsi di fase e analisi sismiche dopo indagini storiche e strutturali preliminari.

L'analisi sismica basata sul DEM fornisce risultati affidabili sulla valutazione della capacità sismica delle strutture murarie storiche e la rappresentazione del loro crollo previsto; l'analisi assicura anche la valutazione dell'intensità del terremoto passato basata sul riconoscimento dei danni strutturali e sull'efficienza delle misure potenziali di rinforzo.

## Абстракт

В настоящей диссертации представлена работа по изучению сейсмической оценки объектов архитектурного наследия с помощью численного анализа основанного на методе дискретных элементов. Под понятие архитектурного наследия попадает множество исторических сооружений выполненных из каменной кладки, от древних памятников до традиционных зданий. Основы метода дискретных элементов рассматриваются на примере их применений для анализа кладочных сооружений в существующем программном коде вместе с вновь внедренными подпрограммами, позволяющими учитывать, во-первых, реалистичное представление геометрии модели и, во-вторых, выполнение сейсмических анализов основанных на квазистатическом и динамическом подходе.

Применимость метода дискретных элементов для анализа исторической кладки рассматривается на трех примерах, таких как Колизей и Акведук Клаудио в Риме и монастырь Беата-Антония в Л'Акуиле. Рассматриваемые сооружения представляют собой примеры памятников архитектурного наследия, расположенных в зонах с высокой сейсмической активностью. Сейсмическая оценка выполняется на основе статического, импульсного и сейсмического анализа после предварительных исторических и структурных исследований рассматриваемых памятников.

На основе сейсмического анализа, базирующегося на методе дискретных элементов, предоставляется возможность получить достоверные результаты по оценке сейсмостойкости исторических каменных сооружений и репродукцию ожидаемого характера их разрушения; также предоставляется возможность оценки интенсивности прошлых землетрясений на базе существующих разрушений и оценки эффективности возможных мер по усилению объекта архитектурного наследия.

## Acknowledgments

The present work has been carried out at the Civil Engineering Department of the Roma Tre University, Italy. The research was performed under supervision of the prof. Gianmarco de Felice.

I am grateful to my colleagues from Structural Group, especially to Alessandra Genoese and Bartolomeo Pantò, who substantially contributed to the quality of this research work with their invaluable advice, knowledge and vast experience in DEM. I would also like to express my gratitude to Stefano De Santis for his patience and professional advices and to Anna Ferrante, Matteo Ammendolia and Pietro Meriggi for their interesting and fruitful discussions.

I would like to record my thanks to all my colleagues from the Engineering Department of Roma Tre for providing a nice and warm working environment as well as their friendship outside the university.

Finally, I would like to acknowledge the SAHC master course, participation on which a year before opened in me a passion for the Cultural Heritage and to prof.de Felice, who allowed of improvement and growth of this passion during my 3 years PhD in Italy.

# Table of contents

<b>LIST OF THE FIGURES.....</b>	<b>XI</b>
<b>LIST OF THE TABLES.....</b>	<b>XVII</b>
<b>LIST OF THE SYMBOLS .....</b>	<b>XVIII</b>
<b>1 INTRODUCTION.....</b>	<b>1</b>
<b>2 MASONRY MONUMENTS AND THEIR SEISMIC ASSESSMENT .....</b>	<b>5</b>
2.1 INTRODUCTION.....	5
2.2 MASONRY IN ARCHITECTURAL HERITAGE.....	5
2.3 MASONRY SPECIFIC FEATURES .....	9
2.4 EARTHQUAKES AND SEISMIC REGIONS .....	12
2.5 SEISMIC ASSESSMENT OF ARCHITECTURAL HERITAGE .....	13
2.6 METHODS OF SEISMIC ANALYSIS .....	17
2.6.1 <i>Pushover analysis</i> .....	18
2.6.2 <i>Dynamic analysis</i> .....	19
2.7 NUMERICAL MODELING OF MASONRY STRUCTURES .....	20
2.8 LITERATURE REVIEW OF DEM APPLICATION ON MASONRY STRUCTURES ANALYSIS.....	23
2.8.1 <i>Ancient structures</i> .....	24
2.8.2 <i>Traditional buildings</i> .....	25
2.8.3 <i>Structural elements</i> .....	26
2.9 SUMMARY .....	28
<b>3 SEISMIC ANALYSIS USING DISCRETE ELEMENT METHOD .....</b>	<b>29</b>
3.1 FUNDAMENTALS OF THE DISCRETE ELEMENT METHOD .....	29
3.1.1 <i>Blocks representation</i> .....	29
3.1.2 <i>Contacts representation</i> .....	30
3.1.3 <i>Contacts Detection and Update</i> .....	31
3.2 UDEC PROGRAM.....	32
3.2.1 <i>Solution algorithm</i> .....	32
3.2.2 <i>Equations of motion</i> .....	34
3.2.3 <i>Contact forces</i> .....	35
3.2.4 <i>Joint constitutive models</i> .....	38
3.2.5 <i>Mechanical damping</i> .....	39
3.3 NEW IMPLEMENTED SEMIAUTOMATIC DE MODEL CREATOR .....	40
3.4 NEW IMPLEMENTED ROUTINE FOR PUSHOVER ANALYSIS .....	43
3.4.1 <i>Ascending branch of pushover curve</i> .....	44
3.4.2 <i>Descending branch of pushover curve</i> .....	50
3.4.3 <i>Verification of the procedure</i> .....	56
3.5 NEW IMPLEMENTED ROUTINE FOR STEP PULSE ANALYSIS.....	59
3.5.1 <i>Detailed algorithm</i> .....	60
3.5.2 <i>Verification of the procedure</i> .....	63
3.6 SEISMIC ANALYSIS.....	64
3.6.1 <i>Damping calibration</i> .....	64

---

3.6.2	<i>Verification of the procedure</i> .....	66
3.7	SUMMARY .....	70
<b>4</b>	<b>SEISMIC ASSESSMENT OF THE PAST DAMAGE ON THE SOUTH-EAST PART OF THE COLOSSEUM</b> .....	<b>72</b>
4.1	INTRODUCTION .....	72
4.2	GEOMETRY AND STRUCTURAL SURVEYS .....	74
4.3	PAST DAMAGE AND RESTORATIONS SURVEYS .....	77
4.4	EXISTING THEORIES ON THE DAMAGE CAUSES .....	88
4.5	SEISMIC ANALYSIS OF THE SOUTH-EAST END OF THE EXTERNAL WALL .....	90
4.5.1	<i>DE Model</i> .....	91
4.5.2	<i>Pushover analysis</i> .....	94
4.5.3	<i>Dynamic analysis</i> .....	96
4.5.4	<i>Damage investigation</i> .....	99
4.6	SUMMARY .....	101
<b>5</b>	<b>SEISMIC ASSESSMENT OF THE CLAUDIO AQUEDUCT</b> .....	<b>103</b>
5.1	INTRODUCTION .....	103
5.2	HISTORICAL SURVEY .....	103
5.3	DE MODEL .....	106
5.3.1	<i>Model geometry</i> .....	106
5.3.2	<i>Material properties</i> .....	109
5.3.3	<i>Boundary condition and loading</i> .....	110
5.4	QUASISTATIC ANALYSIS .....	110
5.4.1	<i>Out-of-plane loading</i> .....	110
5.4.2	<i>In-plane loading</i> .....	111
5.4.3	<i>Sensitivity analysis</i> .....	115
5.5	DYNAMIC ANALYSIS .....	116
5.5.1	<i>Out-of-plane loading</i> .....	116
5.5.2	<i>In-plane loading</i> .....	118
5.6	SUMMARY .....	122
<b>6</b>	<b>SEISMIC ASSESSMENT OF THE MONASTERY OF BEATA ANTONIA</b> <b>123</b>	
6.1	INTRODUCTION .....	123
6.2	HISTORICAL SURVEY .....	124
6.3	DE MODEL .....	126
6.3.1	<i>Geometry and mechanical properties</i> .....	126
6.3.2	<i>Boundary conditions and loading</i> .....	128
6.3.3	<i>Validation of the model</i> .....	128
6.3.4	<i>Retrofitting measures</i> .....	129
6.4	QUASISTATIC ANALYSIS .....	130
6.4.1	<i>Actual state</i> .....	130
6.4.2	<i>Retrofitted states</i> .....	132
6.5	DYNAMIC ANALYSIS .....	133
6.5.1	<i>Pulse excitation</i> .....	134
6.5.2	<i>Seismic excitation</i> .....	140

6.6	SUMMARY .....	148
<b>7</b>	<b>CONCLUDING REMARKS .....</b>	<b>150</b>
	<b>REFERENCES.....</b>	<b>153</b>

## List of the figures

<i>Figure 2.1 Examples of ancient masonry structures: a) Pyramids in Egypt, b) Parthenon in Greece, c) Colosseum in Italy</i> .....	6
<i>Figure 2.2 Examples of the great masonry dome structures: a) Pantheon, Rome and b) Hagia Sophia, Istanbul</i> .....	7
<i>Figure 2.3 Examples of the Romanesque architecture: a) Civita di Bagnoreggio and b) Spoleto in Italy</i> .....	8
<i>Figure 2.4 Examples of the Renaissance architecture: a) the Kremlin and b) Solovetsky monastery in Russia</i> .....	9
<i>Figure 2.5 Failure mechanisms of masonry elements: a) joint tensile cracking, b) joint slipping, c) unit direct tensile cracking, d) unit direct shear cracking, e) masonry crushing (Lourenço 1996)</i> .....	10
<i>Figure 2.6 Out-of-plane (a-g) (D’Ayala and Speranza 2003) and In-plane (l) (Binda et al. 2006) failure mechanisms of the masonry buildings</i> .....	11
<i>Figure 2.7 The global seismic hazard map (Giardini et al. 1999)</i> .....	12
<i>Figure 2.8 Flowchart of the actions for the diagnosis of the building (Pompeu 2010)</i> .....	15
<i>Figure 2.9 Flowchart of the actions in case of structural assessment (Pompeu 2010)</i> .....	16
<i>Figure 2.10 Example of a Capacity Curve</i> .....	18
<i>Figure 2.11 Modeling strategies for masonry structures: a) masonry sample, b) detailed micro-modeling, c)simplified micro-modeling, d)macro-modeling (Lourenço 1996)</i> .....	21
<i>Figure 2.12 General load-displacement diagram for structural analysis (Lourenço 2002)</i> .....	22
<i>Figure 2.13 Examples of numerical analysis of historical structural by a) FEM (Cervera et al. 2004) and b) DEM (Cakti et al. 2016)</i> .....	23
<i>Figure 2.14 Examples of a) 2D DE model of the aqueduct (Sinclairian, Oliveira, and Lemos 1998) and b) 3D DE model of the archeological site (Psycharis et al. 2003)</i> .....	25
<i>Figure 2.15 Collapse mechanisms of a) a traditional rural house (Alexandris, Protopapa, and Psycharis 2004) and b) a church facade (de Felice and Mauro 2010)</i> .....	26
<i>Figure 2.16 Failure mechanisms of the irregular stone models by a) (Lemos, Costa, and Bretas 2011), b) (de Felice 2011)</i> .....	27
<i>Figure 3.1 DEM interface model (Idris, Al-Heib, and Verdel 2009)</i> .....	30



---

Figure 3.2 Contact models: a) Rigid or hard contact model; b) Deformable or soft contact model ( $u_n$ exaggerated) ( J. V. Lemos 2007).....	31
Figure 3.3 Basic logic used in UDEC.....	33
Figure 3.4 Schematic representation of contacts and their forces between rigid blocks.....	35
Figure 3.5 Schematic representation of a) block dimensions and b) contacts between blocks .....	37
Figure 3.6 The joint constitutive laws: a) normal and b) shear, c) Mohr Coulomb yielding criteria .....	39
Figure 3.7 Flowchart of semiautomatic DE model creator .....	41
Figure 3.8 Paths for creating accurate DE mesh .....	42
Figure 3.9 Example of resultant pushover curves.....	43
Figure 3.10 Schematic representation of the mechanism and respective ascending branch .....	45
Figure 3.11 a) Loading scheme and b) detailed algorithm of the ascending branch .....	47
Figure 3.12 Number of cycles to converge to equilibrium.....	48
Figure 3.13 Flowchart of the ascending branch.....	50
Figure 3.14 Schematic representation of descending branch with graph of potential energy, respectively, a) procedure#1 and b) procedure#2	51
Figure 3.15 Schematic representation of the mechanism of descending branch.....	52
Figure 3.16 Flow chart of the algorithm#1.....	54
Figure 3.17 Flow chart of the algorithm#2.....	56
Figure 3.18 The adapted geometry and mechanical properties of the simple walls.....	57
Figure 3.19 Influence of input data on the algorithm#1 results .....	58
Figure 3.20 Influence of input data on the algorithm#2 results .....	58
Figure 3.21 Failure mechanisms of 3 simple walls .....	59
Figure 3.22 Example of representative failure domain of the systems ....	60
Figure 3.23 Schematic representation of the pulse loading and corresponding responses.....	61
Figure 3.24 Flow chart of the implemented pulse analysis .....	63
Figure 3.25 Calibration of a) normalized critical damping ratio with angular frequency (Itasca 2011), b) damping parameters .....	65
Figure 3.27. Numerical and experimental comparison in terms of time history of the relative horizontal displacement at the control point on	

regular (a) and irregular (b) walls: AMT (a1,b1), NCR (a2,b2), AQV (a3,b3) signals.....	69
Figure 3.28. Comparison between the numerical lateral shapes and the experimental failure modes of regular (a) and irregular (b) walls: AMT (a1,b1), NCR (a2,b2), AQV (a3,b3) signals. ....	70
Figure 4.1 A reconstruction of the Amphitheatre (by G. A. Brambilla, 1581).....	72
Figure 4.2 Plan of the valley of the Amphitheatre in IV century AD (De Luca 1985).....	73
Figure 4.3 Plan of the foundation and cross section (De Luca 1985).....	75
Figure 4.4 The cross section of the Colosseum with key for materials (Rea, Beste, and Lancaster 2002) .....	76
Figure 4.5 The current plan of the Colosseum (Coarelli and Gabucci 2001).....	77
Figure 4.6 The hypothetic reconstruction of the Colosseum in 12-13 <sup>th</sup> centuries (Rea, Romano, and Valenzani 2017).....	79
Figure 4.7 The state of the southern end of the external wall in 1570 (by Anonim in Fabriczy from (Frazzoni 2016)) .....	80
Figure 4.8 The South-east part in 1700 (by Gaspar van Wittel).....	81
Figure 4.9 The view on the southern external wall in 1756 (by Piranesi) .....	81
Figure 4.10 Timber shoring in the south-east wall in 1806-1807 (Uggeri 1809).....	82
Figure 4.11 Start of the restoration by Stern (Luciani 1990) .....	83
Figure 4.12 The restoration survey in 1814 (Uggeri 1814).....	84
Figure 4.13 The restoration survey in 1990 (Crocì 1990).....	85
Figure 4.14 The current restoration survey (“Restauro Colosseo” 2017) .....	85
Figure 4.15 The state of the Colosseum in 1776 before the 19 <sup>th</sup> century restorations (by Piranesi).....	86
Figure 4.16 Prospect view of the facade after 19 <sup>th</sup> century restorations (“Restauro Colosseo” 2017).....	86
Figure 4.17 Interventions by Canina (Como 2013) .....	87
Figure 4.18 The current view on the Colosseum .....	88
Figure 4.19 a) ancient course of Fossus Labicano; b) 3D geological map of the site of the Colosseum (Funicello and Rovelli 1998) .....	89
Figure 4.20 Part of the Colosseum under investigation .....	91
Figure 4.21 DE mesh and model geometry.....	92
Figure 4.22 Effective thickness adopted in the model.....	94

---

Figure 4.23 Pushover capacity curve .....	94
Figure 4.24 a) Distribution of velocity along the model during the pushover analysis and b) resultant failure mechanism.....	95
Figure 4.25 Failure pattern based on pulse analysis.....	97
Figure 4.26 Matching of the existing and pulse-by failure patterns.....	98
Figure 4.27 Pushover curves and pulse failure domains of the models without infill and with infill of the second level arches.....	100
Figure 4.28 Failure mechanism with infill of the arches second level ..	101
Figure 5.1 The route of the Aqua Claudia (in red) (adapted form (Droysen 1886)).....	104
Figure 5.2 Upper channel - Anio Novus, made with 'opus testaceum' mixed with 'opus laterazia'; low channel and arcades of Aqueduct Claudio made with 'opus quadratum'.....	105
Figure 5.3 Example of the ancient retrofitting brick works.....	106
Figure 5.4 Geometry of the model and control points .....	107
Figure 5.5 Models of a) actual and b) initial states of transversal section .....	107
Figure 5.6 Models of actual state of longitudinal section depending on upper channel representation: a) simplified, b) well-defined, c) without.....	108
Figure 5.7 Models of a) reinforced and b) ideal states of longitudinal section.....	109
Figure 5.8 Properties of the blocks/joints implemented in the model depending on effective thickness .....	109
Figure 5.9 Collapse mechanisms of a) initial and b) actual states of the transversal section and their c) capacity curves.....	111
Figure 5.10 Collapse mechanisms of actual state a) without, b) with simplified and c) with well-defined upper channel of the aqueduct .....	112
Figure 5.11 Capacity curves of various in-plane models of actual state .....	113
Figure 5.12 Collapse mechanisms of a) ideal state of the structure and after its reinforcing with b) 2 and b) 8 steel bars .....	114
Figure 5.13 Capacity curves of various in-plane models of reinforced state of the aqueduct.....	115
Figure 5.14 Sensitivity analysis on a) friction angle and b) effective modulus of elasticity.....	115
Figure 5.15 Results of out-of-plane pulse loading of the aqueduct initial state in form of a) failure domain and b) failure mechanism.....	116

---

Figure 5.16 Results of out-of-plane pulse loading of the aqueduct actual state in form of a) failure domain and b) failure mechanism.....	117
Figure 5.17 Failure domains of transversal section subjected to step pulse .....	118
Figure 5.18 Failure domain of in-plane pulse loading of the aqueduct actual state .....	119
Figure 5.19 Failure domain of in-plane pulse loading of the reinforced state .....	120
Figure 5.20 Failure mechanisms under in-plane pulse loading of (a) actual and (b) reinforced states of the aqueduct.....	121
Figure 5.21 Failure domains of longitudinal section subjected to step pulse .....	121
Figure 6.1 15th century frescos in the Monastery of Beata Antonia .....	123
Figure 6.2 Current view on the Monastery of Beata Antonia.....	124
Figure 6.3 Plan of the Monastery of Beata Antonia .....	125
Figure 6.4 Longitudinal cross-section of the Monastery of Beata Antonia .....	125
Figure 6.5 Geometry of the model .....	126
Figure 6.6 Adopted mechanical properties for the blocks and joints ....	127
Figure 6.7 Models of the retrofitted states of the monastery .....	130
Figure 6.9 Ultimate states obtained by different pushover techniques a) procedure#1 and b) procedure#2.....	131
Figure 6.10 Pushover results of the retrofitted states.....	132
Figure 6.11 Various ultimate states depending on the intervention a) actual state, b) extra tie-rod, c) backfill, d) combined.....	133
Figure 6.12 Failure mechanism of actual state depending on the pulse direction: a) from right to left and b) from left to right .....	134
Figure 6.13 Failure domain of the actual state of the structure subjected to step pulse.....	135
Figure 6.14 Distribution of velocity and failure mode during applying pulse loading at actual state.....	136
Figure 6.15 Failure domain of retrofitted state of the monastery subjected to step pulse.....	137
Figure 6.16 Distribution of velocity and failure mode after applying pulse loading of the retrofitted model.....	138
Figure 6.17 Failure domain of both investigated states of the monastery subjected to step pulses .....	139
Figure 6.18 Failure mechanisms of a) actual and b) retrofitted states of the monastery .....	139

---

<i>Figure 6.19 Location of the selected stations recorded L'Aquila earthquake 06.04.2009 ("ITACA 2.2 WG" 2017) .....</i>	<i>140</i>
<i>Figure 6.20 Accelerations time histories for L'Aquila earthquake records (horizontal component – black solid line, vertical – red dashed line) .....</i>	<i>141</i>
<i>Figure 6.21 Horizontal acceleration response spectrum for L'Aquila earthquake records.....</i>	<i>141</i>
<i>Figure 6.22 Velocity time histories applied to the model (horizontal component – solid line, vertical component – dashed line).....</i>	<i>142</i>
<i>Figure 6.23 Responses of actual state of the model under 15% AQV and 12.5% AOK records (control points: top wall – solid line, arch keystone – dashed line) .....</i>	<i>143</i>
<i>Figure 6.24 Failure mechanism in the main vault under 15% AOK record .....</i>	<i>144</i>
<i>Figure 6.25 Maximum responses of the actual structure under scaled L'Aquila earthquake records (control points: top wall – dashed line, arch keystone – solid line).....</i>	<i>144</i>
<i>Figure 6.26 Responses of the wall and arch of retrofitted system under 200% AQV and 150% AOK scaled earthquake records (control points: top wall – dashed line, arch keystone – solid line) .....</i>	<i>145</i>
<i>Figure 6.27 States of the retrofitted structure after a) 150% of AOK signal and b) 200% of AQV signal.....</i>	<i>146</i>
<i>Figure 6.28 Maximum responses of the retrofitted structure under scaled L'Aquila earthquake records (control points: top wall – dashed line, arch keystone – solid line).....</i>	<i>147</i>
<i>Figure 6.29 Maximum responses of the actual and retrofitted states under scaled L'Aquila earthquake records (control points: top wall – dashed line, arch keystone – solid line) .....</i>	<i>148</i>

## List of the tables

<i>Table 3.1 Adapted mechanical parameters.....</i>	<i>67</i>
<i>Table 4.1 Damage suffered by Colosseum through the centuries (Funicello et al. 1995).....</i>	<i>78</i>
<i>Table 4.2 Sensitivity analysis on the effective value of a frictional angle</i>	<i>93</i>
<i>Table 4.3 Adapted mechanical properties of the model.....</i>	<i>93</i>
<i>Table 4.4 Sensitivity analysis on step-pulse parameters.....</i>	<i>96</i>
<i>Table 4.5 List of the earthquakes during 1700-1810 (Guidoboni et al. 2007).....</i>	<i>99</i>

## List of the symbols

The following list contains the main symbols that appear in the chapters of the thesis.

$\dot{u}$	<i>Velocity of a rigid body</i>
$t$	<i>Time period of a load applying on a rigid body</i>
$m$	<i>Massa of a rigid body</i>
$\theta$	<i>Rotation of a rigid body about its centroid</i>
$x_i$	<i>X coordinate of the centroid of a rigid body</i>
$F^c$	<i>Contact force of the DE model</i>
$F_n$	<i>Normal component of the contact force</i>
$F_s$	<i>Shear component of the contact force</i>
$u_n$	<i>Normal component of the relative displacement</i>
$u_s$	<i>Shear component of the relative displacement</i>
$\sigma$	<i>Normal stress of an element</i>
$\tau$	<i>Shear stress of an element</i>
$K_n$	<i>Contact normal stiffness of the DE model</i>
$K_s$	<i>Contact shear stiffness of the DE model</i>
$j_{kn}$	<i>Joint normal stiffness of the DE model</i>
$j_{ks}$	<i>Joint shear stiffness of the DE model</i>
$j_{tens}, f_t$	<i>Joint tensile strength of the DE model</i>
$j_{fric}, \varphi$	<i>Joint friction angle of the DE model</i>
$j_{coh}$	<i>Joint cohesion of the DE model</i>

# 1 Introduction

Architectural heritage is defined by ICOMOS as “buildings and complex of buildings (towns, etc) of historical value”. Masonry structures take a great part of the architectural (cultural) heritage that in our days is represented by archaeological sites or partly standing ancient monuments as well as by traditional masonry buildings like churches, cathedrals, castles, etc. Historically, masonry was one of the first and important building materials over the centuries. In time existing masonry structures have suffered damage mainly governed by lack of maintains, material degradation, soil settlements or natural disasters, including earthquakes. Considering all these causes and their combinations, all types of historical structures require careful and periodic assessment in order to evaluate their structural capacity and safety level, that is especially important in case of seismic prone zones.

The recent earthquakes that occurred in Italy highlighted vulnerability of masonry structures and a need on reliable methods for assessing their seismic capacity. Investigation of the seismic behavior of ancient masonry structures is a challenging task due to lack of knowledge on the mechanical characteristics of the used materials and the complexity of the construction techniques. Furthermore, it is useful to remember that some main characteristics of masonry, such as its inhomogeneity, anisotropy and high physical nonlinearity, strongly affect its mechanical behavior. In the engineering practice, it is not always possible to take into account all the characteristics listed above, and often equivalent continuous models are considered in which the macroscopic mechanical quantities are defined.

The preservation of cultural heritage assets must guarantee their capacity to last over time against decay, natural hazards and extreme events without losing their authenticity and use. A strong engineering contribution on assessment and strengthening methods for historic and heritage buildings started from general aspects of Venice charter (ICOMOS 1964) and continued in the ISCARSAH Principles (ICOMOS 2003). Regularly, some attempts are also proceeding in order to develop useful guidelines for historical conservation (Italian Ministry of Cultural Heritage and Activities 2011), (Pompeu 2010), (D’Ayala and Lagomarsino 2015). However, there is still no officially approved European Guidelines for evaluation and mitigation of seismic risk to architectural heritage assets, useful to support their seismic assessment and design of interventions for their preservations.



The scope of the present thesis is to contribute in the development of guidelines for evaluation and mitigation of seismic risk to cultural heritage by developing approach useful for its seismic assessment by means of Discrete Element Method (DEM). The method is especially suitable for analyzing of historical masonry structures that can be viewed as an assembly of discrete bodies and in which failure usually occurs with a collapse mechanism. Thereby, DE numerical model takes into account discontinuity nature of the structure and allows simulating individual movement of each block with its sliding or rocking especially inherent during seismic loading. Another positive aspect of the method is the need for few input parameters that is important for historical monuments, in which destructive tests are not allowed.

The principal objectives of the present work are:

- to evaluate applicability of DEM to simulate the structural behavior of historical masonry constructions, especially in connection with their seismic behavior. This can be achieved by comparing the results of the numerical simulations with experimental data or with observed real seismic damage of the architectural heritage;
- to develop and implement preprocessing code for semiautomatic DE model creator. The algorithm makes possible creating precise models including real geometry of the investigated structures and its material properties in order to obtain further accurate simulation results. Especially valuable since seismic stability of the masonry structures may depend on the masonry arrangements;
- to develop and implement automated routines for seismic analyses of masonry structures with DEM packages (e.g. UDEC). The objective is to provide accurate and easy to use methodology for performing analysis based on quasistatic and dynamic approaches with minimum user interaction and maximum robustness of the algorithms;
- to evaluate applicability of DEM for effective assessment of past earthquakes. The aim is based on an extensive historical survey providing all available information connected with the existing damage to simulate and explain existing damage of the monument;
- to analyze series of architectural heritage structures of different complexity, in terms of their geometry and structural response, failure modes, and damage patterns using the new implemented routines;
- to evaluate applicability of DEM for simulations of masonry strengthening and evaluations of structural upgrade.

The present dissertation is organized in 7 chapters, of which the Introduction constitutes the Chapter 1.

The chapter 2 presents an introduction to the different architectural periods and the relevant development of the masonry constructions, followed by the critical review of their specific features, especially pronounced during seismic actions. Nature of earthquakes and seismic regions are overviewed in connection to the cultural heritage together with the need of their seismic assessment. A review of existing principles and recommendations for structural (seismic) assessment is also presented. After a general overview of methods and numerical approaches a detailed review of the main contributions available in the state-of-the-art for the discrete element method is recalled.

The basics of the Discrete Element Method, as embodied in existing DEM codes, are presented in the Chapter 3. Issues such as mechanics of block interaction, detection and updating of contacts, mechanical behavior of blocks and contacts and numerical algorithms are discussed in details. Based on the DEM formulations several routines were developed for the two-dimensional seismic analysis of structures composed of rigid blocks. These implemented routines provided the means to automate the analyses of masonry structures for the available DEM code and increase its usability. Remarkable capabilities of the DEM are investigated by means of static and dynamic analyses of simple blocky structural components. Within the same chapter some parametric studies are carried out with the scope of providing some insight into the basic aspects and to present problems that can be encountered when a comprehensive seismic analysis is to be done. Finally, some comparisons with experimental tests, carried out in laboratory, are presented, as a verification procedure.

In the Chapter 4 the DEM is used for evaluating the earthquake that had affected important heritage monument. The chapter contains a complete study on the part of the Colosseum external wall, which was restored in 1807 by Stern. The study initiates with extensive structural and geometrical surveys of the structure, together with historical survey of past damage and their respective restorations, and followed by a critical review of the recent studies on the monument. Finally, the numerical model and seismic analysis of the southeast part of the Colosseum is undertaken in order to evaluate the characteristics of earthquake, happened in the beginning of 19th century. Another goal is to investigate the chronology of the monument's interventions preceding the 19th century restorations and their influence on its vulnerability.

The Chapter 5 reports an application of the DEM to seismic assessment of an archeological site before and after its retrofitting. The analysis of arcades of the Claudio Aqueduct is carried out by reproducing the effective shapes and positions of the stone blocks that formed the aqueduct. Several configurations of the model are elaborated aiming to better understand the influence of effective stone representation, existing structural damage or potential retrofitting. The capacity curve of the structure together with pulse failure domain was obtained in order to provide a refined estimate of the seismic vulnerability. Sensitivity analyses on the mechanical parameters were also undertaken to verify their influence on the overall response.

In the Chapter 6 application of the DEM to seismic analysis of traditional heritage building is examined. The chapter contains seismic assessment of the monastery of Beata Antonia in L'Aquila that refers to a high seismic prone zone. The analyses are performed by means of several computational strategies including quasistatic, pulse and dynamic approaches. Several models were created representing the actual state of the monument in order to reproduce its current safety level and after installation of potential reinforcements to analyses their impact. One of the study aims is to evaluate DEM applicability on estimation of the effective strengthening systems that can help to avoid overuse of the reinforcing measures.

Finally, the performances of the proposed methodology and the obtained results are discussed in the Chapter 7. Some further developments that could contribute to a better seismic assessment of architectural heritage are eventually proposed.

## **2 Masonry monuments and their seismic assessment**

### **2.1 Introduction**

Historically, masonry was one of the important building materials over the centuries. In time masonry structures could become damaged mainly by lack of maintains, material degradation, soil settlements or earthquakes. Considering all this causes and their combinations, in our days, all masonry buildings are represented by entire or partially collapsed structures or just archeological remains. Nevertheless, all types of historical structures are required careful and periodic assessment in order to evaluate their structural capacity and safety level in case of possible earthquakes.

The chapter is started from an overview of the different architectural periods and respective development of the masonry constructions. Following by the critical review of the masonry and its specific features, critically pronounced during seismic actions. Nature of earthquakes and seismic regions are overviewed in connection to the cultural heritage together with the need of their seismic assessment. A review of existing principles and recommendations for structural (seismic) assessment of historical structures is presented later in the chapter. After it general overview of methods for seismic analysis of masonry structures is presented. The chapter finalized by detailed review of the fundamentals of discrete element method and its state-of-the-art in the current research.

### **2.2 Masonry in Architectural heritage**

The definition of cultural heritage is very general and depends from culture to culture, but in general it could be represented by existing old buildings with significant cultural value to society (Pompeu 2010). While Architectural heritage is defined by ICOMOS as “buildings and complex of buildings (towns, etc.) of historical value”. Masonry structures take a great part of the architectural (cultural) heritage that in our days is represented by archeological sites or partly standing ancient buildings as well as traditional monuments like churches, cathedrals, castles, etc. Review of the masonry constructions development in time is presented below.



**Figure 2.1** Examples of ancient masonry structures: a) Pyramids in Egypt, b) Parthenon in Greece, c) Colosseum in Italy

History of the masonry constructions is dating back to the prehistoric time and stone was the first masonry material. Remains of one of the first stone house was found near Lake Hullen, Israel (9000-8000 B.C.) presented by dry-stone huts, circular and semi-subterranean (Lourenço 1996). Another example of earliest masonry construction representing the military defending Walls of Jericho (8000 B.C.), which were built from roughly worked limestone with earth filled joints (Crocì 1998).

Historically, religious structures and public places were built with use of better materials and skills than dwellings, so until our days the first ones represent the major part of the best preserved ancient constructions; starting from architecture of ancient Egypt with pyramids and temples (about 2000 BC) (Figure 2.1, a), following by numerous Greek temples (500-0 BC) (Figure 2.1, b) and Roman forums, aqueducts and amphitheatres (0-700 AD) (Figure 2.1, c). Dating back, the structural form of the pyramids was the logical development of the initial stone piles representing one of the most stable structural shapes. However, already Egyptian and Greece temples were constructed using stone columns and lintels based on strict rules of proportion and symmetry between the different elements and played a fundamental role in the history of masonry buildings development. The Romans, with a strong and centralized empire, provided the next important step in development of

the constructions. They introduced many innovations directly related to materials, structural concepts and construction processes. Together with improvement of the dry stone construction, innovative techniques were introduced in the construction of walls, using bricks or stones as facing material, and filling the inner space with 'roman' concrete, made of rubble, lime and pozzolana - special volcanic sand.



**Figure 2.2 Examples of the great masonry dome structures: a) Pantheon, Rome and b) Hagia Sophia, Istanbul**

Another important milestone was in changing from linear structures (columns and beams) to curved structures (arches and vaults). The invention of the archly structure allowed to build more high and complex constructions and take full advantage of the masonry characteristics, which worked mainly in compression. Vaults and domes represent the three-dimensional extension of the arch, which required massive walls or buttresses to prevent any springer movement. Barrel vaults and domes allowed the construction of large-span, durable and fire-resistant roofs. A great example of one of the first masonry dome is Roman Pantheon (125 AD), where gradation in construction thickness was used: it was heavier at the bottom (6 m thickness) and much lighter at the top (2.2 m thickness). Dome lies on massive walls, made of roman bricks and concrete with numerous relieving arches along the perimeter (Figure 2.2, a). Another excellent example of vaulted architecture dated back to the Byzantine period is the Hagia Sophia in Istanbul (6th century A.D.). The building is elegant in geometry but very massive in construction, with also large thickness necessary to accommodate the thrust lines within the domes and vaults (Figure 2.2, b).

A mixture of Roman architecture with strong Byzantine influence evolved the Romanesque architecture (11th - 13th century). Churches were made

with semicircular arches and barrel vaults and marked by the presence of towers. From the other hand, following the historical needs castles and entire towns, at that time, were usually constructed on the top of the hill for protecting purpose. Walls of the buildings were composed by irregular facing stones with a filling made of stones loosely bound with mortar (Figure 2.3).

The next revolution in the architecture and structural behavior took place with the birth of the Gothic structures, in which both the architectural and structural functions were exceptionally well integrated together. This architecture of great proportions, extreme height of the slender columns and the spires pointing to the sky was successfully used for construction of numerous churches and cathedrals starting from 13<sup>th</sup> century.



**Figure 2.3 Examples of the Romanesque architecture: a) Civita di Bagnoreggio and b) Spoleto in Italy**

The period of Renaissance (15<sup>th</sup> -16<sup>th</sup> centuries), which brought a new concept of form and proportions, under the influence of humanistic culture, represented the next step in the history of masonry construction. Many palaces, fortresses and monasteries were built, having regular forms, characterized by a geometrical symmetry in the plans and elevation. The masonry walls were of better quality and were built around a central court. An existed examples of this period can be found all around the Europe like the Kremlin in Moscow or monastery of the Solovetsky Islands in Russia that are listed in the UNESCO World Heritage Sites (Figure 2.4). Churches at that period were made with domes constructed of two shells connected by the main ribs. The most extended examples of such structures are Brunelleschi's Santa Maria del Fiore in Florence and Michelangelo's San Pietro in Rome.

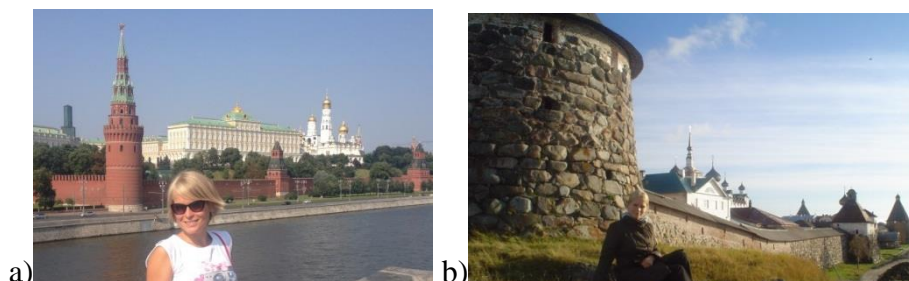


**Figure 2.4 Examples of the Renaissance architecture: a) the Kremlin and b) Solovetsky monastery in Russia**

Probably, the last period, when masonry structures were still used as the main construction material, was Baroque (17-18 centuries), which finished with the industrial revolution. It brought in the structural area new construction materials such as steel and reinforced concrete that led to decrease of the masonry use for new constructions.

### **2.3 Masonry specific features**

Masonry probably is the oldest building material that combines together durability and easy to build characteristics. Usually, it contains of units such as stones, blocks or adobe, connected by mortar, however some ancient constructions consist only by blocks with dry joints. In this case, connections between units and all stability of the structure governed thanks to great mass of the blocks.

There are two fundamental structural problems of the masonry buildings: how to achieve the height and how to span an opening, i.e. how to span vertical and horizontal spaces (Croci 1998). Spanning in a vertical direction is done by columns, walls and towers, while spanning horizontally is achieved by lintels, beams and arches. In addition, some structural elements such as vaults and domes can simultaneously span in both directions.

Primary function of masonry structures is to withstand mainly vertical forces (gravity and dead or live load) however time to time additional loads arise due to earthquakes, winds or settlements, which bring combined shear, flexure and compressive stresses. In this case, mechanical response of masonry depends on many various factors including quality of workmanship or craftsmanship as well as property of materials (units and mortar, if second is presented). Great influence on the structural response also gives a lay-out of masonry (the material pattern), that may contain dry stones or irregular rubble stones with or without



multileaves cross section. Additionally, degradation of the materials (biological, physical and chemical) plays one of the key features in the weakening of the historical buildings.

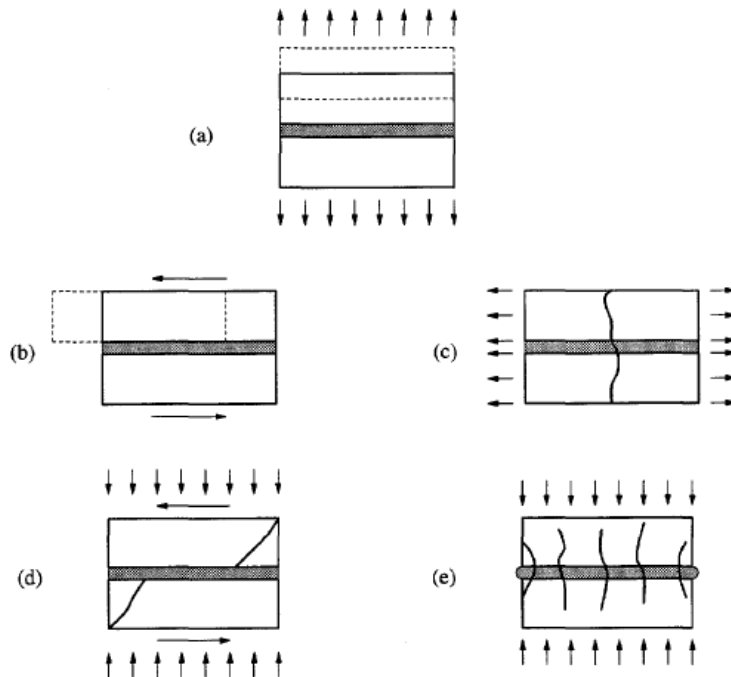


**Figure 2.5 Failure mechanisms of masonry elements: a) joint tensile cracking, b) joint slipping, c) unit direct tensile cracking, d) unit direct shear cracking, e) masonry crushing (Lourenço 1996)**

Masonry, by its nature, is a brittle material, so any external loads result cracking and crushing of its elements (units, mortar, unit/mortar interfaces or all together). Cracks in masonry may open and close depending on the load and its direction, as a rule, cracks less than 0.2mm are not visible to a naked eye and usually not taken in consideration. However, large, progressively propagating and opening cracks may reduce significantly load bearing capacity of the structure and even bring to its collapse. The failure modes (Figure 2.5) depend on magnitude and direction of the normal and shear stresses. The main failure modes of masonry occur in joints due to tensile and shear, in units due to tension and combined in joints and units due to compression.

Masonry is anisotropic composite material with non-linear behavior that mainly controlled by mortar joints. It expires linear elastic behavior at

low level stresses, while with increasing of applied load behavior becomes strongly non-linear with cracks opening and propagation. The mechanical properties of masonry and its characteristics vary significantly even inside one structure, but masonry resistance in compression is always much higher than in tension and shear. The generous strength that responsible for the resistance of masonry to lateral loads is combined shear and compression, which behavior can be described by Mohr-Coulomb failure criterion widely used in masonry modeling.

When walls are subjected to horizontal loads usually occurring during earthquakes, there are two main types of behavior of masonry walls, depending on the direction of external force. In-plane behavior activates the walls parallel to the direction of the horizontal loads, while out-of-plane behavior involves walls subjected to horizontal actions orthogonal to their plane. Historically, masonry structures have shown their great vulnerability to the out-of-plane loading that cause wall's partial or total collapse (Figure 2.6). The main failure mode occurs due to overturning of the wall and governed by lack of the connections between the walls. That can be effectively normalized by presence of connection elements (ties, ring beams) or intrinsic resisting effects (e.g. arch effect of the wall in its thickness) or by strengthening with innovative superficial materials (Mordanova, De Santis, and de Felice 2016). In-plane mechanisms concern the walls parallel to the seismic action and usually cause diagonal cracking of the elements, which often are not able to lead the structure to the collapse, in comparison with the out-of-plane mechanisms (Valluzzi et al. 2004).

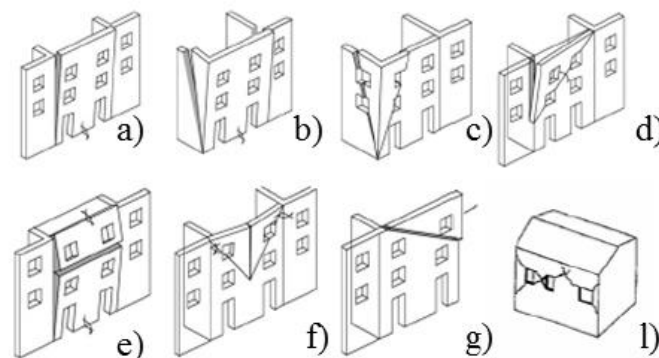


**Figure 2.6 Out-of-plane (a-g) (D'Ayala and Speranza 2003) and In-plane (l) (Binda et al. 2006) failure mechanisms of the masonry buildings**

## 2.4 Earthquakes and Seismic regions

Experience has demonstrated that many masonry building have been damaged or collapsed by historical earthquakes. The ground motions present themselves non-periodic dynamic actions, characterized by inducing additional inertial forces in the structures. Because of their disastrous consequences, the major earthquakes have been noted in chronicles dating back to the beginnings of the civilization (Guidoboni et al. 2007). Earthquakes can occur at any location at any time, following the world earthquake belts (Figure 2.7). A great part of the cultural heritage sites made of stone and brick masonry is situated in earthquake prone areas, such as southern Europe, Asia and America.

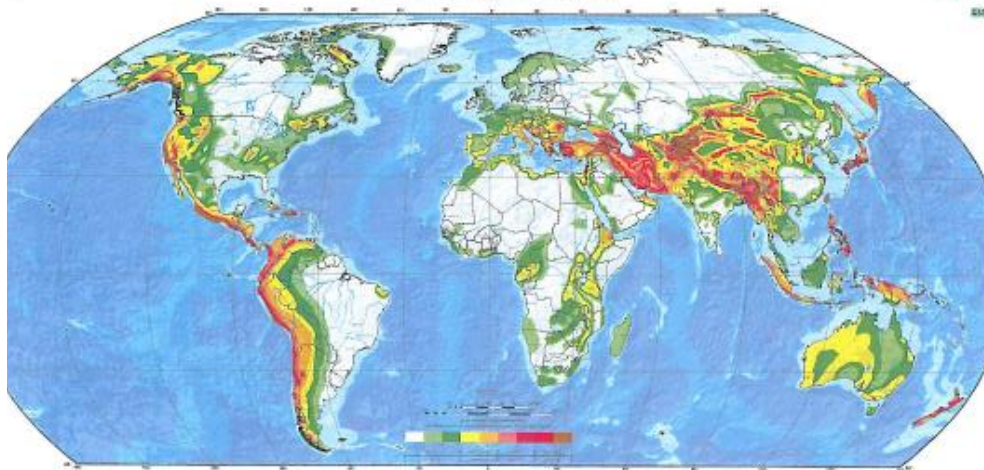


**Figure 2.7** The global seismic hazard map (Giardini et al. 1999)

The earthquakes mechanisms are very complex phenomena and from geological studies it was found out that the rock near the surface of the earth was subjected to permanent deformations in time. Whenever it rupture very high stresses appear. When such ruptures occurred, relative sliding motions were developed between the opposite sides of the rupture surface creating a geological fault. The most important fact about any fault rupture is associated with a sudden release of strain energy that radiates outward in all directions from the rupture point. When such waves are reaching the earth surface, an earthquake creates. Seismic waves can be classified either as dilation waves or shear waves, which produce both horizontal and vertical stresses. Most damage and collapses

are generally produced by the horizontal components of an earthquake. The characteristics of the soil on which the structure is built can amplify or reduce the general seismic effects at foundation level.

To an earthquake engineer, the most important aspect of an ground motions is the effect they will have on structures, such as stresses and deformations or the amount of damage. The severity of the ground motions at any point is called the earthquake intensity, and it is usually measured on the Modified Mercalli scale, ranging from I (no damage) to XII (complete destruction). While, from a seismological point of view the most important measure of the "size" of an earthquake is the amount of strain energy released at the source, which is indicated quantitatively by the magnitude of the earthquake (1-10 on Richter scale).

Ground motion parameters are fundamental to describe the important characteristics of strong earthquakes in a quantitative form, which either can be used for seismic assessment:

- Amplitude - ground motion is usually described with a time history of acceleration, velocity, displacement or all three. The most common measure of ground motion amplitude is the peak horizontal acceleration, also known as peak ground acceleration (PGA);
- Frequency content - the frequency content describes how the amplitude of a ground motion is distributed among different frequencies. The dynamic response of structures is very sensitive to the frequency at which they are loaded;
- Duration - the duration of strong motion can have an important influence on earthquake damage, because many physical processes (e.g. strength degradation) are sensitive to the number of load reversals that occur during an earthquake. A common definition for duration is the time between the first and the last excitations of threshold acceleration (usually 0.05g).

Damage of historical constructions has a cumulative character and mainly not-reversible. In this connection, dynamic assessment by means of numerical simulation is a very fruitful and important tool in Structural and Seismic Engineering.

## **2.5 Seismic assessment of architectural heritage**

Structural assessment of heritage sites is oriented to better understanding of general structural features of the masonry constructions, their present condition and existing damage, together with verification of structural safety and conservation/reconstruction works needed, finalizing by

control of the efficiency of interventions. Seismic assessment of historical masonry structures is particularly challenging task due to structural complexity and partial knowledge of their past, together with specific characteristics of the seismic responses governing by local failures, which occur mainly due to out-of-plane response of the wall (Penna 2014).

A full methodological path for the assessment of cultural heritage sites, with their complex history, according to ICOMOS includes steps similar to those used in medicine:

1. anamnesis - condition survey (visual and historical);
2. diagnosis - identification of the causes of damage and decay (construction knowledge based on non-destructive testing, material parameters, structural identification, followed by structural modeling and seismic analysis of masonry structures);
3. therapy - choice of the remedial measures;
4. controls - control of the efficiency of the intervention (monitoring).

Firstly, the easy available data and information should be collected and analyzed, such as visual and historical survey, based on qualitative approach. That includes direct observation of the structural damage and material decay, together with historical and archeological research. If these data is not sufficient for appropriate diagnoses then more comprehensive research is needed based on quantitative approach. That involves materials and structural tests, structure and damage monitoring as well as structural analysis (ICOMOS 2003).

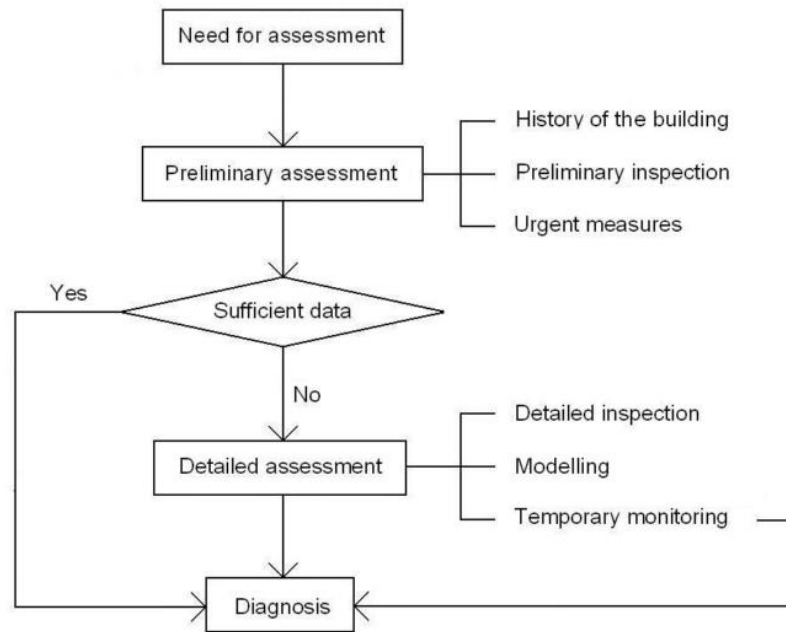


**Figure 2.8 Flowchart of the actions for the diagnosis of the building** (Pompeu 2010)

In general according to (Pompeu 2010) the complete seismic assessment of the heritage building could be divided into two main steps: expended diagnosis and structural assessment. It is important, at the beginning, to determine clearly the cause of damage and decay that possible with the detailed diagnosis (Figure 2.8). Detailed diagnosis is an essential step in the assessment procedure, especially, in the case of historical structures, where the lack of data is more pronounced. A great part of the existing heritage buildings already stays in a damage condition, thus an expended diagnosis based on detailed historical and visual inspection together with numerical modeling is an essential measure. An example of the extended diagnosis of a part of the Colosseum will be presented in the chapter 4 of the present dissertation.

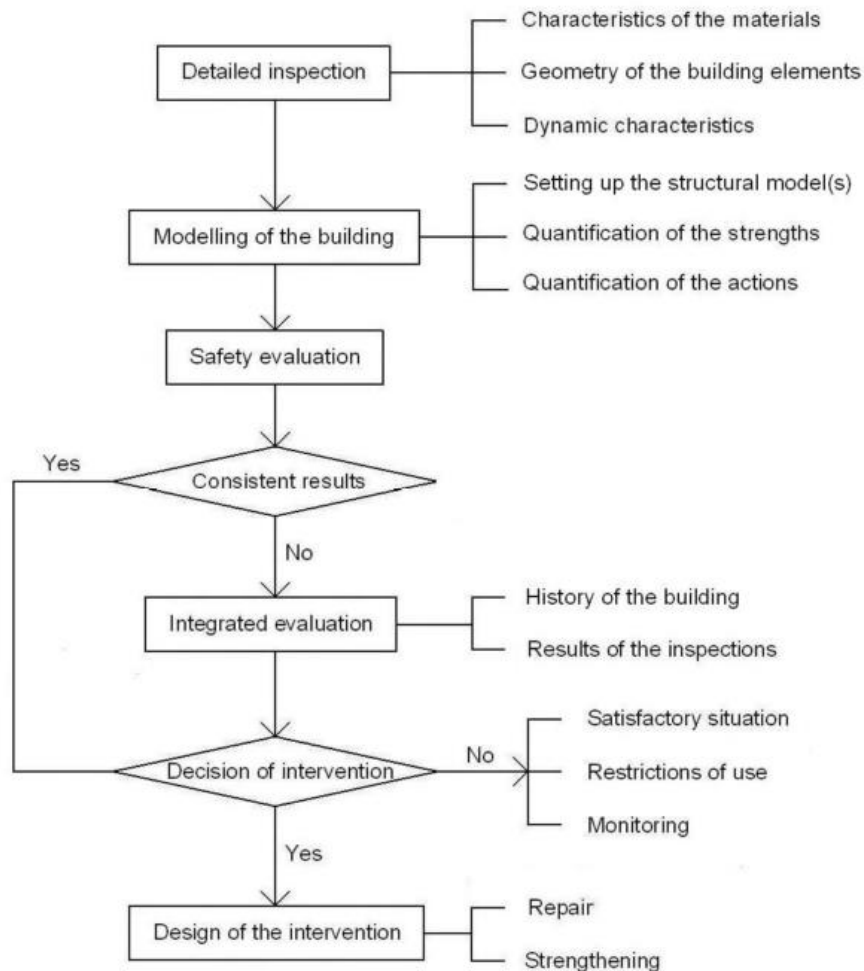


**Figure 2.9** Flowchart of the actions in case of structural assessment (Pompeu 2010)

The second step is an extended structural assessment, which aims to identify the current safety level of the construction and a need for its intervention. The evaluation of the level of structural safety is based on the detailed inspection of the structure identifying its geometry and materials. Obtained data is used for analysis of the structure by means of analytical or numerical modeling. And only based on all these achieved results a decision on need of structural intervention can be made (Figure 2.9). Several examples of the structural assessment of the cultural

heritage sites will be presented in the chapter 5 and 6 of the present dissertation.

If as the result of the full ‘diagnosis’ a need of efficient ‘therapy’ is obtained potential intervention measures should be applied to the investigated monument. According to Venice charter (ICOMOS 1964) and ISCARSAH (ICOMOS 2003) the main aspects of the intervention of cultural heritage sites are:

- durability and compatibility of the new materials with the historical substrate and heritage values;
- removability of the intervention without any harmful effect to the historical construction in case to replace with more suitable measures if new knowledge is acquired;
- minority of the intervention, keeping it minimum to guarantee safety and durability;
- repair is always better to replacement.

## **2.6 Methods of seismic analysis**

According to (Eurocode 8 2005) there are several linear and non-linear, static and dynamic analysis methods for assessment of the resistance of existing building to seismic action:

- lateral force analysis,
- modal response spectrum analysis,
- non-linear static (pushover) analysis
- non-linear time history (dynamic) analysis,
- q-factor analysis.

The first two and the last one belong to linear-elastic type of analysis and based on several assumptions of the mechanical behavior of the system. However, in major part historical masonry structures represent complex geometry and consist of degraded materials, which behavior is hard to describe and well predict using only linear-elastic behavior theories. The non-linear analysis instead could provide more wide results since they already include strength of structural elements and their post-elastic behavior. The mechanical behavior described using force-displacement relationship with elastic stiffness corresponds to cracked sections. Both non-linear analysis are used in the present dissertation and explained more in details in the following section and chapters.



### 2.6.1 Pushover analysis

Pushover analysis is one of the preferred methods for evaluation of structural seismic performance by the major rehabilitation guidelines and codes because of its conceptual and computational simplicity. Pushover analysis allows tracing the sequence of yielding and failure on structural members as well as the progress of overall capacity curve of the structure. The expectation from pushover analysis is to estimate critical response parameters imposed on structural system and its components as close as possible to those predicted by nonlinear dynamic analysis (Magenes 2000).

Pushover analysis is an approximate analysis method in which the structure is subjected to monotonically increasing lateral loads with an invariant height-wise distribution, until a target displacement is reached. Pushover analysis consists of the series of sequential elastic analyses, superimposed to approximate a force-displacement curve of the entire structure. Firstly, a numerical model is created, then gravity loads are applied, after which the predefined lateral load pattern is distributed along the structure height. At every step the lateral forces are increased until some members yield or numerical tolerance is achieved. The process is continued until a control displacement at the top of building reaches a certain level of deformation or structure becomes unstable. The displacement versus base shear is plotted to get the global capacity curve (Figure 2.10).

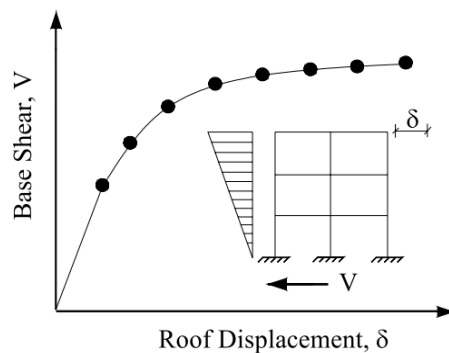


Figure 2.10 Example of a Capacity Curve

Pushover analysis can be performed as force-controlled or displacement controlled procedure. In force-controlled pushover procedure, full load combination is applied as specified, i.e., this type should be used when the load is known (such as proportional to gravity load). While in

displacement-controlled procedure specified drifts are sought because the magnitude of applied load is not known in advance. The magnitude of load combination is increased or decreased as necessary until the control displacement reaches a specified value. Generally, a top control point is chosen to monitor result displacement.

Although pushover analysis has advantages over elastic analysis procedures, anyway it is a static approximation of a dynamic problem, thus the obtained results should be judged carefully. A carefully performed pushover analysis could provide insight into structural aspects that control performance during severe earthquakes. However, the estimate of target displacement, selection of lateral load patterns and identification of failure mechanisms due to higher modes of vibration are important issues that affect the accuracy of pushover results. Perhaps the most critical concern is that the pushover analysis may detect only the first local mechanism that will form in an earthquake (Krawinkler and Seneviratna 1998), for more detailed study the dynamic approach could give some more extended results.

### **2.6.2 Dynamic analysis**

The analysis is called dynamic if magnitude, direction and position of the applying load are various in time. Consequently, response of the system exhibiting this load is also changing in time like during real earthquake. Another main difference between static and dynamic loading is that the last one induce forces of inertia since acceleration is not equal to zero. Thus the time-dependent response of the structure may be obtained through direct numerical integration of the differential equation of motion.

The representation of the displacements of a given system with distributed mass in terms of a finite number of displacements (i.e. discretization) allows to greatly simplify the dynamic problem because inertial forces would develop only at these points. The number of displacement components that must be taken into account to represent the effects of all significant inertial forces of a system is known as the number of (dynamic) degrees of freedom of the system (DOF). A system with continuously distributed mass has an infinite number of degrees of freedom. Discretization allows performing an accurate dynamic analysis involving only a limited number of degrees of freedom.

In order to represent the ground motion real or artificial accelerograms may be applied to the base of the system. The other way of representing

the dynamic loading is to use pulse, which defined as an application of a very large force in a very short period of time to the structure. Generally, pulse is characterized by its force magnitude and time duration. The shape of the pulse may be formed by rectangular, triangular or harmonic function.

## **2.7 Numerical modeling of masonry structures**

Generally, masonry structures are presented by composite material containing units (blocks or stones) and joints (mortars). However, some historical constructions could contain only dry blocks, without any mortar, which was either degraded or not used initially. Thereby, numerical model should take into account discontinuity nature of the structure and allows simulating individual movement of each block with its sliding or rocking that especially essential during seismic loading.

There are several strategies and methods of structural analysis of historical masonry constructions. They could be classified, depending on level of accuracy and desired simplicity, by means of calculating approach (numerical or analytical), by dimensionality (2D or 3D) or by idealization of the structural behavior (linear elastic, plastic or non-linear) (Lourenço 2002),(Roca et al. 2010).

Numerical modeling used for analysis of masonry structures classified into main strategies: detailed and simplified micro-modeling or macro-modeling. The first approach based on the detailed modeling of all components of the masonry – mortar, units and interfaces mortar/units (Figure 2.11, b). It requires a well define geometry of the model and high computational efforts. Thus detailed micro-modeling is used mainly for modeling only small portions of the masonry. Simplify micro-model contains in its geometry generalized joints and expended units on the thickness of the mortar (Figure 2.11, c). The approach is suitable to study structural elements or local behavior of the masonry. The third approach represents masonry as a homogenized anisotropic continuum without any division on units or joints (Figure 2.11, d) and is widely used to study the entire construction with complex geometry.

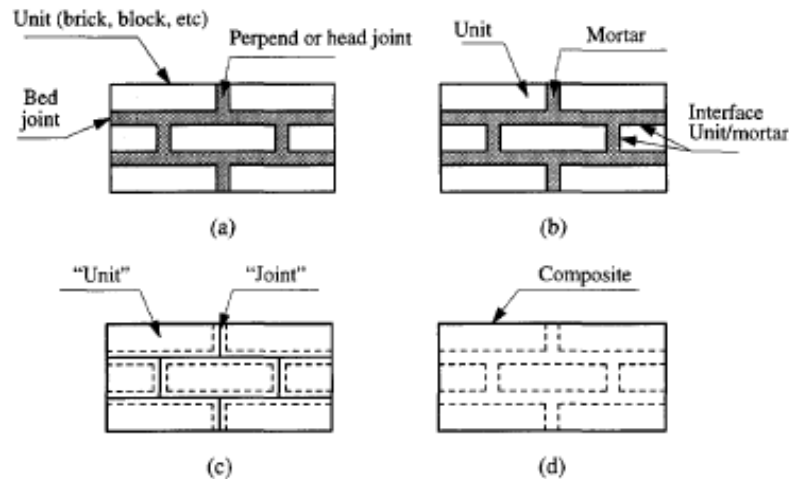


**Figure 2.11 Modeling strategies for masonry structures: a) masonry sample, b) detailed micro-modeling, c) simplified micro-modeling, d) macro-modeling**  
(Lourenço 1996)

From other hand, analysis of masonry structures involves severe simplifications and assumptions about their structural behavior and geometry. The geometry idealizations failed into the general requirements that it “should be kept as simple as possible, as long as it can be considered adequate for a problem being analyzed” (Lourenço 2002). General types of idealized behavior commonly applied to numerical models are elastic, plastic and non-linear (Figure 2.12). The elastic behavior is the ‘basic’ type, which assumes the Hooke’s law for the material mechanical properties and is true for the very low stress levels before the first cracks appear in masonry. Plastic (or limit) analysis based on the main assumptions that 1) material’s compression strength is infinite, 2) masonry’s tensile strength is zero, and 3) sliding between the elements is impossible. While structural non-linear behavior may be explained by physical, geometrical or contact nonlinearity or by their combinations. Application of any structural behavior differ on the results desired - limit analysis aims in evaluation of the ultimate load, linear elastic analysis used as an auxiliary tool in assessment of large structures, while non-linear analysis allows obtaining both ultimate and elastic loads.

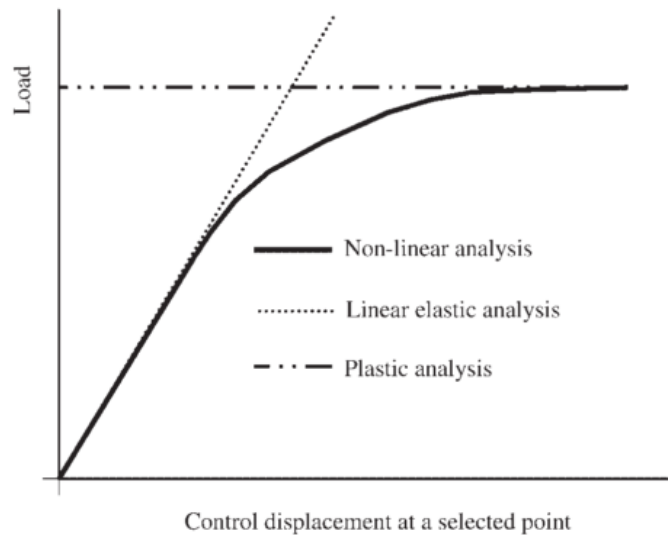


**Figure 2.12 General load-displacement diagram for structural analysis**  
(Lourenço 2002)

Regarding to the computational approaches, structural analysis is divided into two large groups: continuum methods, represented by Finite Element Method (FEM), and discontinuous methods, represented by Discrete Element Method (DEM). Analysis of masonry structures with FEM, based on macro-modeling approach, is widely spread among practitioners as well as among researchers since 1960<sup>th</sup>. The geometry of the models is obtained by its idealizations and assumptions, specifically in application to the large scale objects (Figure 2.13a). The method works well for obtaining the ultimate strength of the model without collapse analysis of the masonry. DEM represents another fundamental methodology that based on discontinuous nature of the analyzed system. Originally, it was created for the rock mechanics (Cundall 1971) but lately was also successfully applied to masonry constructions (Lemos 1995). The numerical model contains of discrete blocks (Figure 2.13b), which could move with large displacements. The method well suits for collapse analysis, and may thus provide support for studies of safety assessment of historical masonry constructions under seismic actions. (Sinclairian 2001), (Bakeer 2009) The fundamentals of the method and its applicability to the analysis of architectural heritage will be critical reviewed bellow and studied in details in the following chapters.

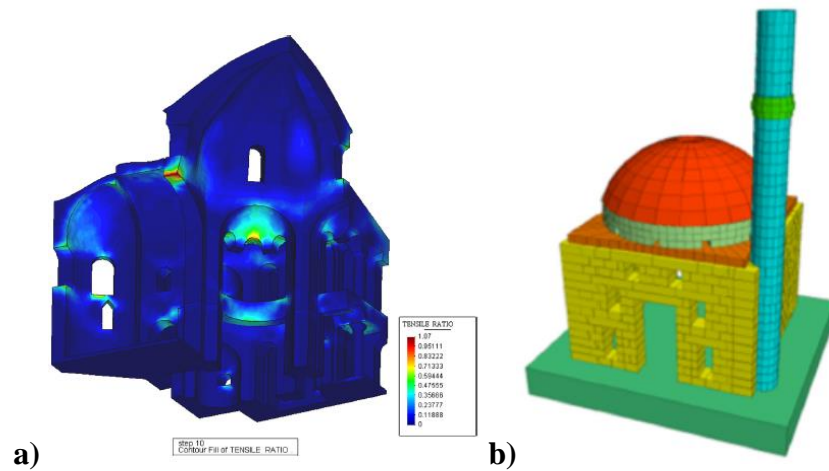


**Figure 2.13** Examples of numerical analysis of historical structural by a) FEM (Cervera et al. 2004) and b) DEM (Cakti et al. 2016)

Generally, results of different approach may differ without meaning of the insufficiency of anyone. Many times a simple approach provides desirable results (Lourenço 2002), that is why the main key aspects affecting the choice of the computation strategy should be availability of tools and initial data for the proceeding analysis as well as availability of the financial resource. In conclusion, particular advantages and disadvantages of various numerical models and strategies for analysis of masonry historical structures, containing also seismic application, could be fined by various publications, such as (Lourenço 2002), (Giordano, Mele, and De Luca 2002), (Roca et al. 2010) , (Soveja, Budescu, and Gosav 2013), (Asteris et al. 2014), (de Felice et al. 2016).

## **2.8 Literature review of DEM application on masonry structures analysis**

Major part of the architectural heritage structures is built by stone dry masonry and represent a great example for DEM application. In case of earthquakes, failure of this kind of constructions is governed by collapse mechanism that is very representative option of DEM analysis. The review of current state of the research based on the DE analysis applied on seismic assessment of the historical masonry is presented below.

One of the first study of historical masonry structure using DEM was presented by (Lemos 1995). The study contained analysis of arch masonry bridge and the effects of load distribution across its width. An

overall seismic behavior of blocky masonry structures with cases of structural systems as well as real structures were studied by (Azevedo, Sincaian, and Lemos 2000). The work has shown applicability of DEM to seismic analyzing of masonry, the obtained results was in accordance with damage and collapse pattern observed in past earthquakes, it also described the possibility of effective simulation of a traditional reinforcing scheme.

### **2.8.1 Ancient structures**

Various numerical studies on seismic behavior of column-architrave classical structures were published by several authors. The DEM research contained analysis of effectiveness of the proposed restoration in case of the Parthenon Pronaos by (Psycharis et al. 2003). Seismic analysis of the Roman Temple of Evola in Portugal (Oliveira et al. 2012) have proved that the construction was in a safe condition also according to the current Eurocode. Another extended study on the current state of the colonnade in Pompeii has been recently published by several articles. The first part of the study presented with 2D DEM static and dynamic analysis (Sarhosis, Asteris, Wang, et al. 2016) where the parameters affecting the seismic behavior of colonnades' structural systems have been examined. The next part of study presented a critical compare between 2D and 3D models' results emphasizing the differences from the selected harmonic and seismic loading (Sarhosis, Asteris, Mohebkah, et al. 2016).

An interesting study on seismic assessment was performed on the tholos in Sardinian "Nuraghe" (Roberti and Soina 2001), in particular on structural elements of an ancient pre-roman construction which consisted of polygonal irregular blocks.

Seismic behavior and stability of narrow and arched constructions built with dry stone masonry were studied by (Sincaian, Oliveira, and Lemos 1998) and by (Drei and Oliveira 2001). Both researches provided models for dynamic analysis of two examples of the Portuguese architectural heritage presented by aqueducts from 16-18<sup>th</sup> centuries.

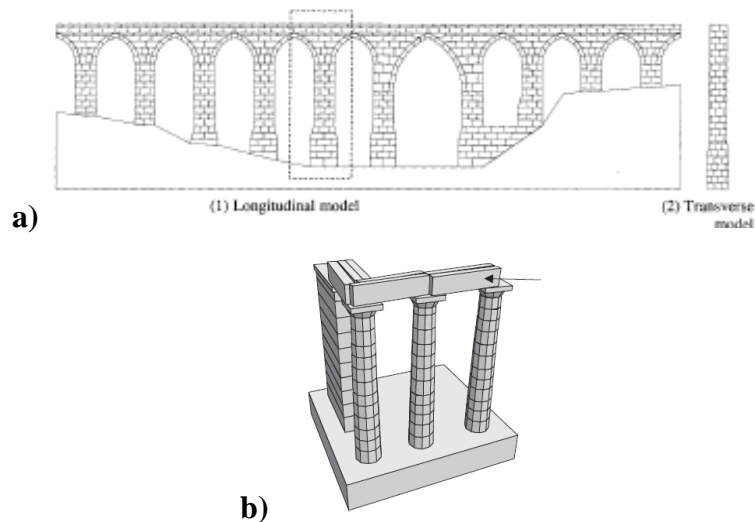


**Figure 2.14** Examples of a) 2D DE model of the aqueduct (Sinraian, Oliveira, and Lemos 1998) and b) 3D DE model of the archeological site (Psycharis et al. 2003)

DE models can be also useful for investigation of the historical hypothesis on the events that damaged or distracted monuments or buildings. Analysis of the temple of Zues at Olimpia was performed using single column models in order to discuss its destruction (Alexandris, Psycharis, and Protopapa 2014). Another pre Doric Greek temple has been studied in order to reconstruct and analyze the seismic response and its possible destruction by a historical earthquake (Young, Schultz, and Lemos 2015).

### 2.8.2 Traditional buildings

Research on traditional architecture is mainly represented by DE analysis of rural houses and religious structures, such as churches and mosques. Parametric study and dynamic analysis of two minarets in Istanbul was published by (Cakti et al. 2014). The research aimed to understand the damage and collapse behavior of minarets under seismic actions. Another study was undertaken on the 15th century Mustafa Pasha Mosque in Skopje (Cakti et al. 2016). The 3D DEM analysis was carried out in order to represent shake table experimental complain that was performed on scaled mosque model. As the result, the DE approach showed the capability to handle the dynamic nonlinear modeling of relatively complex masonry structures.



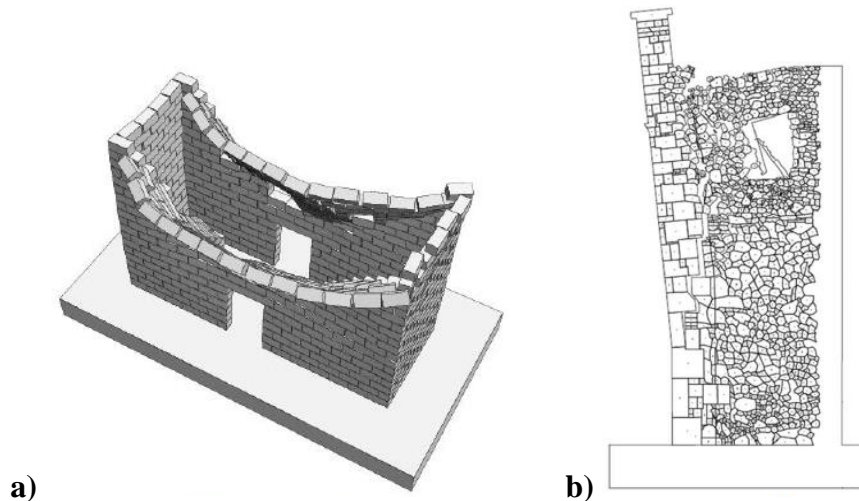


**Figure 2.15** Collapse mechanisms of **a) a traditional rural house** (Alexandris, Protopapa, and Psycharis 2004) **and b) a church facade** (de Felice and Mauro 2010)

Typical structures of traditional rural Cypriot architecture were investigated under dynamic analysis by (Alexandris, Protopapa, and Psycharis 2004). The aim of the research was to obtain the crack patterns and the collapse mechanisms of the stone masonry structures subjected to severe earthquake excitations without and with successive intervention. Similar study on seismic vulnerability of masonry aggregates was published by (Ulrich, Negulescu, and Ducellier 2015), where the 2 floor buildings were efficiently analyzed under pushover procedure.

An interesting research on three case studies damaged during L'Aquila 2009 earthquake were published by (de Felice and Mauro 2010). Seismic behavior of the churches was investigated taking into account the effective morphology of masonry, using both static push-over and dynamic pulse analysis. The effectiveness of evaluation of the seismic capacity by means of quasistatic analysis was also identified by another study performed on the library of the Casamari abbey in Italy (de Felice et al. 2015).

### 2.8.3 Structural elements

Several studies were performed on simulation of the dynamic behavior of ancient masonry columns with DE approach (Papantonopoulos et al. 2002), (Komodromos, Papaloizou, and Polycarpou 2008), (Stefanou, Psycharis, and Georgopoulos 2011), (Dimitri, De Lorenzis, and Zavarise 2011). All works demonstrated appropriate usability of the method in

estimation of the responses to expected earthquake motions that can be used with confidence in the restoration process connected with ancient monuments.

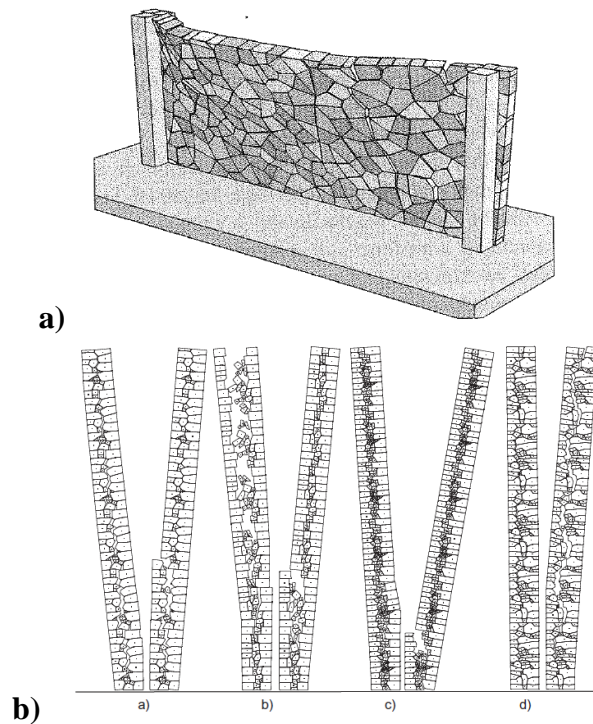


**Figure 2.16 Failure mechanisms of the irregular stone models by a) (Lemos, Costa, and Bretas 2011), b) (de Felice 2011)**

Another extended researches were published on assessment of the out-of-plane seismic capacity of masonry walls analyzed with DEM. (de Felice and Giannini 2001) studied seismic vulnerability of unreinforced masonry buildings depending on the connections with transversal walls. Both static and dynamic techniques were implemented with critical compare of the results. Similar approaches were used in next study by (de Felice 2011), where strength and displacement capacity of rubble stone masonry walls were investigated depending on their morphology. (Lemos, Costa, and Bretas 2011) also presented research on the irregular masonry, showing influence of the DE meshing on the resultants failure loads. (T.-T. Bui and Limam 2012), (Lemos and Campos Costa 2016) developed 3D models to represent shake table experimental results on out-of-plane behavior of masonry buildings.

A study on arch element have been performed by (De Lorenzis, DeJong, and Ochsendorf 2007) and demonstrated good agreement of analytical and numerical results in form of behavior and failure domain of the masonry arch subjected to a ground acceleration pulse.

In addition to stone and clay brick masonry, mud bricks were popular structural materials in ancient time, especially in countries with high sun intensity. Interesting studies were published in order to valid the ability of DEM for modeling adobe housing by (Daudon et al. 2014), as well as rammed earth structures by (Q.-B. Bui, Bui, and Limam 2016).

## **2.9 Summary**

Architectural heritage is mostly based on masonry constructions, from all of the historical periods that endured along the centuries. Earthquake is periodical and the most dangerous natural disaster that continuously creates hazard and damage on the masonry structures. Due to damage accumulated with time, these structures require periodic inspections in order to assess their actual safety level. To perform the structural assessment of a historical masonry structure, several principals and recommendations are developed by ICROM and ICOMOS. Numerical simulations are the great tool for structural analysis of masonry constructions, in order to fulfill the special requirements associated to the architectural heritage.

In this connection, the DEM is one of the most powerful numerical methods for seismic assessment of historical masonry structures, and the only one able to trace the complete structural response from the elastic range, through joints cracking and crushing, up to its failure. Simple constitutive models are easy to use and require few input data, which is very important in the case of historical structures, where there is lack of data and distractive tests are not allowed. The DEM will be followed and used in the present dissertation.

## **3 Seismic analysis using Discrete Element Method**

### **3.1 *Fundamentals of the Discrete Element Method***

Discrete Element Method (DEM) firstly was presented by (Cundall 1971), as was mentioned earlier, to model rock's materials as an assembly of rigid blocks. The name "discrete", according to author, could be applied to a computer approach only if

- a) it allows finite displacements and rotations of discrete bodies and
- b) new contacts between the blocks recognized automatically and updated as calculation progresses.

However, within the general classification it falls into discontinues analysis techniques. A discontinues medium is distinguished from a continuum one by introducing of contacts or interfaces between the discrete bodies comprising the system. A numerical DE model mainly represents two types of mechanical behavior, containing behavior of the solid material and the discontinuities. Thereby, it is a suitable tool for numerical modeling of the historical masonry structures and their seismic assessments. The best advantage could be achieved by applying DEM on analysis of structural failure, which may be modeled either as quasi-static or fully dynamic process in the context of safety assessment studies and which will be critically discussed further in the chapter.

The essential features of the DEM that makes it an excellent tool to approach the highly non-linear behavior of masonry are reviewed below.

#### **3.1.1 Blocks representation**

Blocks in DEM can have representation in two different ways: the material may be assumed rigid or deformable. If the deformation of the solid material cannot be neglected, deformable blocks are used. To introduce deformability, the body is divided into internal elements, for instance, a finite element mesh is created for each block. The complexity of the deformation depends on the number of elements into which the unit is divided.

The assumption of material rigidity is used in the physical system where the most of the deformation is accounted by movements on discontinuities. In this case, the movements consist mainly of sliding and rotation of blocks and of opening and interlocking of interfaces. The rigid

block representation is very suitable approach for simulation of the masonry constructions, as all the non-linearity concentrated in the joints and failure by mechanism is common. Thus, analysis based on DEM allowed getting the most possible realistic modeling results on the chained mechanisms failure. In order to effectively use this DEM features the shape and the arrangement of the blocks together with existing damage should be included precisely in the model. For this reason an automatic procedure for DE geometry creating is developed and successfully implemented, that will be discussed further in the chapter.

### 3.1.2 Contacts representation

Contacts in DEM are represented in form of point contact hypothesis, where interaction between the blocks is represented by set of contacts. Generally, point contacts are assigned to corners of a rigid block otherwise to each grid points of a deformable unit. Block displacement at each point is a function of the relative contact force. Stresses can be calculated following joint constitutive law usually formulated in terms of stresses and displacements. The point contact is assigned to a specific length or an area, in a way that the sum of lengths or area of all contacts in a row equal to the total joint length or area. The simplest way is to assume a representation of the contacts as a normal and shear elastic springs (Figure 3.1), where the contact forces are proportional to the relative displacements between the blocks. Generally used constitutive laws of the joints are reviewed further.

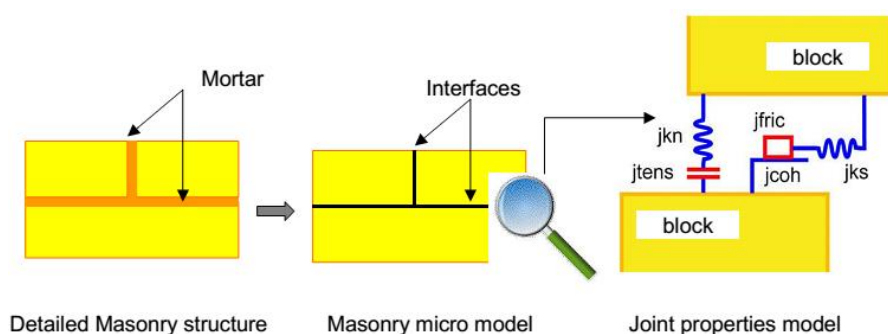


**Figure 3.1 DEM interface model** (Idris, Al-Heib, and Verdel 2009)

There are two main classifications of contacts in DEM:

1. Rigid or hard contact model, when no any overlap of blocks is allowed, shear displacement  $u_s$  only due to sliding (Figure 3.2a);
2. Deformable or soft contact model, where a small overlap of units is possible in order to obtain relative block displacements in the normal  $u_n$  and shear  $u_s$  directions thanks to defined contact stiffness (Figure 3.2b)

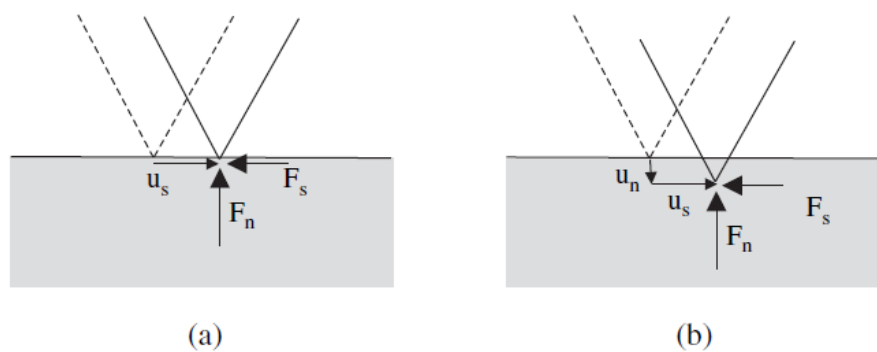


**Figure 3.2 Contact models: a) Rigid or hard contact model; b) Deformable or soft contact model ( $u_n$  exaggerated)** (J. V. Lemos 2007)

In the most DEM approaches the deformable contact model is applied. In case of masonry modeling, the normal stiffness can be directed to the mortar thickness and its characteristics; or in case of dry masonry the normal stiffness parameters could be obtained from the blocks mechanical characteristics.

### 3.1.3 Contacts Detection and Update

DE analysis by the default involves large displacements that also required in masonry studies, in order to visualize and understand the structural behavior. Thus, the contact detection process is the principal time consuming task in DEM simulations and depends on the complexity of each block's geometry as well as the number of blocks being simulated.

Theoretically, the detection of contacts requires simple geometric calculations, while the major problem lays on computational time. Generally, the rule is that the new contact should be detected automatically before the blocks actually touched. Contact detection is basically made by means of two steps (Cundall 1988): firstly, the blocks

which do not have any possibility of coming in contact are eliminated, and secondly, the blocks left are strictly checked. In order to save computational time, the contact detection procedure is performed periodically depending on chosen tolerance, as an indicator of the certain block movements. Since the contact detection test is not realized every step, it is important to anticipate the possible contacts that could be formed between two successive steps. For this reason a virtual contact is introduced, in which forces are equal to zero. Once the blocks come closer, some virtual contacts may become real with interaction forces. On the contrary, when blocks move apart, with exceeding of the given tolerance the virtual contacts are eliminated.

### **3.2 UDEC program**

There are many computational approaches fall within DEM, such as distinct elements, discontinuous deformation analysis, combined finite-discrete element, discrete element particle, etc., detailed list of which can be found in (Lemos 2007),(Sarhosis, Bagi, et al. 2016). In this connection, in the present dissertation DEM is utilized by mean of commercial software UDEC (Itasca Ltd).

Initially, UDEC (Universal Distinct Element Method) was developed mainly for dynamic analysis of rocks, but later the program was successfully adapted for analysis of masonry structures. The essential principals of the UDEC such as solution algorithm, equation of motion, mechanical damping and joints constitutive law is discussed in the present chapter. However, more detailed info about the program can be found in the user's manual (Itasca 2011).

Additionally, during the analysis performed in the present dissertation several build in UDEC features have been also beneficially used. For example, structural elements, such as reinforcement and cables, initially developed for strengthen of the rocks were successfully implemented in the simulation of masonry retrofitting. A programming language *FISH* embedded within *UDEC* enables the user to access the entire internal data structure, add requirement features or implemented analysis routines.

#### **3.2.1 Solution algorithm**

The calculation performed in the distinct element method alternate between application of a force-displacement law at all contacts and Newton's second law at all centroids of rigid blocks or grid points of

deformable blocks. Thanks to the force-displacement law contact forces are found from known (and fixed) displacements. The next step is based on the known (and fixed) forces that give the motion of the blocks from the Newton's second law. For the deformable blocks it also gives stresses within the elements by the application of the material constitutive law. The basic logic used in UDEC is shown schematically in Figure 3.3. The approach uses an explicit integration scheme in order to solve the equation of motion directly.

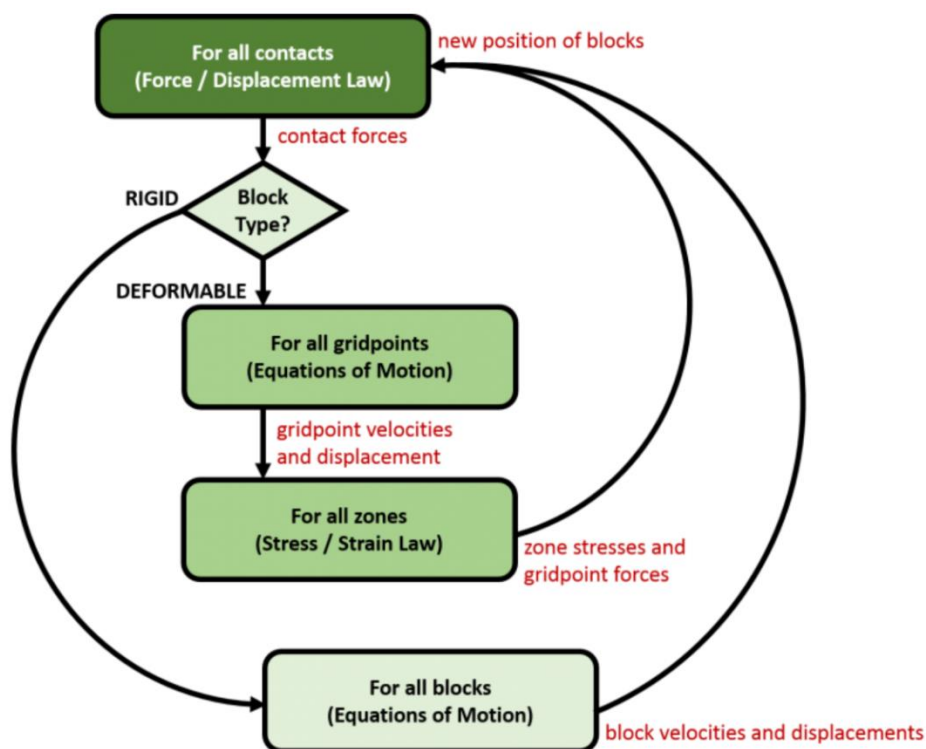


Figure 3.3 Basic logic used in UDEC

The numerical analysis is represented dynamic behavior of the system by time stepping algorithm where the time step is limited by the numerical stability requirements of the central difference method. It is assumed that the time step in DEM is sufficiently small that during one unite the disturbance can propagate only between immediate neighbors and velocity and acceleration are constant within it. Thereby, at any time step the resultant forces on any block are determined exclusively by its interaction with the neighbor contacting blocks. The last feature makes it



possible to follow non-linear interaction of a large number of blocks without excessive memory requirements or the need for an iterative process within a time step. The time step restrictions depend on several parameters such as the block mass and interface stiffness for rigid blocks; the zone size and the stiffness of the system for deformable blocks.

By the definition the algorithm is the dynamic one, but may also be used for quasi-static problems under particular circumstance. The static analysis can be performed if the time scale is fictitious and if a large amount of viscous damping is introduced to dissipate the kinetic energy, and obtain convergence to a static solution or to a failure mode. This approach is conceptually similar to dynamic relaxation technique. The disadvantage of the explicit time integration method is to be only conditionally stable under use of very small time step that may lead to time consuming computations.

### 3.2.2 Equations of motion

The motion of an individual block is determined by the magnitude and direction of resultant out-of-balance moment and forces acting on it. The equation of one-dimensional motion that describe translation and rotation of a single mass acted on by a varying force,  $F(t)$ , can be expressed using Newton's second law of motion as following

$$\frac{d\dot{u}}{dt} = \frac{F}{m} \quad (3.1)$$

where  $\dot{u}$  – velocity,  $t$  – time,  $m$  – mass.

For models containing rigid blocks, the central difference method is used to integrate the equations of motion of each block. For models with deformable blocks, the equations of motion are solved for each node and the variables are 2 nodal degrees of freedom in 2D. While, for rigid body in 2D the variables are 2 displacements and 1 rotation, which are defined as following.

$$x_i^{(t+\Delta t)} = x_i^{(t)} + \dot{u}^{(t+\frac{\Delta t}{2})} \Delta t \quad (3.2)$$

$$\theta^{(t+\Delta t)} = \theta^{(t)} + \dot{\theta}^{(t+\frac{\Delta t}{2})} \Delta t \quad (3.3)$$

where  $\theta$  – rotation of block about centroid,  
 $x_i$  – coordinates of block centroid.

Finalizing, each time step produces new block positions that generate new contact forces. Resultant forces and moments are used to calculate linear and angular accelerations of each block. Block velocities and displacements are determined by integration over increments in time. The procedure is repeated until either a satisfactory state of equilibrium or one continuing failure results. Mechanical damping utilized in the equations of motion to provide both static and dynamic solutions will be reviewed further in the chapter.

### 3.2.3 Contact forces

When two blocks come into contact, a force develops between them and can be resolved into normal and shear components. Moreover, the simplest representation is to assume that the blocks are connected by normal and shear elastic springs. In this connection the mechanical interaction forces are functions of the relative displacement between the two blocks and the contact stiffness containing deformability of the joint (Figure 3.4).

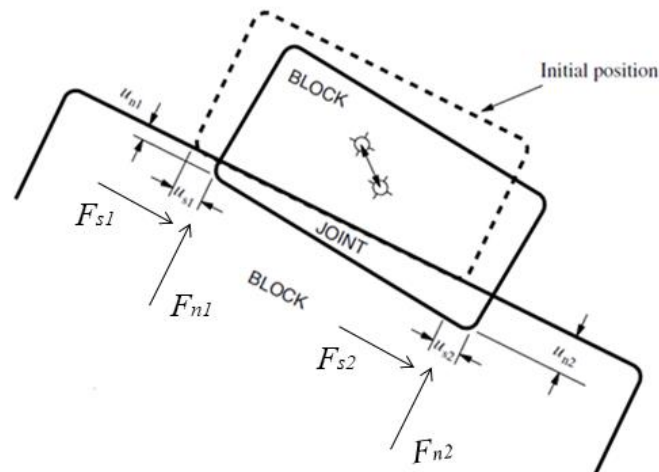


Figure 3.4 Schematic representation of contacts and their forces between rigid blocks

$$F^c = F_n + F_s$$

(3.4)

where  $F^c$  –contact force,

$F_n$  and  $F_s$  - respectively, normal and shear components of contact force.

The forces components of the mechanical interaction could be found using following elastic spring formulations

$$F_n = K_n \Delta u_n \quad (3.5)$$

$$F_s = K_s \Delta u_s \quad (3.6)$$

where  $K_n$  and  $K_s$  – normal and shear stiffness of the contact,

$\Delta u_n$  and  $\Delta u_s$  – normal and shear displacement increment at the contact.

From the other hand, in general, force could be expressed in terms of stresses at each point contact as following (normal force used as an example)

$$F = \sigma A \quad (3.7)$$

where  $\sigma$  – normal stress,

$A$  – associated area of the contact,  $A = b \cdot s$

with  $b$  – length of the block and  $s$  – thickness of the block.

Consequently, stresses according to Hook's low can be found

$$\sigma = E \cdot \varepsilon \quad (3.8)$$

where  $E$  – elastic modulus of the blocks,

$\varepsilon$  – strain expressed by following formula  $\varepsilon = \frac{\Delta u}{h'}$ ,

with  $h'$  – associated height of the contact

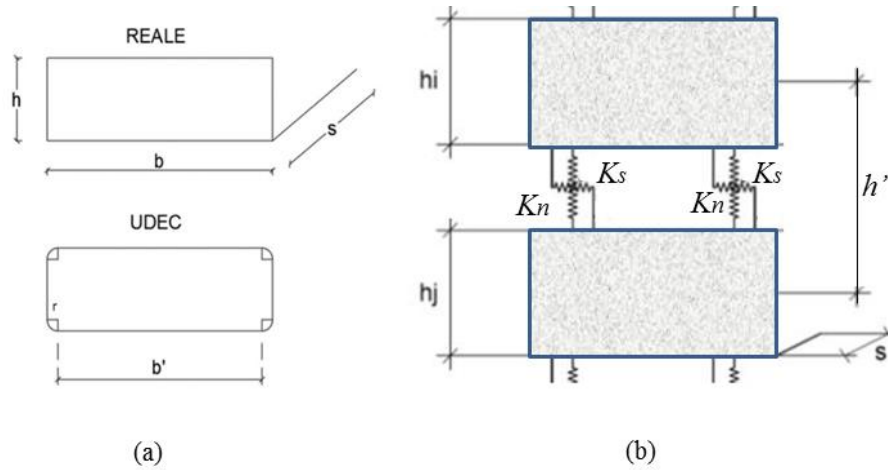


**Figure 3.5 Schematic representation of a) block dimensions and b) contacts between blocks**

Finally, merging all the formulas together the contact normal stiffness can be expressed as following

$$K_n = E \frac{b \cdot s}{h'} \quad (3.9)$$

Respectively the shear contact stiffness

$$K_s = G \frac{b \cdot s}{h'} \quad (3.10)$$

Thereby the joint stiffness used in UDEC for Coulomb friction constitutive law can be implemented as an effective stiffness density depending on an effective joint length (Figure 3.5a)

$$jk_n = E \frac{b \cdot s}{h' \cdot b'} \quad (3.11)$$

$$jk_s = G \frac{b \cdot s}{h' \cdot b'} \quad (3.12)$$

Additionally, based on masonry average Poisson's ratio the value of shear stiffness is assumed  $j_{k_s} = 0.4j_{k_n}$  for most of the performed analysis in the present dissertation.

### 3.2.4 Joint constitutive models

The general model used in UDEC for representing masonry joints is the Coulomb slip model. The essential parameters to define the mechanical behavior of the joints are:

- Normal stiffness ( $j_{k_n}$ )
- Shear stiffness ( $j_{k_s}$ )
- Friction angle ( $\varphi$ )
- Cohesion ( $c$ )
- Tensile strength ( $f_t$ )

In the Figure 3.6 the force-displacement relationships are presented both for the shear and normal components. In the normal direction, the stress-displacement relation is assumed to be linear and governed by

$$\Delta\sigma_n = -j_{k_n}\Delta u_n \quad (3.13)$$

where  $\Delta\sigma_n$  – the effective normal stress increment,  
 $\Delta u_n$  – the normal displacement increment.

For computing of relative normal displacement an overlap between the blocks is assumed as a mathematically convenient measure. This is the soft contact assumption as was described earlier. If normal joint stiffness is increased, overlaps can be assumed as small as desired. There is also limiting joint tensile strength, exciding which the normal stress becomes zero. However, in the most analysis of historical dry masonry the value of tensile strength assumed to be zero.

In the shear direction, the response is controlled by constant shear stiffness and the shear stress is limited by a combination of cohesive and frictional strength. An increment of the shear stress is defined as following:

$$\Delta\tau_s = -j_{k_s}\Delta u_s \quad (3.14)$$

if

$$|\tau_s| \leq c + \sigma_n \tan \varphi = \tau_{max} \quad (3.15)$$

otherwise

$$\tau_s = \text{sign}(\Delta u_s) \tau_{max} \quad (3.16)$$

where  $\Delta u_s$  – the shear displacement increment.

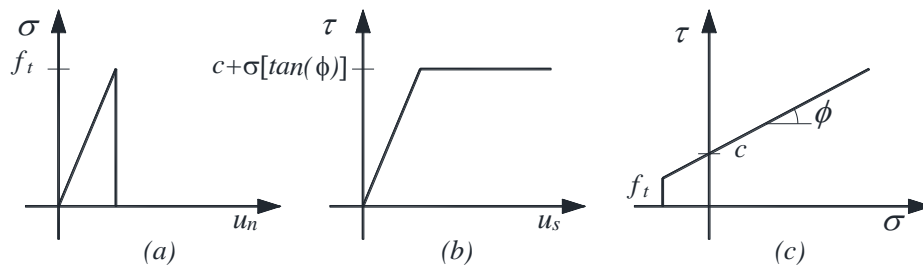


**Figure 3.6 The joint constitutive laws: a) normal and b) shear, c) Mohr Coulomb yielding criteria**

In addition, joint dilation or residual strengths values can be used in the Coulomb slip model to approximate a displacement-weakening response. As shown in (Lourenço 1996) dilation and residual strength are more important in confined masonry, thus these values are equal to zero in all the simulations performed in this dissertation.

### 3.2.5 Mechanical damping

Mechanical damping is used in UDEC to solve two general classes of problems: static (non-inertial) and dynamic solutions. For each type of problem a different form of damping is used.

For static analysis, the approach is conceptually similar to dynamic relaxation, where the equations of motion are damped to reach the equilibrium as fast as possible. The resultant damping is velocity-proportional, that means that the damping magnitude is proportional to the velocity of the blocks. Thus, two build-in damping forms in UDEC may be used for solving static problems. *Auto damping* is an adaptive global damping, which adjusts the damping constant automatically. Viscous damping forces are used, but the viscosity constant is

continuously adjusted in such a way that the power absorbed by damping is constant and proportion to the rate of kinetic energy change in the system. The adjustment to the viscosity constant is made by a numerical servo-mechanism that seeks to keep the ratio,  $R$ , equal to a given ratio (e.g., 0.5).

$$R = \frac{\sum P}{\sum \dot{E}_k} \quad (3.17)$$

where  $P$  – damping power for a node or a rigid block,  
 $\dot{E}_k$  – rate of change of nodal or block's kinetic energy,  
 $\sum$  - represents the summation over all nodes or blocks.

At the moment when system approaches steady state (equilibrium or steady flow), the rate of kinetic energy change approaches zero and, consequently, the damping power tends to zero too.

Another form of damping provided in *UDEC* is when the damping force on a rigid block is proportional to the magnitude of the unbalanced force. For this scheme, referred to as *local damping*, the direction of the damping force is such that energy is always dissipated. The local damping to translational and angular velocities

$$\dot{u}^{(t+\frac{\Delta t}{2})} = \dot{u}^{(t-\frac{\Delta t}{2})} + \left( \sum F_i^{(t)} - \gamma \left| \sum F_i^{(t)} \right| \text{sgn} \left( \dot{u}^{(t-\frac{\Delta t}{2})} \right) \right) \frac{\Delta t}{m} \quad (3.18)$$

where  $\gamma$  is a constant (set to 0.8 in *UDEC*). Local damping may be preferred for analyses involving sudden load changes or progressive failure (such as caving of many blocks), for which different amounts of damping are required in different regions of the model. Analyses with local damping are observed to be slightly underdamped in general. It is the main damping used in the present dissertation for quasistatic analysis. For a dynamic analysis, the damping in the numerical simulation should approximately reproduce the energy losses in the natural system when subjected to a dynamic loading. Rayleigh damping is used in *UDEC* for dynamic analysis it will be described further in the chapter.

### **3.3 New implemented semiautomatic DE model creator**

As was mentioned earlier, DE analysis allows getting the most possible and realistic simulation results on the chained mechanisms failure,

especially if the DE model contains an effective reproduction of the blocks shape and arrangement. Unfortunately, it is inconvenient to obtain a complex and precise geometry using directly UDEC interface since the user is able to create geometry only using coordinates of single lines. In order to reduce complexity of the DE model generation as well as needed amount of time, a semi-automatic model creator was developed, which allows user to draw a model in the CAD graphic software and then produce a ready UDEC input file. The algorithm contains the following steps as illustrated in the Figure 3.7.

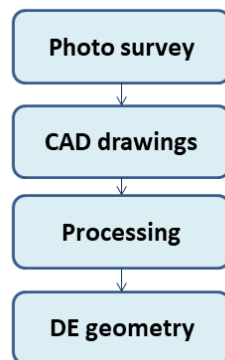


**Figure 3.7** Flowchart of semiautomatic DE model creator

The initial step is an appropriate photo survey, aimed to obtain qualified pictures of the monument. Firstly, the pictures should be with high resolution permitting to observe masonry arrangement including existing damage usually presented in form of cracks and fissures. Secondly, the picture should contain the monument on the right angle, saving as much as possible its original shape and proportions.

The next step is to attach obtained corresponding photo to the CAD and to perform scaled drawings of the investigated structure. The drawings should reproduce the real masonry texture with all the damage. Generated mesh contains only polygons representing masonry blocks, while the joints are assumed as interfaces between the blocks and recognized by the UDEC automatically without intrusion an additional unit. Thereby, the border of each reproduced block excides the real one on the half joint thickness in order to keep the entire system's geometry equal to the original monument dimensions.

The CAD drawing should include several layers containing input information, such as:



- a layer with a polygon representing perimeter of the model;
- a layer with lines or polygons representing masonry arrangement and existing cracks;
- a layer with polygons representing existing openings;
- layers with polygons representing domains, each domain reflects a specific mechanical parameter like material density or joint normal/shear stiffness, friction angle, cohesion and tensile strength.

The mechanical properties variant depending on materials typology or/and model effective thickness. As was mentioned earlier in the Chapter, the Mohr-Coulomb criteria is widely applied for masonry modelling, thus it is used as a default constitutive law in the developed pre-processing code.



**Figure 3.8 Paths for creating accurate DE mesh**

Finally, a pre-processing code is used to automatically generate an UDEC model. In this connection, a final *.dxf* file containing all the CAD data is processed using C++ language code in order to obtain UDEC ‘friendly’ *.txt* file. The target file contains required input data including vector coordinates for geometry and text with adapted mechanical parameters. In the final model, stones are represented as polygonal rigid bodies with certain value of mass density and the joints as interfaces between the blocks defined by Coulomb friction law.

The algorithm represents the real geometry of the investigated structures including orderly arrangement of blocks and existing damage. It also applies material and joint properties to different parts of the model depending on the material types and its effective thickness. The implemented semi-automatic model creator makes possible to easily obtain precise models with use of widely spread graphical software and consequently obtain accurate simulation results.

### 3.4 New implemented routine for pushover analysis

An automated routine has been implemented in UDEC in order to obtain a capacity curve based on pushover analysis. The analysis was performed using a quasi-static technique, in which the gravity load was applied first and then horizontal increasing accelerations were introduced in successive steps up to the failure of the structure. The ascending part of the push-over curve was obtained by collecting the static equilibrium points reached by explicit integration of the equation of motion at each load step. Once the last equilibrium point was reached under increasing horizontal acceleration, a further load step activated the collapse mechanism, which was followed up to the attainment of the ultimate displacement and then to failure. The descending branch of the push-over curve was obtained by joining the last equilibrium point of the ascending branch, with the ultimate displacement corresponding to the unstable mechanical equilibrium of the structure. Example of resultant pushover curves are illustrated in the Figure 3.9 that represents the lower capacity curve by dashed line and a solid red curve with higher capacity in terms of both strength and ductility.

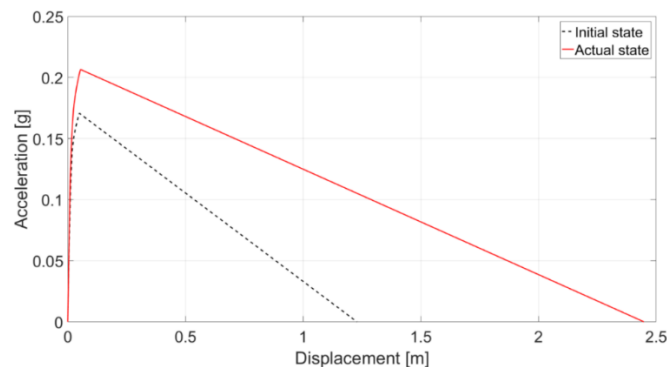


**Figure 3.9** Example of resultant pushover curves

In general, implemented pushover analysis is based on force-control technique, where a known value of acceleration has been applied to the system. Consequently, it is worth noting that the original dynamic problem was solved as a quasi-static problem using artificial damping to reach the equilibrium state as soon as possible. A build-in ‘local’ damping has been used for all the parts of pushover analysis, and principles of which were explained earlier in the Chapter.

The theoretical basis of the analysis is based on the concept of the both static and mechanical equilibriums. Thereby, the most important

parameters of the seismic response were found at the last static and mechanical equilibrium points of the system. Consequently, the algorithm's calculation paths were destined to define strength and ductility parameters at the critical stages of the structure that respectively represents its capacity curve.

Practically, the implemented pushover routine was divided into two respective algorithms. The first one allowed defining a maximum bearing acceleration of the structure, while the second one obtained a value of ultimate displacement. In the following paragraphs the two corresponding steps denoted as ascending and descending branches of pushover curve are provided with extended explanation of the new implemented routine in UDEC.

### **3.4.1 Ascending branch of pushover curve**

Initially the model is defined with its geometry and mechanical properties of the materials. The model is run under the gravity loads until a default equilibrium state in UDEC that could be determined by 'solve' command, and which corresponds to a steady state condition defined by tolerance of velocity and unbalanced force.

The pushover routine starts with the application of the first horizontal acceleration increment  $\Delta a_1$ , which in UDEC is implemented as a horizontal component of acceleration applied to the centroid of each block using 'grav' command. As soon as static equilibrium is reached, the parameters of displacement  $d1$  and acceleration  $a1$  will be recorded as the first point of the pushover curve (Figure 3.10). After that the cycle repeats by applying further acceleration increments and collecting equilibrium points.

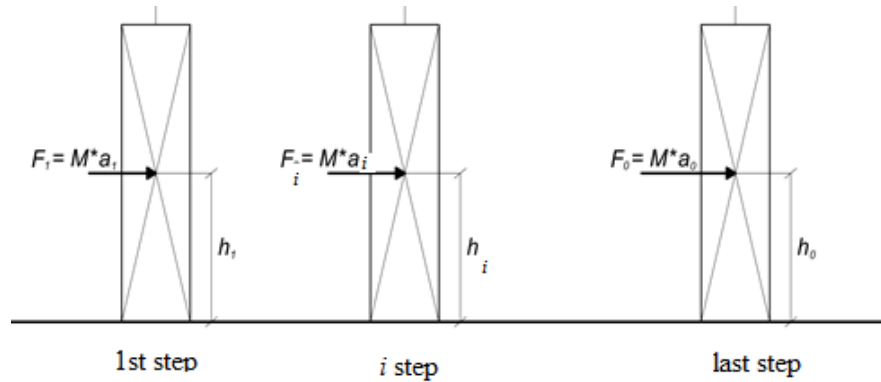


**Figure 3.10 Schematic representation of the mechanism and respective ascending branch**

By repeating the procedure the ultimate equilibrium condition  $(d_0, a_0)$  can be determined, which represents the peak of the capacity curve as well as the maximum resistance in terms of bearing acceleration. Generally, at this stage of the analysis, displacements are very limited and appear only due to deformability of the geometry without any damaging phenomena such as joints openings or sliding.

### **3.4.1.1 Detailed algorithm**

The detailed algorithm in order to obtain corresponding coordinates  $(d_i, a_i)$  of the ascending branch of the pushover curve is presented below in more details. The logic is built on the concept of the static equilibrium and addressed to follow the capacity curve until the last static equilibrium point of the investigated system.

**INPUT DATA**

$a$  – initial acceleration (i.e.  $a = 0 \text{ m/s}^2$ ),

$\Delta a$  – initial acceleration increment, should be rather small to respect static character of the analysis (i.e.  $\Delta a = 0.05 \text{ m/s}^2$ ),

$\Delta a_{min}$  – the minimum value of the acceleration increment, should be fairly small to provide good accuracy of the procedure (i.e.  $\Delta a_{min} = 1 \cdot 10^{-4} \text{ m/s}^2$ ),

$vel_{max}$  – the maximum possible velocity to identify the last equilibrium point (i.e.  $vel_{tol} = 2 \cdot 10^{-6} \text{ m/s}$ )

$cyc_{max}$  – maximum number of cycles to find an equilibrium of the system (i.e.  $cyc_{max} = 1 \cdot 10^5$  as default value in UDEC)

$last$  – indicator if the logic passed at least once over  $vel_{tol}$  or  $cyc_{max}$  (i.e.  $last = 0$ )

**LIST OF STEPS**

1. Entering the input parameters with the model already under gravity loads
2. Application to the structure of a horizontal acceleration value equal to  $a = a + \Delta a$
3. Executing the SOLVE command – running the model until the steady state of the system
4. Calculating the average velocity of all blocks in the system  $vel$  and the number of cycles  $cyc$  used during executing solve command
5. Controlling  $cyc > cyc_{max}$  – if YES proceed to the step#9, if NO proceed to the step#11 (after passing YES at least once then  $last = 1$  and always proceed to the step#9)
6. Controlling  $vel > vel_{max}$  – if YES proceed to the step#9, if NO proceed to the step#11 (after passing YES at least once then  $last = 1$  and always proceed to the step#9)
7. Decreasing the acceleration increment  $\Delta a = \Delta a/2$
8. Controlling  $last = 1$  – if YES proceed to the step#2, if NO proceed to the next step
9. Controlling  $\Delta a < \Delta a_{min}$  – if YES proceed to the end, if NO proceed to the next step
10. Storing the current values ( $a, d$ ) and go back to step#2.

The list of operations implemented in UDEC is useful to describe the algorithm in details and clarifies the meaning of all parameters, but the structure of the program is certainly clearer if represented in flowchart format (Figure 3.13).

In the routine, in order to define an adequate acceleration increment a dichotomy algorithm is used. It means that the algorithm launches with a certain value of the initial acceleration increments. When the applied acceleration reached a value when convergence of the algorithm is not found, the applied initial increment is divided by 2 and the calculation continues with decreased  $\Delta a$ . Once reaching a non-convergence condition every subsequent value of the increment will be twice lower than the previous one. Accordingly, as a convergence condition the value of maximum velocity tolerance  $vel\_max$  was chosen. If the equivalent velocity of the system  $vel$  was below the tolerance, it was assumed that the structure stayed in the static equilibrium. Oppositely, if the equivalent velocity exceeds the tolerance and the system is not in the steady state condition anymore that means the current value of acceleration overpassed the sought-for value. Thus, the calculation step should be repeated with reduced value of the acceleration increment and so on up to reaching a secondary convergence condition. As a secondary convergence condition a minimum acceleration increment tolerance was determined.

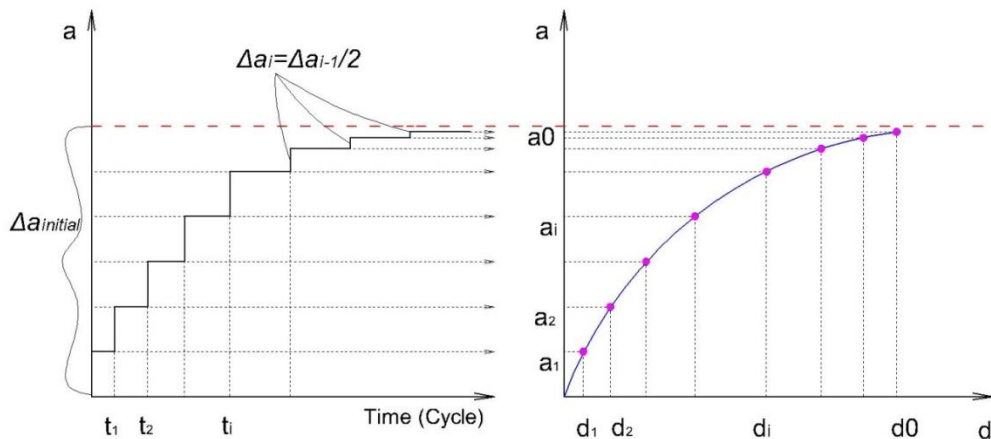


**Figure 3.11 a) Loading scheme and b) detailed algorithm of the ascending branch**

Since under  $a_{i+1}$  the system is not in corresponding ‘equilibrium’ any more, the required value of  $a_0$  is between  $a_i$  and  $a_{i+1}$ . In this condition

dichotomy logic may be successfully applied as demonstrated in the Figure 3.11.

The dichotomy logic can be expressed as following

1. Initial acceleration increment  $\Delta a_{initial}$
2.  $a_{i+1} = a_i + \Delta a_{initial}$
3. check if  $vel > vel_{tol}$ , then  $a_{i+1}$  is too great and  $\Delta a_2 = \Delta a_{initial}/2$
4.  $a_{i+1} = a_i + \Delta a_2$
5.  $\Delta a_{initial} = \Delta a_2$  and go back to step#2

In general, the run time that expressed by number of required cycles is not constant during calculation steps. The number of cycles needed to converge the equilibrium state of the system rise with increasing the value of applied acceleration. Since the system is moving towards unstable condition, it is more time consuming to define its steady state even under artificial damping (Figure 3.12).

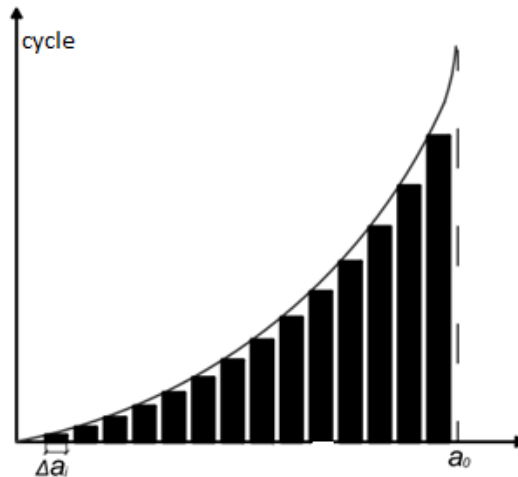


Figure 3.12 Number of cycles to converge to equilibrium

The procedure of calculating the value  $vel$ , utilized in the first convergence condition, depends on the nature of the investigated structure:

- For a structure containing mainly arches the  $vel$  is defined as an average velocity of all the blocks of the system as following

$$vel = \frac{\sum m_i v_i}{\sum m_j}$$

(3.19)

---

where  $m_i$  and  $v_i$  – mass and velocity of a block of the system,  
 $m_j$  – mass of a moving block of the system.

• For a rigid structures, system of which works as a rigid body, the  $vel$  value is obtained as a velocity of the center of gravity of the mechanism, the coordinates of which defined using following implemented formulas

$$\begin{aligned} X_g &= \frac{\sum m_i x_i \Delta x_i}{\sum m_i \Delta x_i} \\ Y_g &= \frac{\sum m_i y_i \Delta y_i}{\sum m_i \Delta y_i} \end{aligned} \tag{3.20}$$

where  $m_i$  – mass of a block of the system,  
 $x_i$  and  $y_i$  – coordinates of centroids of a block,  
 $\Delta x_i$  and  $\Delta y_i$  – displacement of a block.

The final value of  $vel$  for a rigid system is obtained as a velocity of a block nearest to the centroid of the mechanism ( $X_g, Y_g$ ).



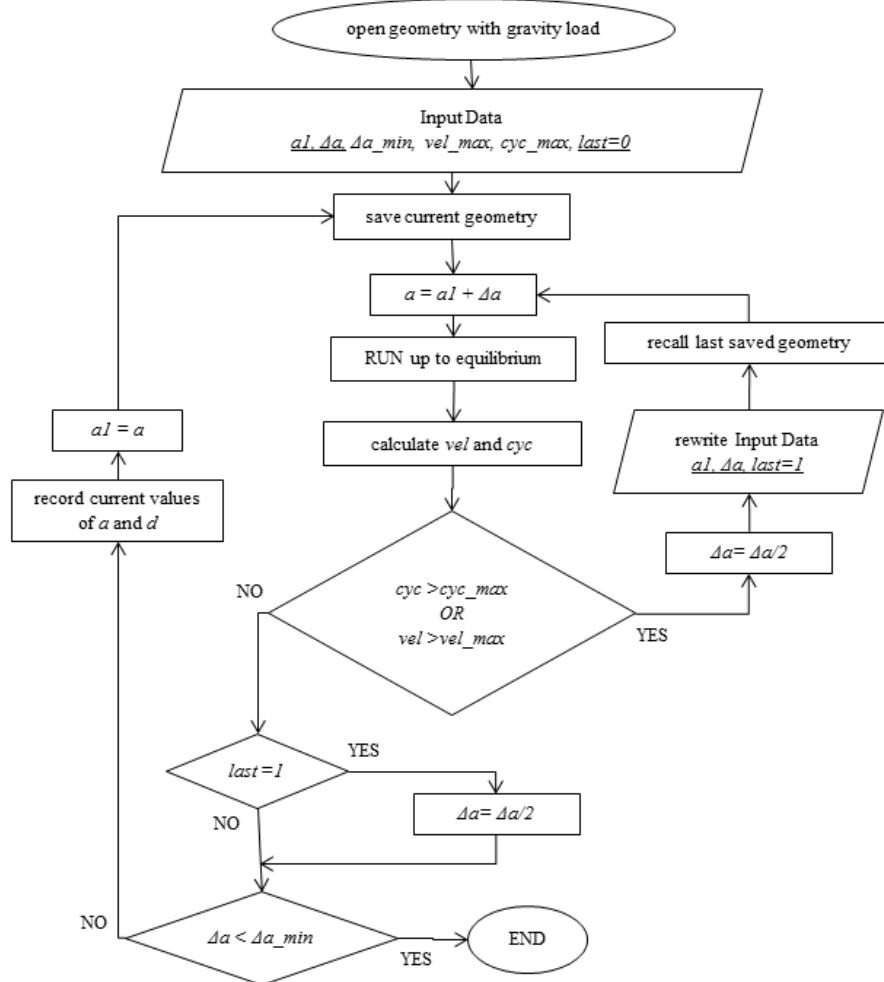


Figure 3.13 Flowchart of the ascending branch

### 3.4.2 Descending branch of pushover curve

The second part of the pushover analysis continues modulating the structure by the action of horizontal loading, which destined to create an imbalance condition and advance structure towards its collapse. Two algorithms for obtaining the descending curve have been developed based on different approaches. The main difference is in the way of determining a value of acceleration applied during the analysis:

algorithm#1 - a constant slightly higher acceleration than was in the maximum strength condition,

algorithm#2 – variable values of acceleration depending on the total base shear of the system.

The descending branch of the pushover curve starts from the found point of the last static equilibrium ( $d_0, a_0$ ) and continues up to the point of the last mechanical equilibrium ( $d_u, a_u$ ) that is schematically demonstrated in the Figure 3.14.

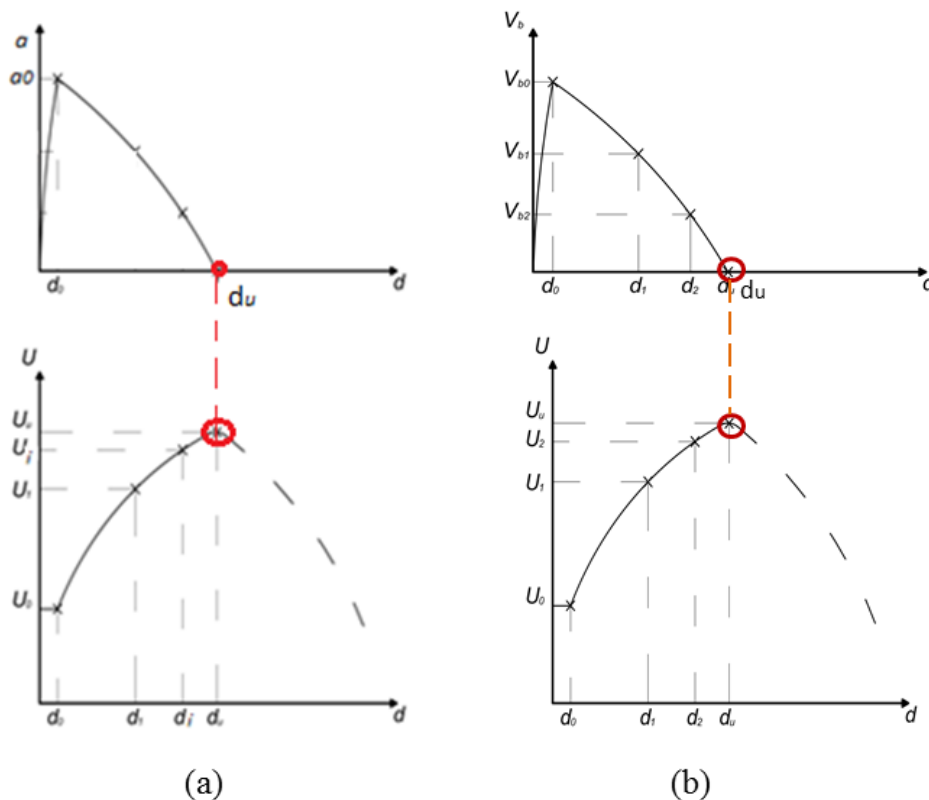


**Figure 3.14 Schematic representation of descending branch with graph of potential energy, respectively, a) procedure#1 and b) procedure#2**

Both algorithms are based on the theory of mechanical equilibrium, and it is gain to find an ultimate displacement which corresponds to unstable configuration of the system. It means that the system has zero value of base shear, and that with addition of any arbitrary small loads the system will no longer be able to return to its initial equilibrium configuration. An important property of unstable mechanical equilibrium is that the function of potential energy of the system stays at its local maximum. A small displacement away from that position results in a decrease in potential energy and a tendency to move farther away from the equilibrium towards

a failure. In this way, the routines continue calculation's cycles until the extremum of potential energy is defined, that corresponds to the ultimate displacement  $d_u$  of the structure (Figure 3.15).

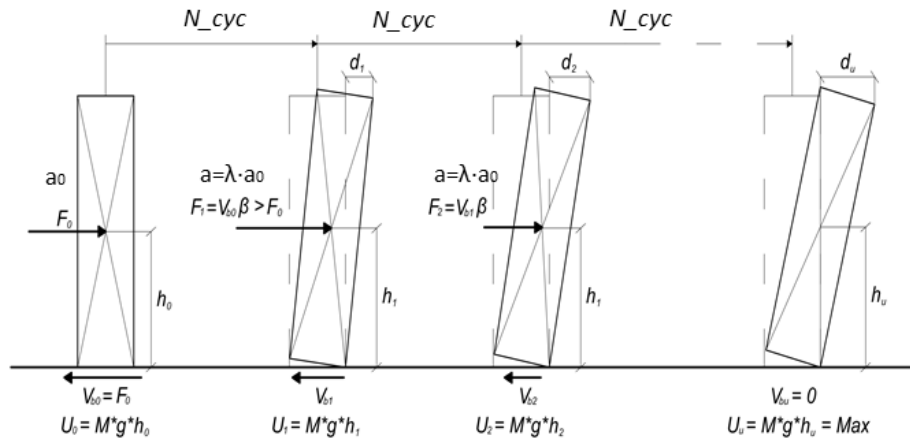


**Figure 3.15 Schematic representation of the mechanism of descending branch**

Both developed procedures for descending branch are explained in details below with their further verification.

### 3.4.2.1 Detailed algorithm#1

The algorithm starts from the last saved model geometry, when the system stays in the last static equilibrium point. The analysis is performed under a constant value of an external horizontal acceleration  $a$  that is enough to initiate a failure mechanism. Hereby, after a calculation step, containing a predetermined number of calculation cycles  $N_{cyc}$ , the value of potential energy of the system  $U_1$  is obtained and compare with initial potential energy  $U_0$ , which was defined at the last equilibrium point. If new value of potential energy is higher than the previous one  $U_1 > U_0$  the running will continue and the next values of energy will be compared again. In this way, the calculation proceeds until the current value of system's potential energy is less than one during the previous step, which is a main convergence criterion of the algorithm. Detailed list of input data and steps of the algorithm#1 are presented below together with a flow chart, which is illustrated in the Figure 3.16.

A UDEC built-in damping for static analysis called '*local*' was used, which has been reviewed earlier in the Chapter.

---

#### INPUT DATA

$a_0$  – the maximum bearing acceleration, obtained from the first half of the pushover routine,

$\lambda$ – acceleration multiplier to create an unbalanced condition

(i.e.  $\lambda = 1.4$ ),

$N_{cyc}$  – number of cycles during one calculation step, enough to provide a modest shift of the system (i.e.  $N_{cyc} = 1 \cdot 10^4$ )

#### LIST OF STEPS

1. Entering the input parameters with the model in the last static equilibrium state
2. Calculating the initial value of the potential energy of the system  
 $P_{ini} = \sum m_i g h_i$
3. Application to the structure of a horizontal acceleration value equal to  $a = \lambda \cdot a_0$  during  $N_{cyc}$  cycles
4. Calculating of potential energy of the system after applying the acceleration  $a$  during cycling run  $P = \sum m_j g h_j$
5. Controlling  $P < P_{ini}$ – if YES record the current values of displacement  $d$  and proceed to the end, if NO proceed to the next step
6. Updating the value of initial potential energy  $P = P_{ini}$  and go back to step#4

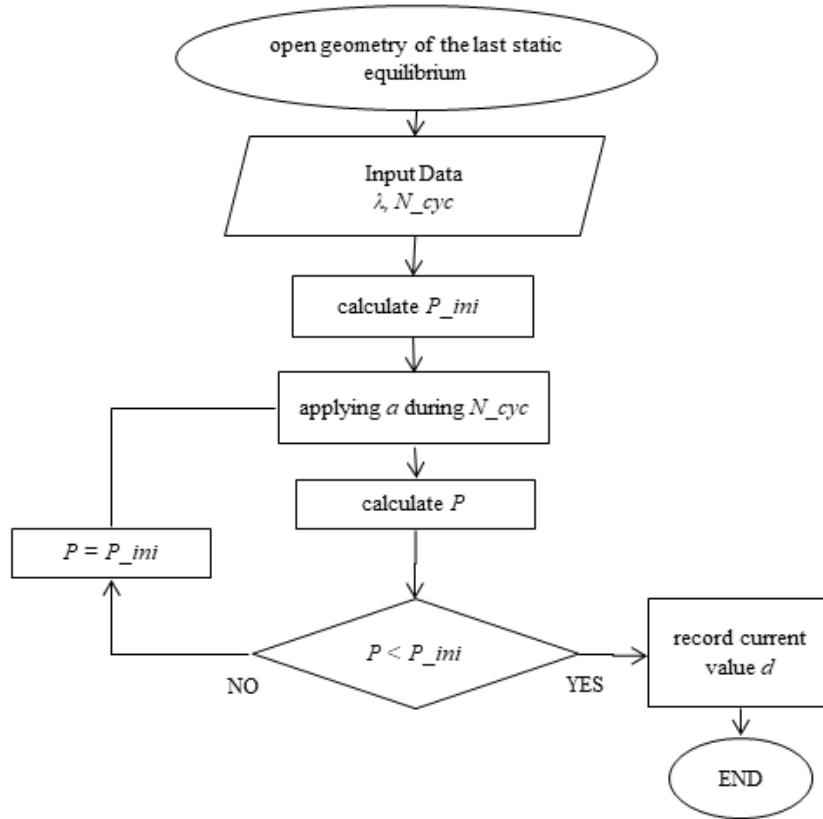


Figure 3.16 Flow chart of the algorithm#1

### 3.4.2.2 Detailed algorithm#2

The algorithm initiates from the last saved geometry after ascending branch was obtained. The analysis progresses by applying variations of acceleration, but it is more useful to represent the curve and the algorithm in the force-displacement plane. In the initial condition, the shear base  $Vb_0$  is recorded and a slightly higher load  $F_1 = \beta \cdot Vb_0$  is applied to create an imbalance condition that begins to advance the structure towards collapse. After a predetermined number of calculation cycles  $N_{cyc}$ , the base shear is recorded again, which value would rationally decrease ( $Vb_1 < Vb_0$ ) as the structure is no longer in elastic phase and the base joint is opening progressively decreasing its resistance. At this point, the applied load is updated with its proportional reduction  $F_2 = \beta \cdot Vb_1$  and the calculation proceed as described until meeting the convergence

criterion. Hereby, the base shear of the structure ( $Vb_i$ ) is recorded at every calculation step and next applying load is equal to  $F_i = \beta \cdot Vb_{i-1}$ . This condition of imbalance allows tracing the entire push-over curve, "accompanying" the structure to the collapse condition. The ultimate displacement  $du$  of the system is defined at the last calculation step, when the structure no longer has any resistance reserve ( $Vbu = 0$ ).

From other side, observing a trend of potential energy can also provide useful information to determine the collapse condition: as soon as rotation begins, energy starts growing and reaches its maximum at the ultimate equilibrium state.

An UDEC built-in damping for static analysis was used called 'auto' that have been reviewed in details earlier in the Chapter.

#### INPUT DATA

$\beta$  – ratio of the external forces  $F_i$  applied to the structure to the total base shear  $Vb_i$  (i.e.  $\beta = 1.02$ )

$N_{cyc}$  – number of cycles for one calculation step, during which forces maintained constant (i.e.  $N_{cyc} = 5 \cdot 10^3$ )

$Vb_{tol}$  – tolerance of the base shear (i.e.  $Vb_{tol} < 0$ ).

#### LIST OF STEPS

1. Entering the input parameters with the model in the last static equilibrium state
2. Calculating the mass  $M$  of the system
3. Calculating the base shear  $Vb_i$  and the potential energy  $P_i$
4. Controlling  $Vb_i > Vb_{tol}$ , if YES record the current values of displacement  $d$ ,  $Vb_i$ ,  $P_i$  and proceed to the next step, if NO proceed to the end
5. Application to the structure of a horizontal acceleration value equal to  $a_i = \beta \cdot \frac{Vb_i}{M}$  during  $N_{cyc}$  cycles
6. Proceed to the step#3

The parameters that influence the trend of the descending branch are  $\beta$  and  $N_{cyc}$ , analysis on their sensitivity is performed further in the verification part. A flow chart of the algorithm#2 is illustrated in the Figure 3.17.

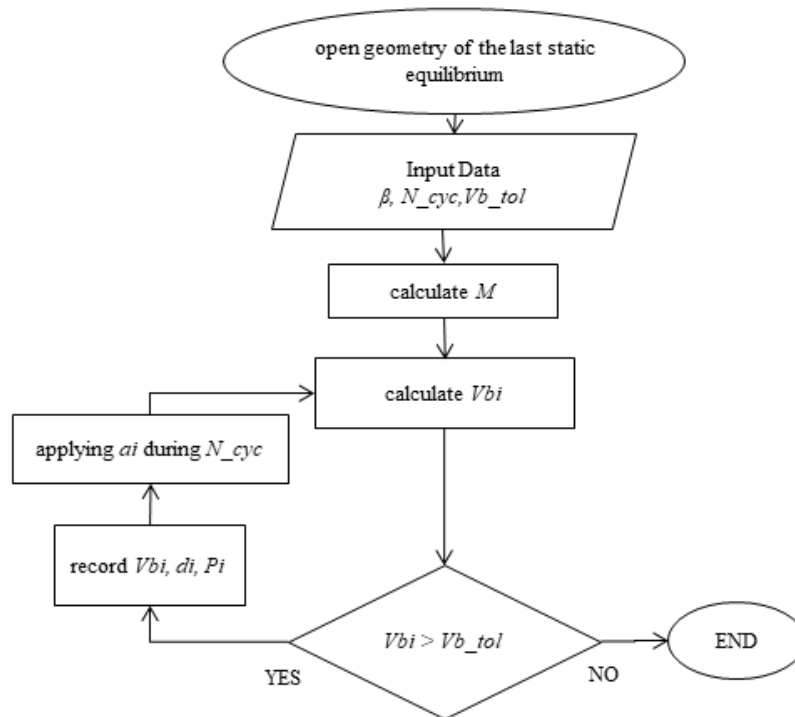
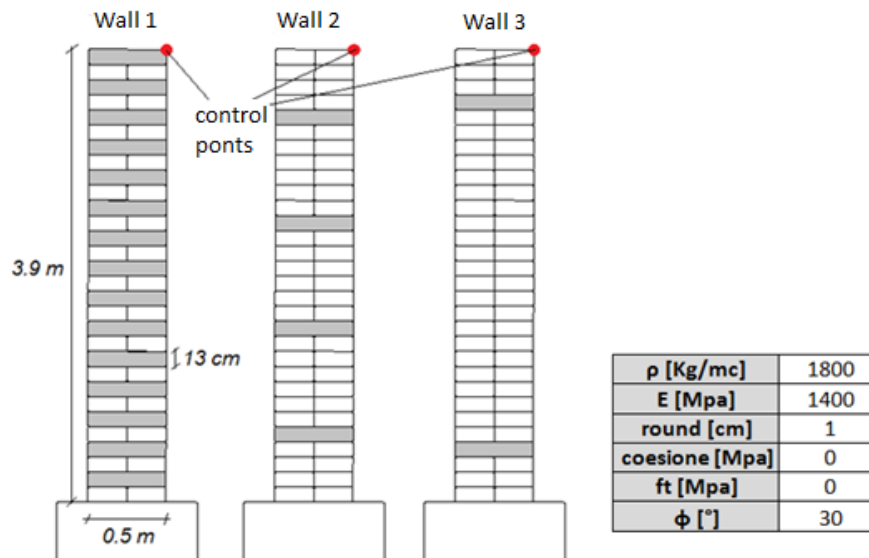


Figure 3.17 Flow chart of the algorithm#2

### 3.4.3 Verification of the procedure

In order to validate the procedure and check its dependents on the input parameters several analyses on simple structures have been performed and compared with the published result (de Felice 2011). Three configurations of simple standing 2-leaves walls was chosen, which have different number of headers and their positions along the height of the walls. The geometry as well as the mechanical properties was considered similar as in the literature and illustrated in the Figure 3.18.



**Figure 3.18** The adapted geometry and mechanical properties of the simple walls

A number of analyses have been performed in order to identify sensitivity of the implemented pushover procedures on the input parameters. For the ascending branch both routines demonstrated stable results not depending on the input data. The only suggestion could be to keep velocity tolerance  $vel\_max$  and initial acceleration increment  $\Delta a$  small enough in order to satisfy 'static' character of the analysis. However, the initial value of  $\Delta a$  is suggested to be not less than 0.05 m/s otherwise the algorithm is not able to proceed, since the mechanism could not be activated yet.

Nevertheless, the second part of both routines demonstrated some dependence on the input data, most likely due to more 'dynamic' character of the algorithms.

The influence of the acceleration multiplier  $\lambda$  and number of running cycles step  $N\_cyc$  on the algorithm#1 was performed and the results are the following. The graphs shown in the Figure 3.19 demonstrate that the values of  $\lambda$  from 1.05 to 1.6 had moderate influence on the result displacement, with less scattered results for  $\lambda < 1.6$ . From other side, the  $N\_cyc$  parameter provided good convergence of the analysis with its value of about  $10e4$ . Oppositely, the lower number of cycles did not provide any displacement, since the value was not sufficient to shift the system. While, the number of cycles greater than  $1.5e4$  overloaded structure during calculation step and brought it to immediate collapse. Thus, in



order to provide appropriate results the values of acceleration multiplier and of cycle numbers are kept, respectively, 1.4 and  $10^4$  for most analyses.

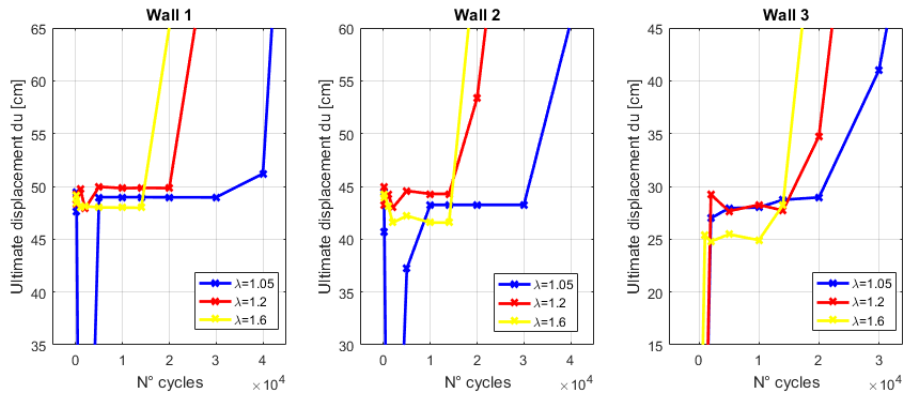


Figure 3.19 Influence of input data on the algorithm#1 results

Similarly, influence of the input data  $N_{cyc}$  and  $\beta$  on the algorithm#2 was investigated and results are illustrated in the Figure 3.20. It is notable that results obtained for the first two walls had a very good correlation, while the results of the wall 3 had a very scattered character independently on values of  $N_{cyc}$  or  $\beta$ . It was identified that the algorithm#2 worked well with 'simple' systems when failure appeared mainly in the base joint, how it happened in cases of wall 1 and 2 (Figure 3.21). Though, in case of more 'complex' failure happening not only along the base joint (wall 3) or in case of more complex geometry of entire system (will be identified in the Chapter 6) the algorithm#2 delivered inappropriate results.

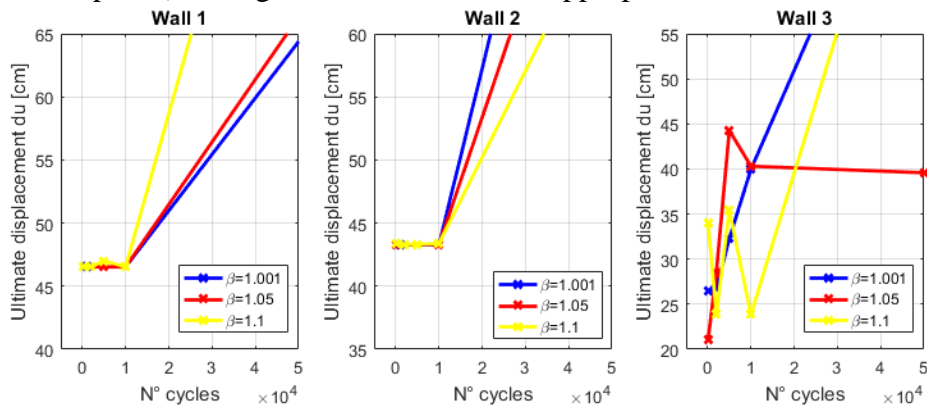
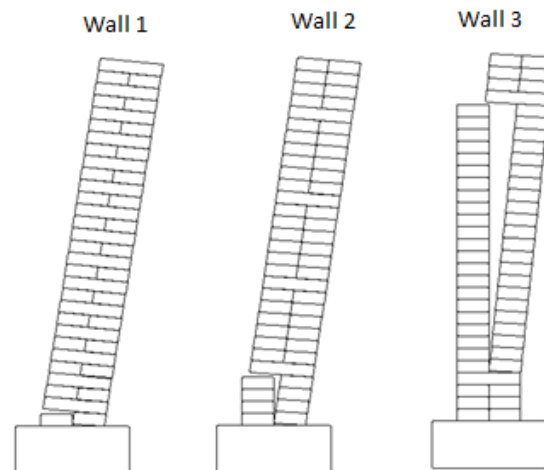


Figure 3.20 Influence of input data on the algorithm#2 results

In general, results of the implemented pushover routine are potentially stable and provide good correlation especially for ascending branch of the capacity curve, independently on the input parameters. The input data for proceeding second part of the pushover routine should be employed according to the presented sensitivity analysis.



**Figure 3.21 Failure mechanisms of 3 simple walls**

In this connection, further analysis presented in present dissertation will be performed using algorithm#1 as the one demonstrated more stable and reliable average results. Application of the implemented routine will be presented on several case studies in the further chapters together with discussion of its applicability.

### **3.5 New implemented routine for step pulse analysis**

The implemented pulse analysis is based on the application of horizontal acceleration to centroids of every block of the system during a short time period. The procedure is gained to define maximum pulse parameters that structure could withstand. The analysis by its nature is dynamic analysis, where response of the system depends on time parameter. The function implying character of applying load may be either step or harmonic pulse. However step pulse is more representative for simulating seismic action, since it incarnates a single 'spy' at the real time history accelerogram. The implemented algorithm performed without using any artificial damping parameters, as a pulse signal has instantaneous character and viscous damping usually does not contribute significantly (Chopra 2012).

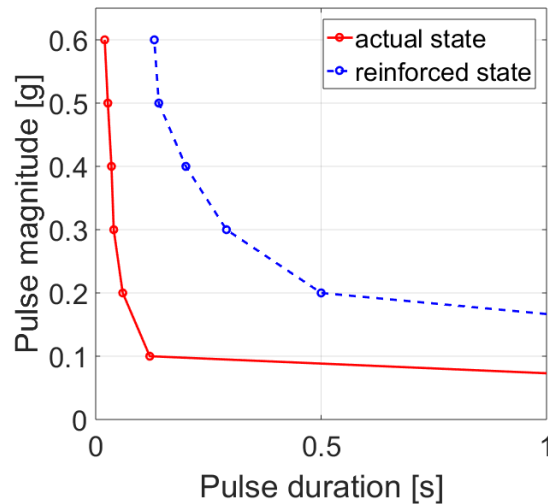


**Figure 3.22 Example of representative failure domain of the systems**

The results of the implemented pulse analysis may be delivered in a form of representative failure domain of the system. As an example on the Figure 3.22 are illustrated 2 failure domains of the systems with different seismic capacity. It is demonstrable that the dashed line refers to the more resistant system than the red one, since it can withstand similar values of magnitude corresponding to the higher values of the pulse duration.

### 3.5.1 Detailed algorithm

The algorithm is based on the controlling response of the system at each pulse parameter. The main pulse parameters are its magnitude and duration. For example, with a certain magnitude value the routine applies continuously various time durations of the load. As soon as it meets a convergence criterion, the value of magnitude and respective maximum duration is stored and the algorithm restarts with a next value of magnitude. As a convergence criterion the maximum displacement of a demonstrative control point, which foreruns the failure, is chosen. A detailed representation of the phenomena is illustrated in the Figure 3.23.

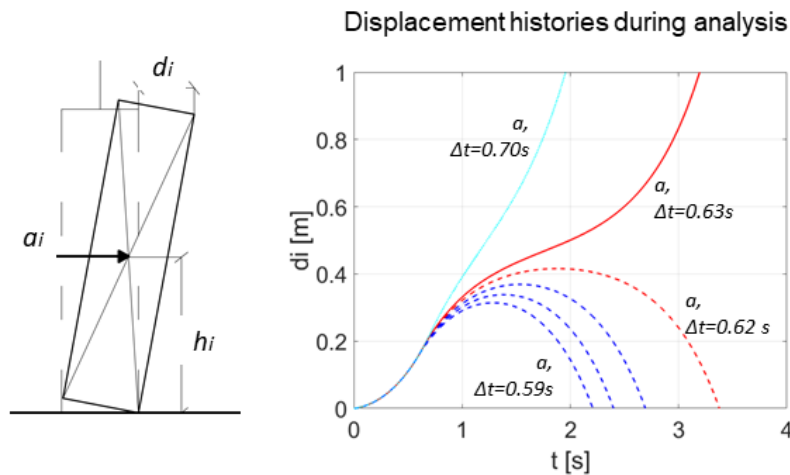


**Figure 3.23 Schematic representation of the pulse loading and corresponding responses**

A detailed routine destined for defining an ultimate response of a rigid blocks system under certain pulse magnitude is presented below.

#### INPUT DATA

$a$  – initial pulse magnitude (i.e.  $a = 1 \text{ m/s}$ ),

$a_{max}$  – maximum tolerance of pulse magnitude (i.e.  $a_{max} = 10 \text{ m/s}$ ),

$\Delta a$  – increment of pulse magnitude (i.e.  $\Delta a = 1 \text{ m/s}$ ),

$time$  – initial pulse duration (i.e.  $time = 0 \text{ s}$ ),

$time_{max}$  – maximum tolerance of pulse duration (i.e.  $time_{max} = 1 \text{ s}$ ),

$\Delta t$  – time increment of pulse duration (i.e.  $\Delta t = 0.01 \text{ s}$ ),

$T_{cyc}$  – running time during one calculation step (i.e.  $T_{cyc} = 0.3 \text{ s}$ )  
enough to provide a modest shift of the system

$mm_{max}$  - maximum number of calculation steps (i.e.  $mm_{max} = 10$ )

$d_{max}$  - maximum tolerance of ultimate displacement of the system (i.e.  $d_{max} = 0.5 \text{ m}$ ),

#### LIST OF STEPS

1. Entering the input parameters with the model under gravity loads
2. Calculating current duration of the pulse  $time = time + \Delta t$
3. Controlling  $time > time_{max}$  – if YES proceed to the step#11, if NO proceed to the next step

4. Controlling  $a > a_{max}$  – if YES proceed to the end , if NO proceed to the next step
5. Application to the structure of a current pulse magnitude equal to  $a$  and
6. Introducing iteration counter  $mm = 0$
7. Executing the ‘cycle’ command – running the model only under gravity load during  $T_{cyc}$  sec and updating the iteration counter  $mm = mm + 1$
8. Controlling  $d > d_{max}$  – if YES proceed to the step#11, if NO proceed to the next step
9. Controlling  $mm > mm_{max}$  – if YES proceed to the next step, if NO proceed to the step#7
10. Rewrite Input Data with the current value of time, recall the initial geometry and proceed to the step#2
11. Restore current values of  $a$  and  $time$
12. Update the values  $a = a + \Delta a$  ,  $time = 0$
13. Rewrite Input Data with the updated value of  $a$  and  $time$ , recall the initial geometry and proceed to the step#2

The analysis is performed under various values of magnitude and duration of pulse signal. The calculation under a certain pulse magnitude is proceeding until it meets a main convergence criterion, when the current value of displacement of the system is greater than the tolerance. Displacement of a representative control point is controlled right after pulse load applied, when the system stays only under gravity load. The time, during which the displacement is monitored, is user controlled parameter and equal to  $(T_{cyc}) \cdot (mm_{max})$ .

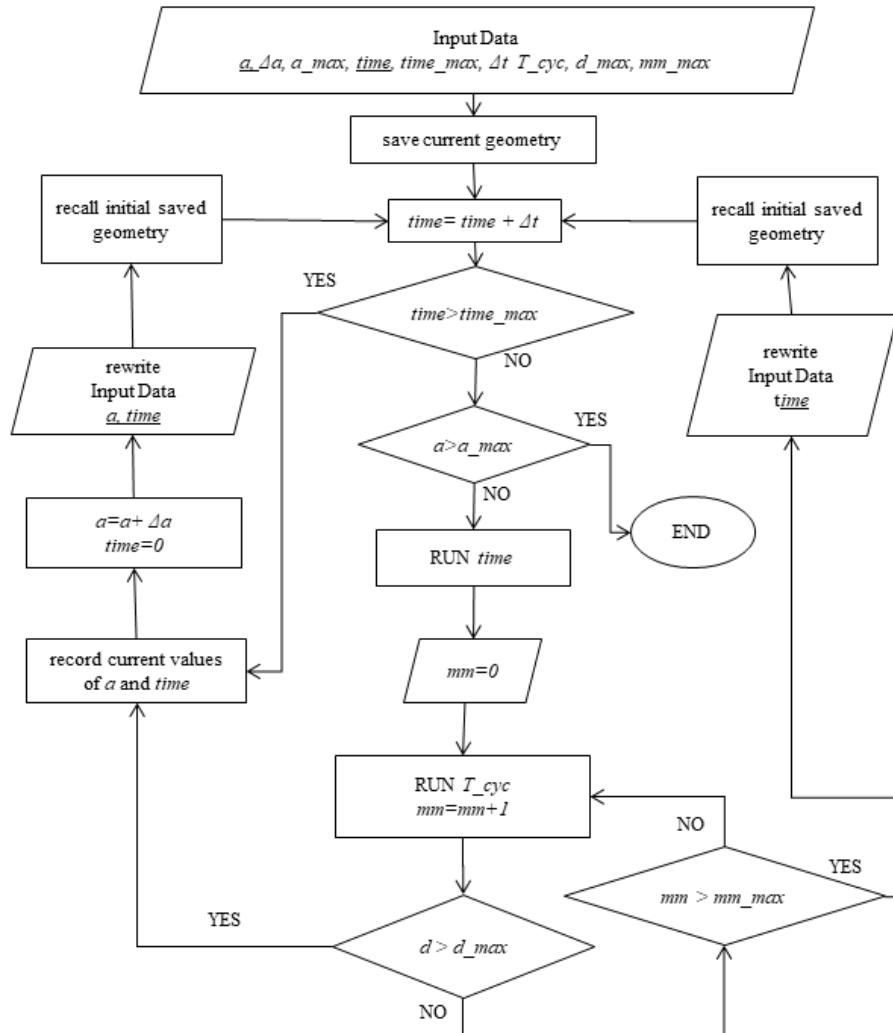


Figure 3.24 Flow chart of the implemented pulse analysis

### 3.5.2 Verification of the procedure

The value of input data depends on the nature and size of the system, some sensitivity analysis on that parameters may be needed before starting main pulse analysis. Especially, it is important to be aware of the possible ultimate displacement value  $d_{max}$  in order to obtain appropriate results. Similarly, the choice of the running 'after' pulse time  $T_{cyc}$  can be changing depending on the structure and the required accuracy of the

analysis. However, during verification of the algorithm it was noted that for majority of the analyzed simple and complex systems the running time  $T_{cyc}$  up to 5 sec with time step  $\Delta t$  0.1-0.2 sec was sufficient to catch the structural collapse precisely. Thereby, these values of the input data were used for all performed analysis in the present dissertation using pushover results as starting value for the  $d_{max}$ .

### **3.6 Seismic analysis**

The dynamic calculation in UDEC is based on the explicit finite difference scheme as discussed earlier, but in order to solve the full equation of motion the real rigid-block masses are used rather than scaled ones as for static analysis. Consequently, the time step of the calculation algorithm becomes rather various for dynamic analysis.

Seismic analysis is performed by applying a ground velocity time history on the base block of the model. The base block in this case is represented by deformable block, while the rest of the model may consist of only rigid blocks. Dynamic input is usually applied to the boundary of deformable block with a history function that is expressed in form of a harmonic function or a time history record. Subsequently, dynamic input can be applied in  $x$  and  $y$  directions corresponding to the  $x,y$  axis of the model. The applying signal, time history record, could be defined by integrating of a real accelerogram of the past earthquake or rather of an artificial accelerogram. The signal can be easily scaled in UDEC, thus providing a possibility of critical study different levels of PGA magnitude.

One of the main issues connected with the dynamic analysis is the choice of the appropriate damping.

#### **3.6.1 Damping calibration**

Rayleigh damping is originally used in the structural analyses to damp the natural oscillation modes of the system. A damping matrix  $C$  is used with components proportional to the mass ( $M$ ) and stiffness ( $K$ ) matrices

$$C = \alpha M + \beta K \tag{3.21}$$

where  $\alpha$  and  $\beta$ — respectively, mass and stiffness proportional damping constants.

The mass-proportional term is analogous to a dashpot connecting each corner or gridpoint to “ground”, while the stiffness-proportional term is analogous to a dashpot connected across each zone (responding to the

strain rate). Although both terms are frequency-dependent, an approximately frequency-independent response can be obtained over a limited frequency range, with the appropriate choice of parameters.

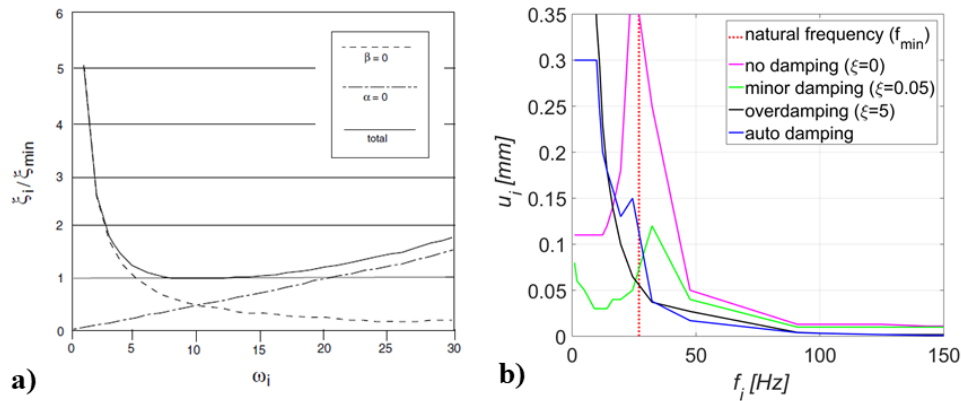


**Figure 3.25 Calibration of a) normalized critical damping ratio with angular frequency (Itasca 2011), b) damping parameters**

Rayleigh damping in UDEC is specified with the parameters  $f_{min}$  (central frequency) in Hertz and  $\xi_{min}$  representing the minimum of the variation of the normalized critical damping ratio with angular frequency (a), with mass and stiffness components only, and the sum of both components. As shown, mass-proportional damping is dominant at lower angular frequencies, while stiffness proportional damping dominates at higher angular frequencies. The curve representing the sum of both components reaches a minimum at

$$\begin{aligned}\xi_{min} &= (\alpha\beta)^{1/2} \\ \omega_{min} &= (\alpha/\beta)^{1/2}\end{aligned}\tag{3.22}$$

The final central frequency is defined as

$$f_{min} = \omega_{min}/2\pi\tag{3.23}$$

and is usually chosen to lie in the center of the range of frequencies present in the numerical simulation – either natural frequencies of the model or predominant input frequencies or a combination of both. Hysteretic damping is thereby in UDEC simulated in an approximate fashion. Thus the calibration of the damping parameters was performed on a simple structure represented by column, which geometry and



parameters were taken from the literature (Komodromos, Papaloizou, and Polycarpou 2008). A model composed of rigid blocks was analyzed under harmonic excitation using various parameters of signal frequency and amplitude. Maximum top displacement of the column before its failure was monitored and collected under various UDEC damping parameters. The analyses were performed with  $f_{min}$  equal to the natural frequency of the structure and with varied  $\xi_{min}$  in order to simulate damping combination from minor to considerable (b). It is interesting to note that the results demonstrated numerical stability with various parameters of the damping coefficients as well as without any viscous damping. The use of an appropriate damping value still is an open issue. Therefore, in the present dissertation, based on the above calibrations and following verification, all the dynamic analysis has been performed with zero value of Rayleigh damping, thus including only dissipation due to friction occurring in the contacts.

### **3.6.2 Verification of the procedure**

Finally, some comparisons with experimental tests, carried out in ENEA laboratory, are presented below as a verification of seismic analysis in UDEC (Meriggi et al. 2018).

#### **3.6.2.1 DE models**

The 2D models represent cross-sections of the out-of-plane loaded URM walls represented. The wall's models contained assembly of rigid blocks with horizontal joints and brick shaped unites for the regular wall and random shape units with inclined joints for the irregular wall, respectively. Both models limited by two blocks representing the top restrain and the shaking table. The dimensions of walls were about 3.4 m in height, 0.25 m in width and 1.5 m in length (Figure 3.26).

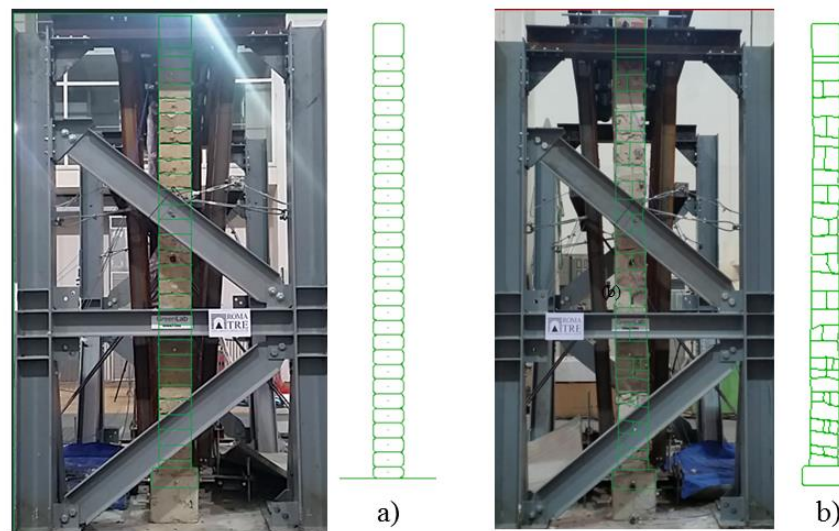


**Figure 3.26** UDEC models of the regular wall (a) and the irregular wall (b)

Since blocks representing the masonry units were modeled as rigid bodies, the deformability was allocated to the interfaces representing the mortar joints. The joint deformability was characterized by normal ( $k_n$ ) and shear ( $k_s$ ) stiffness. The normal behavior of the joints was considered elastic in compression with a limited strength in tension ( $f_t$ ). The sliding behavior of the joints was governed by an elastic-perfect plastic constitutive law, represented as usual with the Mohr-Coulomb yielding criteria characterized by cohesion ( $c$ ) and friction angle ( $\varphi$ ). In case of tensile or shear failure, both the cohesion and the tensile strength were set to zero, while the friction angle was set unchanged.

The average masonry mass density was estimated  $1200 \text{ kg/m}^3$  for the tuff wall and  $1600 \text{ kg/m}^3$  for the stone walls, while the mass density of the top masonry beam was estimated to be  $1800 \text{ kg/m}^3$  including additional vertical load. The final mass density of the model was computed by multiplying it by the wall length 1.5 m.

The mechanical parameters of the joints and materials adapted in the models are indicated in the Table 3.1.

**Table 3.1** Adapted mechanical parameters

Prototype (wall)	Block mass density [ $\text{kg/m}^3$ ]	Joint normal stiffness [ $\text{GPa/m}$ ]	Joint tangential stiffness [ $\text{GPa/m}$ ]	Joint friction angle [ $^\circ$ ]
Regular	1900	from 4.2 - to 0.5	from 2.1 - to 0.25	33
Irregular	3500	from 10 - to 3	from 5 - to 1.5	33

In the model, the dynamic input was applied at the base block, representing the shaking table, and at the top support block, representing the vertical restraint. The wall models were loaded in two steps: firstly, the gravity load was applied as vertical acceleration of  $9.81 \text{ m/s}^2$  together with additional vertical axial restraint on the top (600 kg) that was included into the mass density of the model top block. Secondly, the time domain dynamic analysis was performed, by applying velocity histories to the base block in vertical and horizontal directions and to the top block only by horizontal component, with allowing of its rotation. The signals were derived from the displacement time histories of the base recorded during the test campaign by an optical measurement system. Depending on the wall type, 100 and 75% scale factor of signals were utilized for the regular and irregular wall models, respectively. The measured PGAs range from 0.12 to 0.77g for the AMT (2016 Amatrice earthquake), NRC (1997 Umbria-Marche) and AQV (2009 L'Aquila earthquake) signals.

### **3.6.2.2 Results and comparisons**

The comparison between experimental and numerical results was performed based on relative displacement of the control points and lateral deformed shapes of the walls. The models demonstrated a complex nonlinear behavior with response depending on the geometry and properties of the blocks and stones. The level of viscous damping was various between the models to better match the experimental results, but in general its value was minor with only 0.2% and 0.5% damping coefficient for, respectively, AMT and NCR signals. Moreover all the analysis on irregular wall was performed without any additional damping.

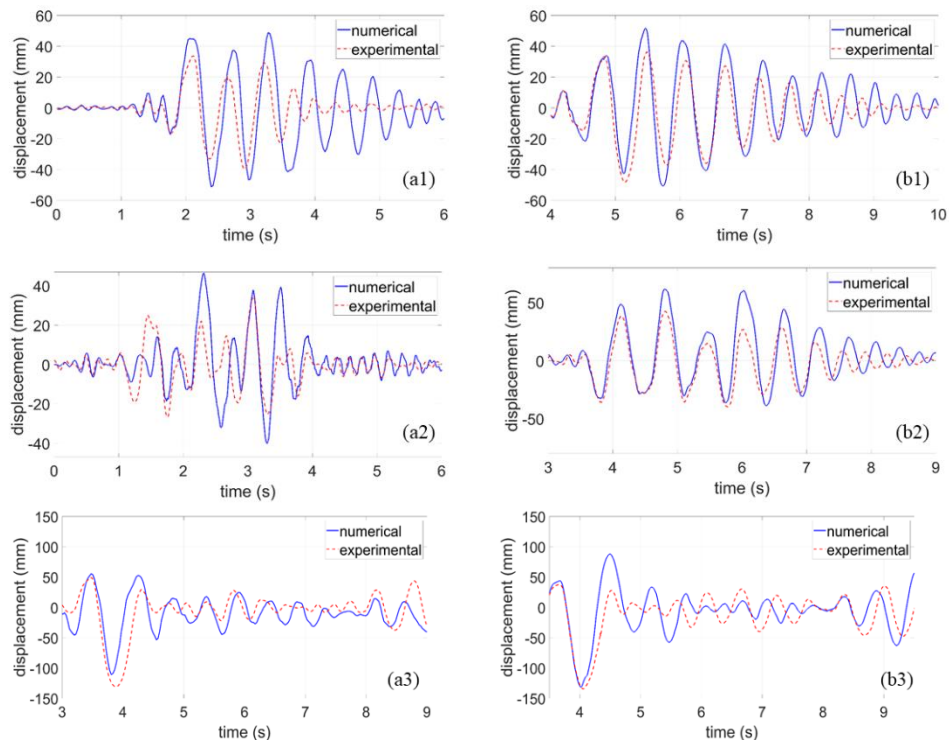


**Figure 3.27. Numerical and experimental comparison in terms of time history of the relative horizontal displacement at the control point on regular (a) and irregular (b) walls: AMT (a1,b1), NCR (a2,b2), AQP (a3,b3) signals.**

The displacement time histories of experimental and numerical results of the control point placed on the height of about 2.4 m from the base were performed (Figure 3.27). The following results demonstrated that the numerical models were able to represent the experimental results properly, especially for the high level signals (NRC, AQP), with error of the peak response value of about 20% for the regular wall and less than 5% for irregular one.

The experimental failure modes and the numerical maximum lateral shapes of the regular and irregular walls were also obtained demonstrating sufficient coincide of the both results (Figure 3.28). The average error of the maximum displacement was less than 10% with better catching of the mechanism for the strongest L'Aquila signal.

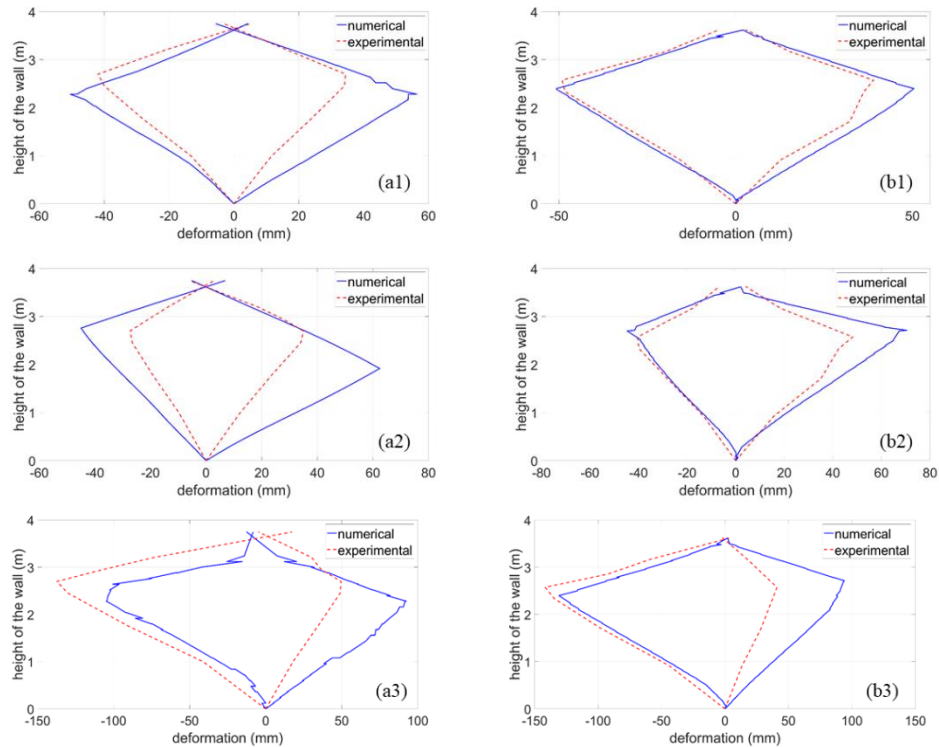


**Figure 3.28. Comparison between the numerical lateral shapes and the experimental failure modes of regular (a) and irregular (b) walls: AMT (a1,b1), NCR (a2,b2), AQV (a3,b3) signals.**

### 3.7 Summary

The first part of the chapter presents the fundamentals of the Discrete Element Method containing its main features that include blocks and contacts representation and contacts detection. Then corresponding formulations embodied in existing two-dimensional computer program UDEC are overviewed. Fundamental issues such as the mechanics of block interactions, the mechanical behavior of blocks and contacts and solution algorithms for the equations of motion are analyzed in detail. The most important features of the DEM relevant to the modeling of masonry structures with rigid blocks are emphasized.

The second part presents new implementations integrated to an existing DE code, which are intended to provide the analyses of masonry structures with representative and accurate results to ensure proper seismic assessment of masonry monuments with DEM. Firstly, an

algorithm with semi-automatic model creator is illustrated that aims to create DE model with realistic geometry and mechanical properties. Secondly, seismic analysis routines are developed and verified on simple walls in order to provide some insight of the implemented approaches and their sensibility on input parameters.

The first implemented routine is based on quasistatic approach when increments of horizontal acceleration are applied to each block in successive steps up to the failure of the structure. The results represent by capacity curve contained maximum bearing acceleration and ultimate displacement of the structure. Initially, it was proposed two independent algorithms that differed by the way to obtain the ultimate displacement. However, after some verification studies the only one algorithm was chosen for further analysis as demonstrated the most stable results. The second implemented routine is based on dynamic approach represented by step pulse analysis, when horizontal acceleration applied to every block of the structure during short period of time. The results represent in form of corresponding failure domain of the system obtained by collecting respective extreme parameters of pulse magnitude and duration. The last routine is based on seismic approach performed by applying time histories to the base block of the DE model. Main aspect of seismic approach is in calibrating of an appropriate damping solution for the analysis. The verification of dynamic analysis is performed by comparison numerical and experimental results, and finally, it was selected to use no additional viscous damping in dynamic analyses contained in the present dissertation.

## 4 Seismic assessment of the past damage on the south-east part of the Colosseum

### 4.1 Introduction

The Colosseum, probably, is the most famous example of the roman amphitheaters (Figure 4.1) that was built in the center of the ancient Rome by the Flavian dynasty (Parker 1876). Its construction was begun in 72 AD in a valley between Fagatal, Oppian, Velia and Palatine hills, precisely on a spot of the artificial lake (Figure 4.2), which previously was a part of the Neron palace. “The choice of this place helped to use the lake bed as ground for building the solid foundations of the construction and speed up the project without need of great excavation work “ (Manzione 1999). The construction took place 8 years without interruption and finished in 80 AD. It was the first stone amphitheater in Roman Empire providing seats for about 70000 spectators during almost 400 years. The last famous games were organized by Emperor Theodoric in 523 AD in an attempt to revive the ancient way of living. Built as the Flavian amphitheater, it had been named Colosseum at the Middle Ages, probably due to its colossal size or after the nearby statue of Colossus.

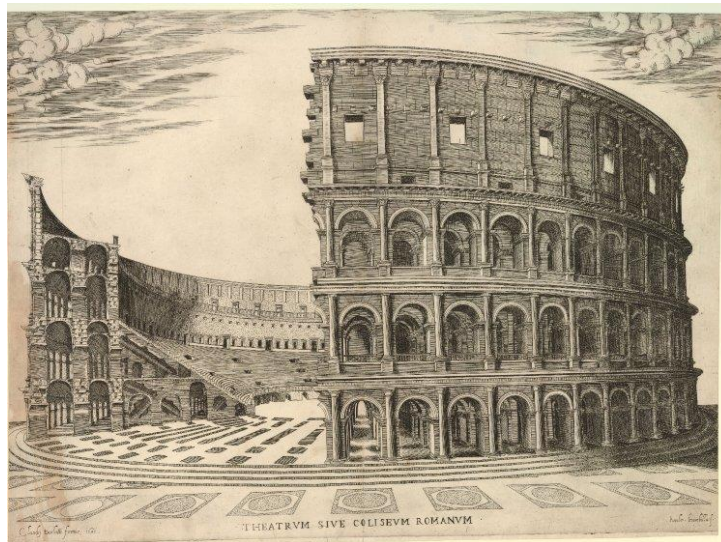


**Figure 4.1** A reconstruction of the Amphitheatre (by G. A. Brambilla, 1581)

The decrease of population at that time, the general state of decay of the amphitheater and the change in economic conditions were among the



primary causes leading to the abandonment of the building. After the last games the Colosseum became a shelter, a castle, a warehouse and a stone quarry. Only from 19<sup>th</sup> century the Colosseum was recognized with its symbolic and monumental value and the necessary work on its care and maintenance has begun and continued until now. However, there are still many questions from the past, such as what was the cause that brought the monument to its current condition? Until now there are several existing hypothesis on it, however none of them is confirmed as final.

- |   |                                   |
|---|-----------------------------------|
| 1 Piattaforma del Tempio del Divo Claudio | 9 Arco di Costantino              |
| 2 Circo Massimo                           | 10 Meta Sudans                    |
| 3 Mura «serviane»                         | 11 Nuova posizione del Colosso    |
| 4 Aqua Claudia                            | 12 Tempio di Venere e Roma        |
| 5 Terme di Traiano                        | 13 Domus Tiberiana                |
| 6 Terme di Tito                           | 14 Domus Flavia e Domus Augustana |
| 7 Ludus Magnus                            | 15 «Stadio»                       |
| 8 Anfiteatro Flavio                       | 16 Domus Severiana                |

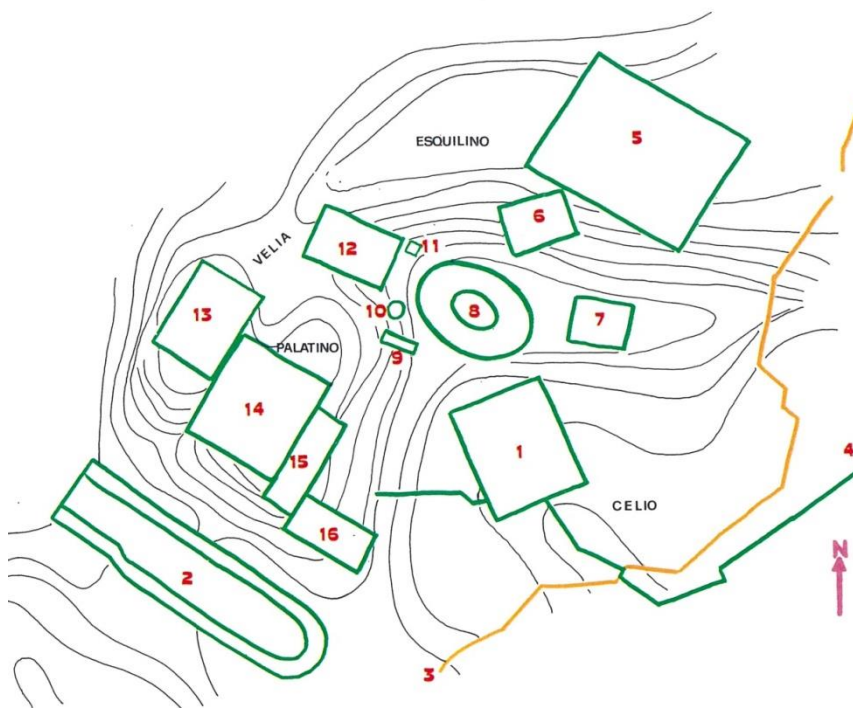


Figure 4.2 Plan of the valley of the Amphitheatre in IV century AD (De Luca 1985)

In this chapter, firstly, the structural and geometrical survey of the Colosseum will be overviewed. Followed by history of past damage and



respective restorations, together with the critical review of the recent studies on structural behavior of the monument. Finally, the numerical model and seismic analysis of the southern part of the Colosseum will be undertaken. One goal of the chapter is to evaluate the effective earthquake characteristics, happened in the beginning of 19th century, based on comparing of real and UDEC model structural damage. Another one is to investigate the chronology of the monument's interventions preceding the 19th century restorations and the influence on its vulnerability.

## **4.2 Geometry and Structural surveys**

Initially, Amphitheater Flavian contained 2 separate structures: substructures (underground chambers) and amphitheater itself, which were lying on separate foundations and which are in various proportions remained until our days (Figure 4.5). The whole structure of the amphitheater laid on a massive foundation, 12-13 meters high and 50 meters width, made from roman concrete mixed with rubble stones – *opus caementicium*. The foundation, which resembled a compact donut, filled up a part of Nero's lake (Figure 4.3). The underground structures, where activities connected to the preparation of the show took place, were not visible for the spectators and was covered with arena - wooden floor covered with sand. The substructure formed ellipse measured 76 by 44 meters along the major and minor axes, respectively, and its floor laid about 6.5 meter below the arena. The underground areas were on 2 levels connected by wooden stairs and bordered by a 2.8 meters thick brick retaining wall. The substructure was supplied with well-organized drainage system, which is still partly functioning.

The main structure of the Colosseum was an ellipse (Rosin and Trucco 2004), with a minor axis of 156 meters, oriented toward north-northeast and south-southwest, and a major axis of 188 meters. A series of radial masonry walls connected to concentric annular walls and by inclined concrete vaults creates concentric wedge cell. The exterior was composed of four levels, each corresponding to the four levels of the interior. All of the tiers of the interior together were called *cavea*, which were divided into horizontal seating areas of individual seats and every level belonged to defined social group. The different levels of the amphitheater were composed of concentric corridors descending in numbers from bottom to top and on the upper level stood the colonnaded portico. The building was about 48.5 meters high with four floors and contained 80 entrances, also

separated by the social groups, with 2 vestibules at the ends of the minor axis.

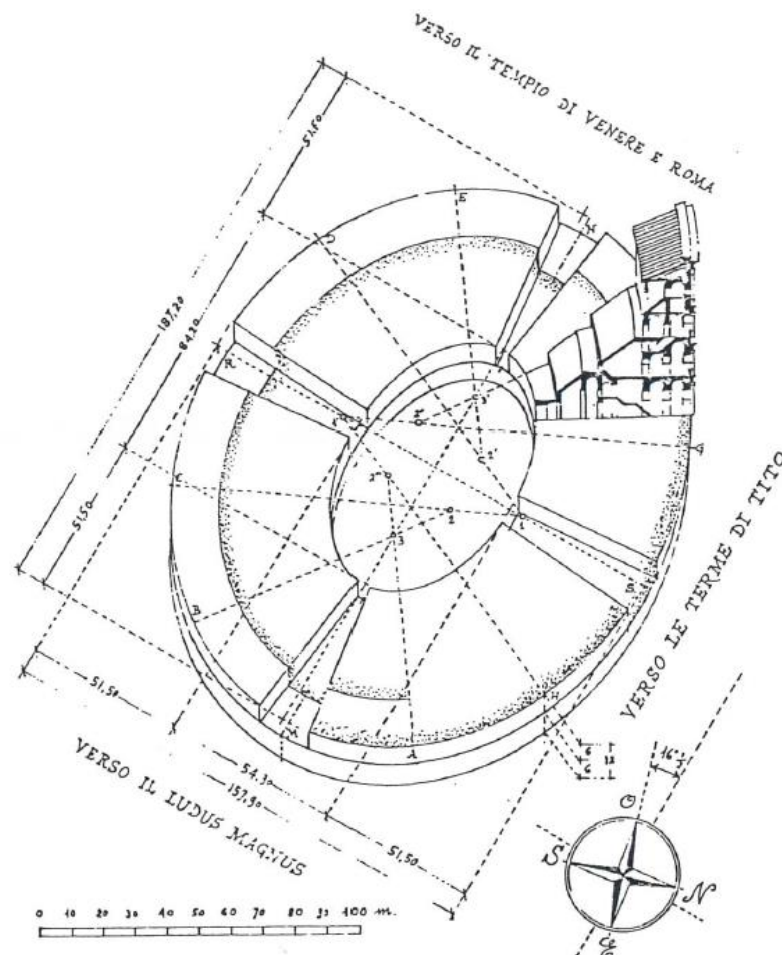


**Figure 4.3 Plan of the foundation and cross section (De Luca 1985)**

The first three exterior walls were each composed of 80 arches, with openings 4.2 meters high, set upon pillars with semi columns about 2.7 meters wide (Figure 4.1). The height of the first level's arches was 7 meters, while the second- and the third-level varied around 6.5 meters. The arches typically consist of 9 or 11 varying in size voussoirs with a keystone at the very top. The fourth level, the attic, was constituted by a full wall in which pilasters placed on very high, jutting pedestals divided 80 panels with 40 windows spaced at regular intervals.

The materials used at the construction of the Colosseum are (Rea, Beste, and Lancaster 2002):

- Travertine – mainly at the structural elements (columns, arches and cornice, external face of the attic floor) that quarried from nearby Tivoli;
- Tuff – at all internal parts of the masonry as infill material;
- Masonry brick – in the upper part of the radial walls, in the arches which support the *ambulacrali* vaults, in the arena substructure. The brick employed is generally the *bipedales* type;
- Concrete - in the vaults that cover passage ways and in the inclined section of the *cavea*, in the vaults supporting the stairs and into the foundation bed. (Figure 4.4)

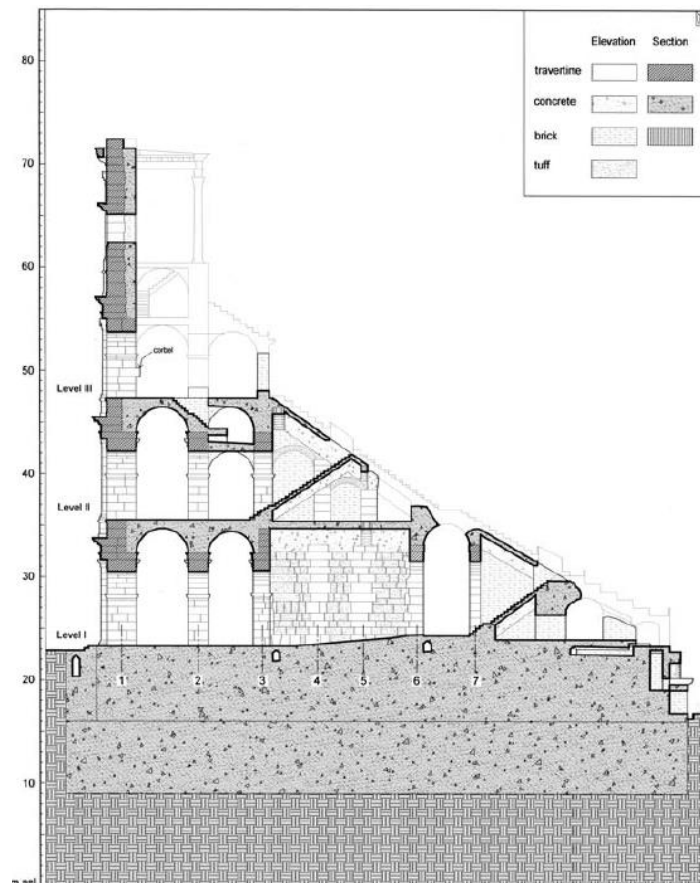


Figure 4.4 The cross section of the Colosseum with key for materials (Rea, Beste, and Lancaster 2002)

The entire restricted area around the amphitheater, about 17.5 meters wide, was paved with travertine blocks. Stone boundaries of the same material were placed around the external parameter at regular intervals, and five of them are still visible at the original setting. These stones were also used to fix the cover of the entire arena in case of rain or sun, with an enormous awning called *velarium*.

### 4.3 Past damage and restorations surveys

The current state of damage of the monument is the result of nearly 20 centuries of the Colosseum existence, during which it suffered various exceptional events that led to its weakening and partial collapse. The Figure 4.5 shows the plan of the first level of the amphitheater in its present state. The entire southern part of the monument, both the external and intermediate walls with all corresponding piers, had been destroyed, while the northern part of the monument remained in relatively good condition. There are several theories trying to explain the damage sources yet none of them are certainly defined, however they will be discussed further in the chapter. Firstly, let us follow the historical path of Colosseum with dating the damage and respective interventions, inquiring more about the south-east part of the monument.

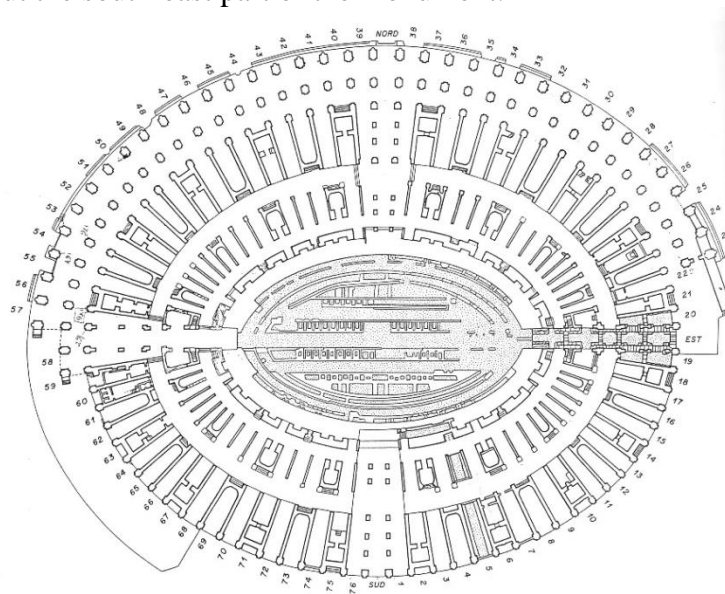


Figure 4.5 The current plan of the Colosseum (Coarelli and Gabucci 2001)

The list of the damage suffered by Colosseum since its construction is displayed in the Table 4.1. It is notable that the first serious damage and following reconstructions already happened at the time when the Colosseum was still used under its main activity (Croci 1995).

**Table 4.1 Damage suffered by Colosseum through the centuries** (Funicciello et al. 1995)

Year	Type of damage	Notes
138-161	Fire	Antonino Pio
217	Fire or lightning	Alessandro Severo/Macrinio
250	Fire	
443	Earthquake	Engraving still visible inside Colosseum
508	Earthquake	Damage to podium and arena; three engravings on reutilized marble stones, still visible inside (fig. 2)
615-618	Earthquake	Adeodato (uncertain account)
795-816	Earthquake	Leone III (uncertain account)
801	Earthquake	Reported by various sources
847	Earthquake	Pillars supporting the wooden ceiling of the upper arcade collapsed
1032-1048	Earthquake	Benedetto IX (uncertain account)
1073-1085	Earthquake	Gregorio VII (uncertain account)
1091?	Earthquake	Engraving in church of S. Maria in Trastevere
1231-1255	Earthquake	(uncertain account)
1332	Restoration	Bull hunt in honor of Frederick of Bavaria; at this time the monument is intact suggesting that previous damage had been mild or already repaired
1349	Earthquake	After several hystorical sources, arcades of southern external ring collapsed («cecidit aedificiarum veterum neglecta civibus, stupenda peregrinis moles»; Petrarca)
The amphitheater begins being demolished; according to various available documents, the peak of this activity dates to the XVII century. The structure of the Colosseum is weakened, such that in		
1703	Earthquake	Restorations begin in 1807 by Pope Pio VII. Before end of restorations three external arcades (second ring) collapsed
1812	Earthquake	Another arcade in the second ring collapsed

The most important restoration work from ancient times dates back to the Severan period after a great fire took place in 217 AD. At that time the building contained many wooden elements that burned out degrading and destroying metal clamps and stone blocks. Thus the timber was no longer used and changed for mainly stone elements. Later, in 5th century Rome was shaken by several earthquakes and the amphitheater suffered partial collapse, especially of the upper parts. The structure was not rebuilt properly and started to be used partially. Moreover, already during the next centuries the monument was used as a quarry for building materials with the first construction yards located in its southern side, while the northern part was never dismantled (Coarelli and Gabucci 2001). Additionally, the metal pins, which had been used to anchor the travertine

blocks one to another, were removed during the Middle Ages. Until now innumerable irregular holes are visible in the points of junction between the blocks, by some approximate calculation the quantity of metal (bronze, iron and lead) amounts to roughly 300 tons (Manziona 1999). All those weakening factors and others brought monument to its partial collapse that was already significantly noticeable in 12-13 century. According to the recent archeological finds during excavation works for the new metro line in Rome (Rea, Romano, and Valenzani 2017), it was possible to recreate a hypothetical appearance of the Colosseum during its use as a fortress by the Frangipane family (Figure 4.6). It gives an idea that the southern edge of external wall at that time could have been already in similar configuration with the current state. The next picture made in 16<sup>th</sup> century confirmed the possible use of Colosseum as the fortress (Figure 4.7), with the rests of additional walls and infilled arches that partially remained. Thereby, for many centuries the monument had been used not in appropriate way - as a fortress for the noble families, as a shelter for homeless, as a church, as wells as a store for nearby gun-powder factory.



**Figure 4.6** The hypothetic reconstruction of the Colosseum in 12-13<sup>th</sup> centuries  
(*Rea, Romano, and Valenzani 2017*)



**Figure 4.7 The state of the southern end of the external wall in 1570** (by Anonim in Fabriczy from (Frazzoni 2016))

The image of the southeast part of the Colosseum in 1700 demonstrated absolutely matching of the south-east wall edge with its present state (Figure 4.8). On the picture it is also notable the representative, still existed, vertical crack going through the middles of the extreme arches' row. It is also interesting that at that time the arches of the first level were partially grounded, while arcades of the second level were still filled-in with brick masonry, probably from the time of its use by the Frangipane family. Another picture made by Piranesi (Figure 4.9) confirms that the southern external wall in 1756 was at the same dimension as the present one having 16 arches left from the main northern entrance (marked 'A') as it is in our days. It is also seen that as that time the last 6 arches of the second level were still infilled with the bricks, while the lower arches were partly infilled with the ground. Obviously, the bricks infill had consolidated the south-east outer wall and prevented its progressive failure at this certain point. However, the structure had stability problems that demonstrated with the already visible vertical cracks along the extreme row of the wall.





Figure 4.8 The South-east part in 1700 (by Gaspar van Wittel)



Figure 4.9 The view on the southern external wall in 1756 (by Piranesi)



From the next available picture of the Colosseum it is notable that the arches of the second level had been freed by 1806 (Figure 4.10). Was it done as a part of the archeological works started on the monument at the beginning of 19<sup>th</sup> century, immediately with the start of the legislation of the cultural property in Italy? There is no a certain information about when the filled-in brick was removed, and if the illustrated timber shoring of the last 2 rows of the arches was built before or after 1806 earthquake, however the structure was in danger and required an immerge intervention.



**Figure 4.10** Timber shoring in the south-east wall in 1806-1807 (Uggeri 1809)

The reconstruction started in November 1806 with accepted project of Palazzi, Camporesi and Stern that contained construction of a masonry buttress on travertine base to consolidate the east wall. When the work started, the part of the Colosseum was found to be even in worse conditions than expected. The extreme pillar had serious cracks, which

were constantly opening. Thus, the first step was to provide a strong support of the wall against the thrust caused by detached elements (Figure 4.11). Then, the extreme 3 arches were walled-in in order to consolidate them internally, thus the extreme row of arches entered into the buttress that was built wider than the wall. On its base the brick buttress replaced 3 rows of the arches, and arrived to the top at an acute angle. Lastly, a cross wall was built to ensure further lateral support and to link all the external structural elements with the inner structures. This cross wall was built in imitation of the original radial arched walls. The entire intervention was made rapidly and took about 6 months. Finally, the idea of Stern was to finish up the brick works with the travertine in order to create an esthetic outcome of the intervention, which was never realized (Jokilehto 1986).

The image survey of the Stern intervention shows that the consolidation works stayed under unchanged condition since the work was completed in 1807 as illustrated in the Figure 4.12, Figure 4.13 and Figure 4.14. The only difference is the absence of the vegetation, which was cleaned out about 10 years after the intervention, in 1815.

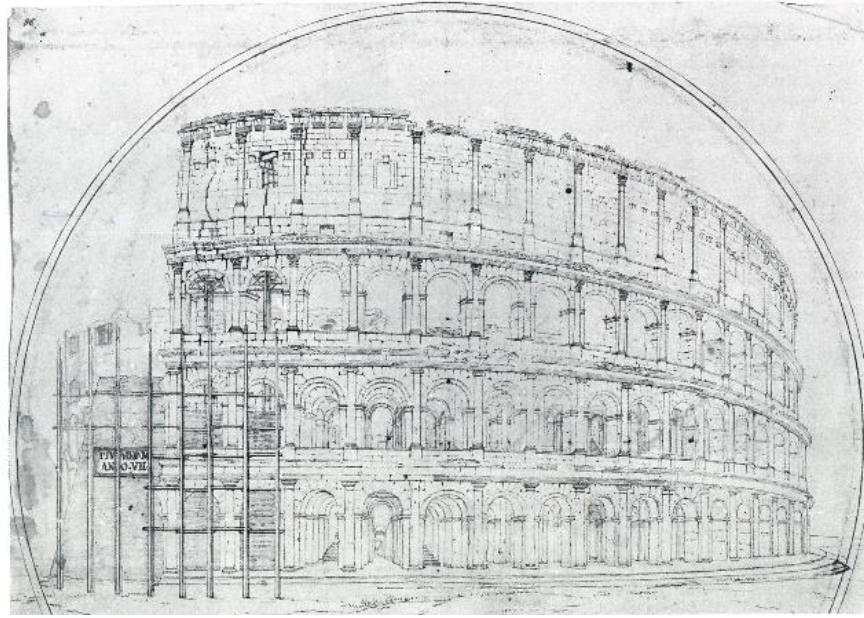


**Figure 4.11 Start of the restoration by Stern (Luciani 1990)**

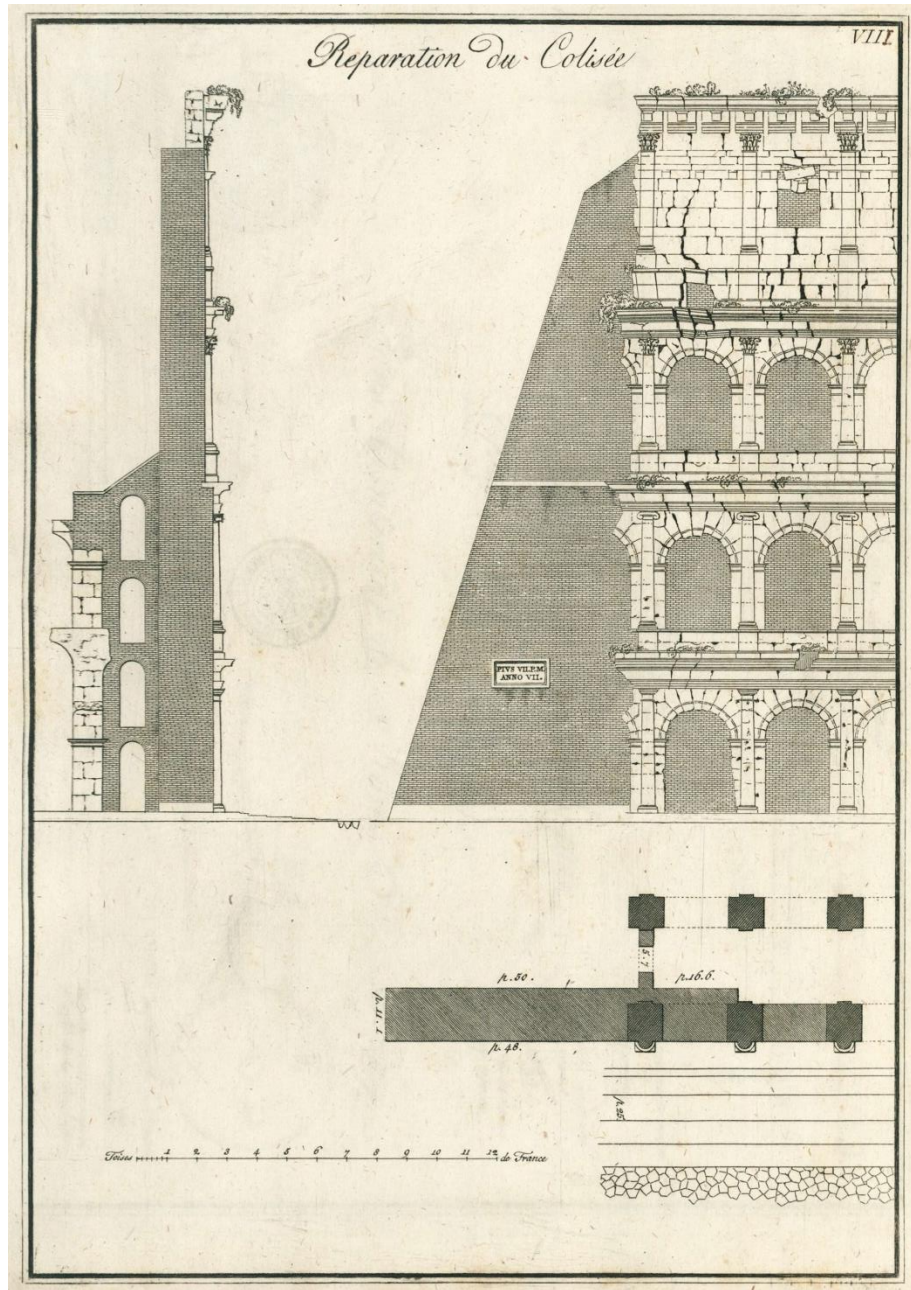


Figure 4.12 The restoration survey in 1814 (Uggeri 1814)



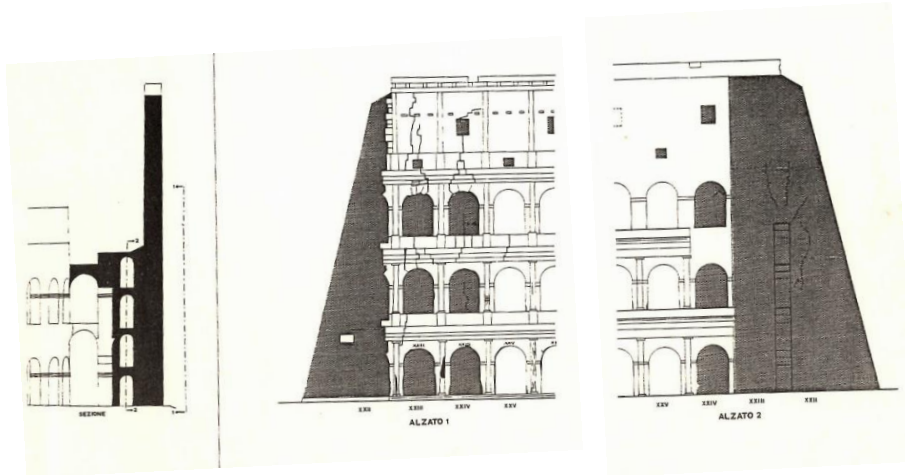


Figure 4.13 The restoration survey in 1990 (Croci 1990)

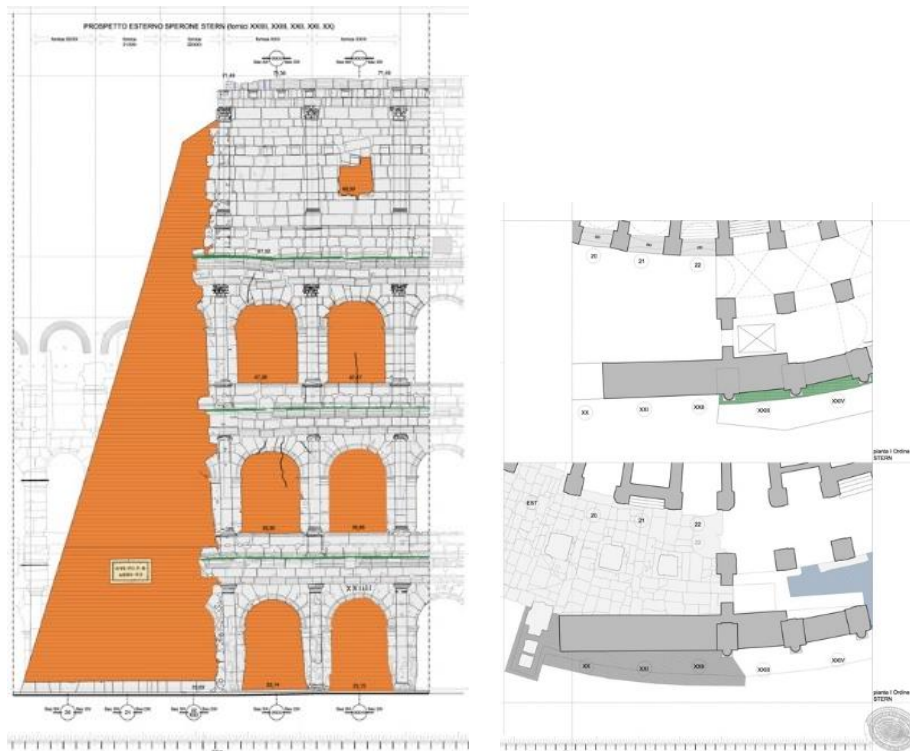
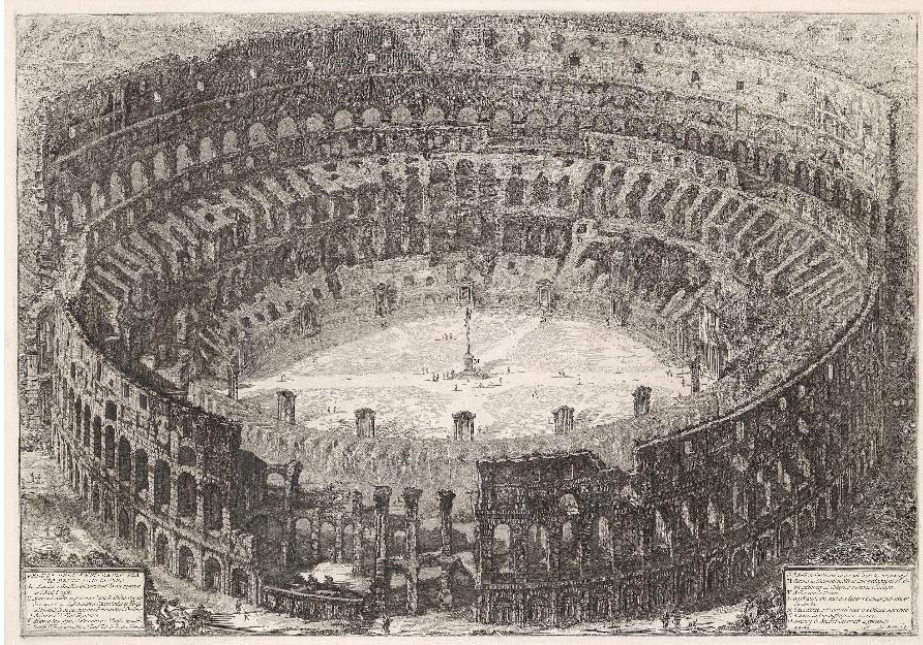
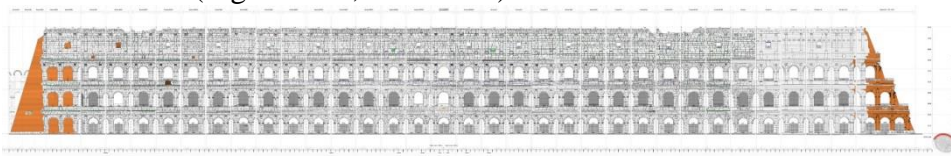


Figure 4.14 The current restoration survey ("Restauro Colosseo" 2017)



**Figure 4.15** The state of the Colosseum in 1776 before the 19<sup>th</sup> century restorations (by Piranesi)

Suchwise, as it was stated before more than half of outer ring of the Colosseum collapsed and the structure was in unstable condition (Figure 4.15). In this connection, at the beginning of the 19th century the conservation works began with two completely different approaches of restoration. The first buttress in 1806 was built by Stern, Camporesi and Palazzi on the southern end of outer ring and it tended to conserve even the smallest fragment of the monument as it was without any reconstruction (Figure 4.16, on the left).



**Figure 4.16** Prospect view of the facade after 19<sup>th</sup> century restorations (“Restauro Colosseo” 2017)

Almost twenty years later, Valadier constructed the second buttress at the northern end of Colosseum’s outer ring that was intended as a partial reconstruction of the monument. It’s involved rebuilding a part of the missing structure and forming a buttress. The work was partly made in

travertine - up to the first pillars, some part of arches and pillars, and the rest was made in brick covered with a patina to imitate travertine (Figure 4.16, on the right). Despite the works done, the external wall continued to rotate outwards and in 1850 Canina installed a triple order of chains corresponding to the 13 central arches (Figure 4.17). Some removing of the plants roots, consolidation with iron straps and works on the missing parts of the southern inner wall were also done. (Jokilehto 1986)

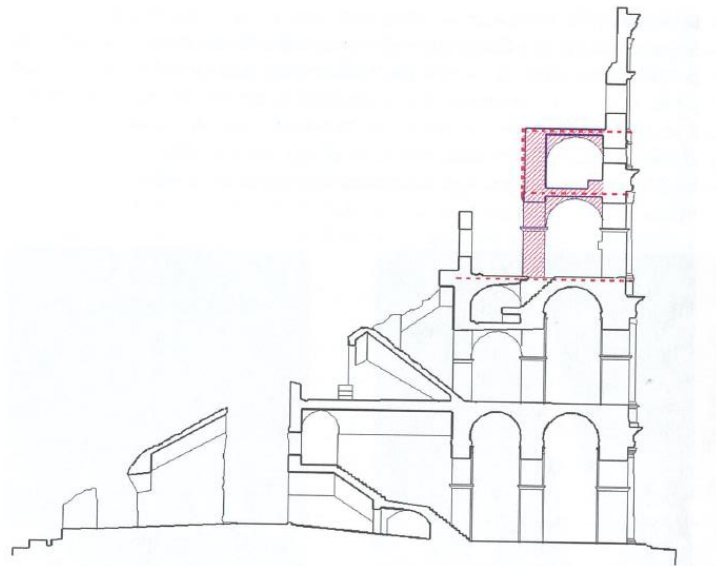


**Figure 4.17 Interventions by Canina** (Como 2013)

During the following decades, the conservation works were continued and contained reconstruction of the southern part with 8 rebuilt arches, restoration of the western entrance towards the Forum, and a partial rebuilding of the small area in travertine above the northern entrance. In first two cases, the new constructions were made in yellow brick, using travertine only in some structurally important parts. At this time, more iron straps were used to consolidate the structure as well as smaller iron crams for minor repairs. At the end of 19<sup>th</sup> century, the Colosseum was the object of numerous restorations. The most extensive one was in 1892, with the construction of some radial walls and their end pillars along 15 arches along the 3<sup>rd</sup> ring on the 2<sup>nd</sup> level. After that only in the 1970<sup>th</sup> the first scientifically conducted archeological studies were set in motion following with restoration that respected the ancient structure was carried out. The last intervention is still in the process contained cleaning of the monument's surface and its respective consolidation.





Figure 4.18 The current view on the Colosseum

#### **4.4 Existing theories on the damage causes**

Still until now we have many open questions about Colosseum, about its history and about past damage that has brought the monument to its current condition. At the present time, exist several hypotheses on what was the main cause of the Colosseum damage during the centuries...were it earthquakes or man-made or mix between geology and seismic actions? The most recent studies and researches on the Colosseum were published by Giorgio Croce (Croci 1990), Renato Funicello (Funicello et al. 1995) and Mario Como (Como 2013) with the following theories and explanations on the Colosseum's damage.

For the first time (Croci and D'Ayala 1989) have published their work on hypothesis based on seismic nature of the Colosseum damage. The research was corroborated by detailed historical survey of the building, respective chronology of damage in time and connected them with successive earthquakes. The research has been continued in successive publication (Croci 1990) that also contained extended study on the monument with linear and nonlinear analysis of the structural parts. The work was confronting the monument critical capacity with the existing seismology of the territory and resulted damage with the existing failure and cracks of the monument. As a consequence of the work the damage of the Colosseum were connected with the past earthquakes happened frequently in Rome.

Next research was published by (Funicello et al. 1995), which agreed with the seismic nature of the amphitheater damage, consequently adding some geological details (Figure 4.19). "The Colosseum built over a small

fluvial valley...and contained sedimentary deposits of the Fosso Labicano, a third-order tributary of the Tiber River ....The structure of the subsurface beneath the Colosseum, showing that the southern section of the amphitheater lies directly above an elbow formed by the Labicana Valley...” In this connection, the failure and concentrating of the damage mainly in the southern part of the monument were explained by the amplification of the seismic action due to local geological heterogeneity (Funicciello et al. 2006).

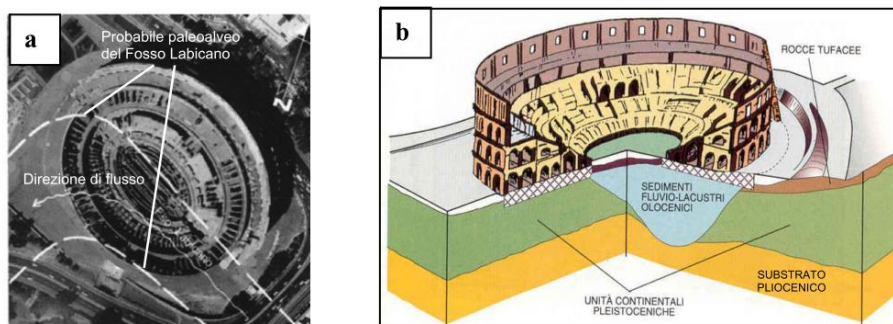


**Figure 4.19 a) ancient course of Fossus Labicano; b) 3D geological map of the site of the Colosseum (Funicciello and Rovelli 1998)**

The work by (Como 2013) presented another theory priority focusing on the static source of the Colosseum’s problems. The work contains numerical and analytical calculations providing values of the strength of the monument and its seismic capacity. The idea is that the initial source of the damage was “intentional deconstruction of the monument...by the destruction of piers of the first level of the external wall” (Coccia et al. 2006). After the man-made action the structure became more vulnerable and following man or earthquake interactions have produced further failure.

Noticeable, that all the studies admitted the influence of the seismic action on the existing damage of the Colosseum. On the behalf of the present study, the source of the existing damage on the part of the Colosseum will be investigated. The south-east edge of the external wall, which was restored by Stern in 19<sup>th</sup> century, until now contains and demonstrates intricate damage pattern (Figure 4.20). What was the source of the damage that led the south-east end of the wall to its critical point needed consolidation works? Was it a specific earthquake or a start of the archaeological works on the Colosseum or both these reasons together?



#### **4.5 *Seismic analysis of the south-east end of the external wall***

The seismic analysis of the south-east edge of the external wall of the Colosseum was performed using UDEC. The goal of the investigation was to recreate the action that caused the damage to the investigated wall. (Figure 4.20) The wall was restored in 1807 but the damage pattern is still perfectly visible on the structure. Firstly, numerical analysis in terms of pushover approach is obtained in order to examine the seismic capacity of the investigated structure. Then, step pulse analysis applied to the model and aimed to reproduce the intensity of the horizontal load causing existing damage, reproducing historical magnitude of the earthquake of 1806.

The investigated wall is studied by means of two models. The first and the key models tend to represent the state of the structure in 1806, how it was before restoration and during the investigated earthquake. The second model represents the studied wall with the infilled arches of the second level, the state of the structure preceded the 19<sup>th</sup> century as was described earlier in the chapter.

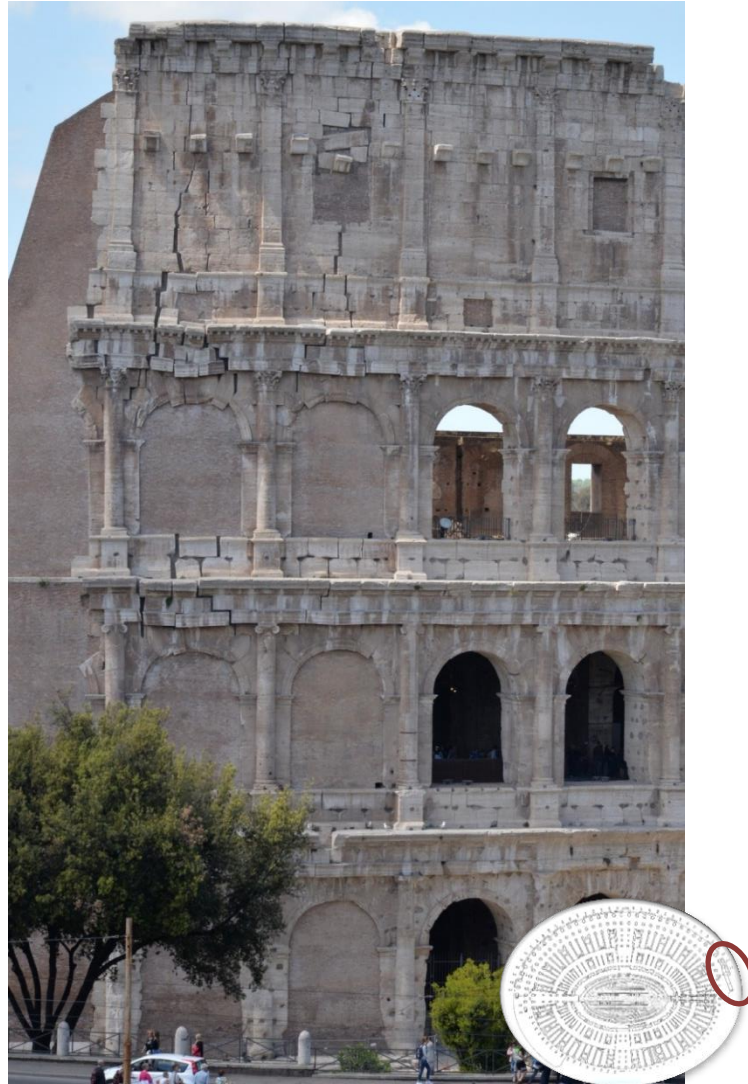


**Figure 4.20** Part of the Colosseum under investigation

#### **4.5.1 DE Model**

The geometry of the model is built using photographic survey by creating the mesh in CAD, following the real pattern blocks. The analyzed part of the external wall is 28 m in length and 48 m in height and contains 12 arches in 3 rows with the attic part also containing openings. (Figure 4.20) The average dimension of the blocks is 0.7x0.7 m, so the model contains about 1000 blocks. On the right side the model is confined by the

fixed block in order to consider the existing rest of the structure. The analyzed part of the façade assumed to be straight, neglecting the curvature of the external wall in plan (Figure 4.21). Elliptical shape of the Colosseum has a great radius that not affecting the results of the present study. The control point was chosen as a corner of an extreme left block placed on the 3<sup>rd</sup> level of the arches, that is assume to represent the displacement of the structure.

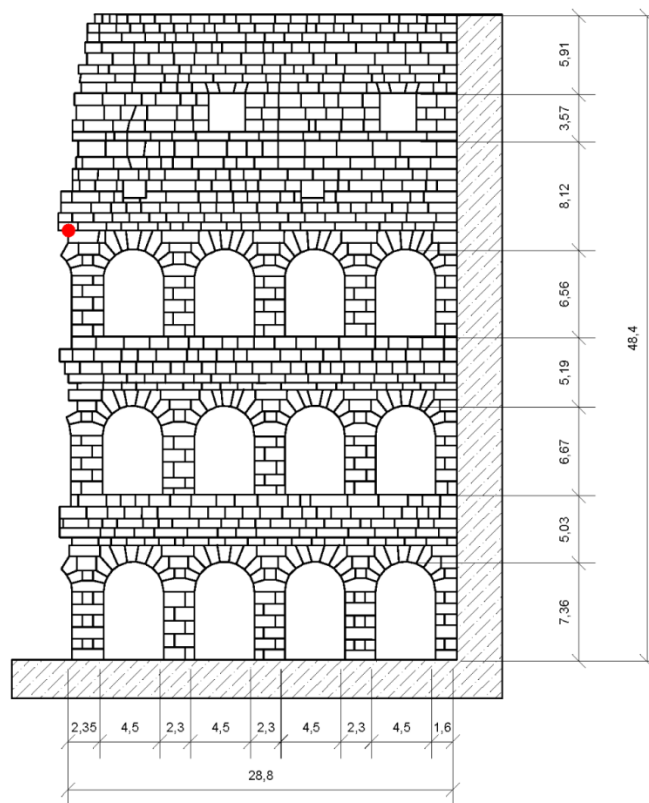


**Figure 4.21 DE mesh and model geometry**

The materials of the analyzed wall mainly are represented by travertine stone blocks on the façade and roman concrete on the interior part of the attic and in the cross vaults. (Figure 4.22) The mechanical properties of the materials obtained from the former studies on the Colosseum (Crocchi 1990) and are the following: for the travertine stone -  $E=30\text{GPa}$ ,  $f_s=60\text{MPa}$ ,  $r=2500\text{ kg/m}^3$ , for the roman concrete  $E=12\text{GPa}$ ,  $f_s=7\text{MPa}$ ,  $r=1350\text{ kg/m}^3$ . The value of the friction angle for the travertine stone varies in the literature from  $35^\circ$  (Pentecost 2005) to  $25^\circ$ - $35^\circ$  (Giampaolo

and Aldega 2013). In order to obtain the most suitable value for the UDEC model, a sensitivity analysis on frictional angle was performed using step pulse signal, which results are presented in the Table 4.2.





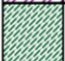
**Table 4.2 Sensitivity analysis on the effective value of a frictional angle**

Step pulse signal	friction angle [degrees]		
	30	35	40
0.3g, 0.3s	failure	1.05	0.8

The final mechanical parameters applied to the UDEC model summarized on the Figure 4.22. The mechanical properties such as density of the blocks as well as normal and tangential stiffness of the joints obtained depending on effective thickness of the walls and its materials. The tensile strength and cohesion are set to zero, while the frictional angle equal to 35. The parameters of the existing crack that has been already opened before the investigated earthquake (Figure 4.8) was adopted with decrement factor 0.1.

The geometry and mechanical parameters of the second model are the same as of the main one; without creating openings on the second level and using as arch infill the material parameters of the travertine.

**Table 4.3 Adapted mechanical properties of the model**

Lgnd	Effective thickness (m)	Density (m/kg <sup>3</sup> )	Normal stiffness (GPa)	Shear stiffness (GPa)	Friction angle(°)	Cohesion, Tensile strength (MPa)
	Travertine - 1.6 Concrete - 1.0	5400	88	44	35	0
	Travertine - 1.6 Concrete - 3.5	8900	132	66	35	0
	Travertine - 2.3 Concrete - 1.0	7150	118	59	35	0
	Travertine - 3.3	8250	144	72	35	0
	Travertine - 2.6	6500	114	57	35	0

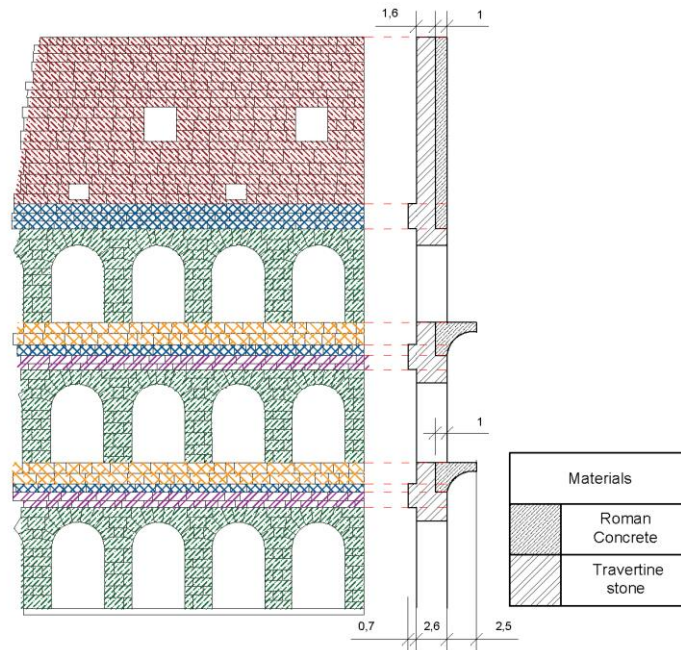


Figure 4.22 Effective thickness adopted in the model

#### 4.5.2 Pushover analysis

Pushover analysis was performed by applying gradually increasing horizontal acceleration to all the blocks of the model. From the resultant capacity curve (Figure 4.23) the maximum bearing horizontal acceleration of the investigated part was  $0.07g$  with ultimate displacement equal to  $0.25$  m.

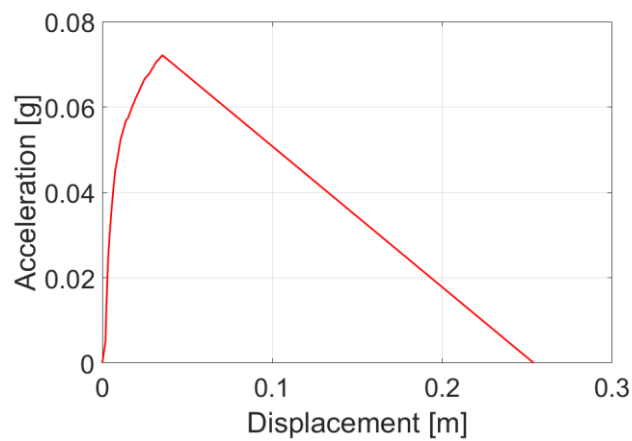
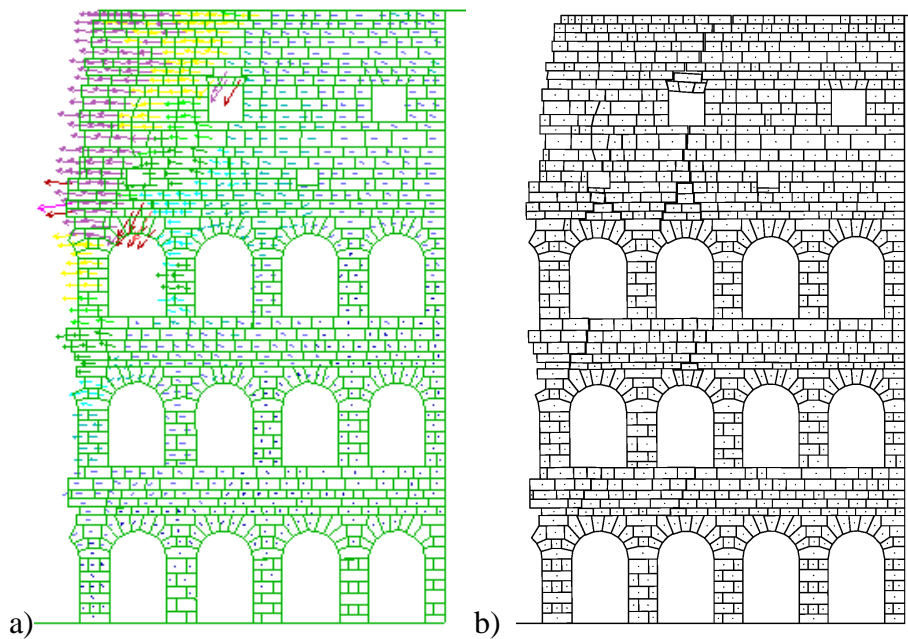


Figure 4.23 Pushover capacity curve

It is interesting to examine the distribution of the velocity in the model during the second half of the pushover analysis (Figure 4.24a). The major part of the moving blocks concentrated in the upper left portion of the model, representing the most vulnerable part and forming the further failure mechanism.



**Figure 4.24 a) Distribution of velocity along the model during the pushover analysis and b) resultant failure mechanism**

The ultimate state of the structure showed good agreement with the current damage pattern of the monument (Figure 4.24b). In both cases the failure mechanism took place on the 2 extreme rows of arches accompanied by corresponding vertical cracks. Only, the numerical result demonstrated less pronounced collapse since the analysis was interrupted due to fractional failure of the masonry.

The pushover analysis demonstrated the lack of the seismic capacity of the investigated part of the external wall of the Colosseum to resist the horizontal load without any additional restrain. In the past the consolidation role took infilling of the extreme arches with the bricks, which effects on the structural stability will be investigated further in the chapter.

### 4.5.3 Dynamic analysis

Analysis was performed applying step pulse signal in terms of acceleration to all the blocks of the model simultaneously. The applied acceleration value was from 0.1 to 0.4 g with duration 0.1 - 0.5 sec. The duration of each analysis was about 6 seconds, in order to assess the behavior of the structure during and after application of the pulse. The results of the sensitivity analysis on step-pulse parameters showed below (Table 4.4) that were performed in order to define the equivalent values of the required signal and corresponding displacement of the chosen control point in order to match the existing damage pattern.

**Table 4.4 Sensitivity analysis on step pulse parameters**

step pulse parameters		displacement of control point [m]
acceleration [g]	duration [sec]	
0.25	0.3	0.61
0.28	0.3	0.84
0.29	0.3	0.94
<i>0.3</i>	<i>0.3</i>	<i>1.05</i>
0.3	0.4	failure
0.4	0.1	0.21
0.4	0.2	0.87
0.4	0.3	failure

From the photographic survey it was defined an approximate value of the existing displacement of the investigated part that was about *0.9 m*. The best matching was achieved by applying horizontal acceleration of 0.3g during 0.3sec with maximum displacement of control point *1.05 m*. The numerical model under step pulse signal showed perfect matching of its main failure mechanism with the existing damage pattern of the structure. The failure primarily appeared on the 2 extreme rows of the arches with vertical cracks opening along their vertical axis with partial failure of the voussoirs as seen on the Figure 4.25.

The investigated earthquake (26.08.1806) was the one that produced damage on the south-east end of the wall and had a relatively low intensity (Table 4.5). It had coincident location with the geological substructure of the Colosseum (Funicello et al. 1995) that probably may have produced amplification of the PGA . The earthquake intensity was approximately 6-8 MMI, that according to (Bolt 1993) may satisfy with

0.1-0.3g, and that also confirms the obtained numerical results with 0.3g pulse magnitude. Additionally, this magnitude can be confirmed according to current Italian seismic map, in which Rome is located on the 2A seismic zone with corresponding PGA 0.15-0.25g (Pericolosità Sismica Di Riferimento per Il Territorio Nazionale 2006).

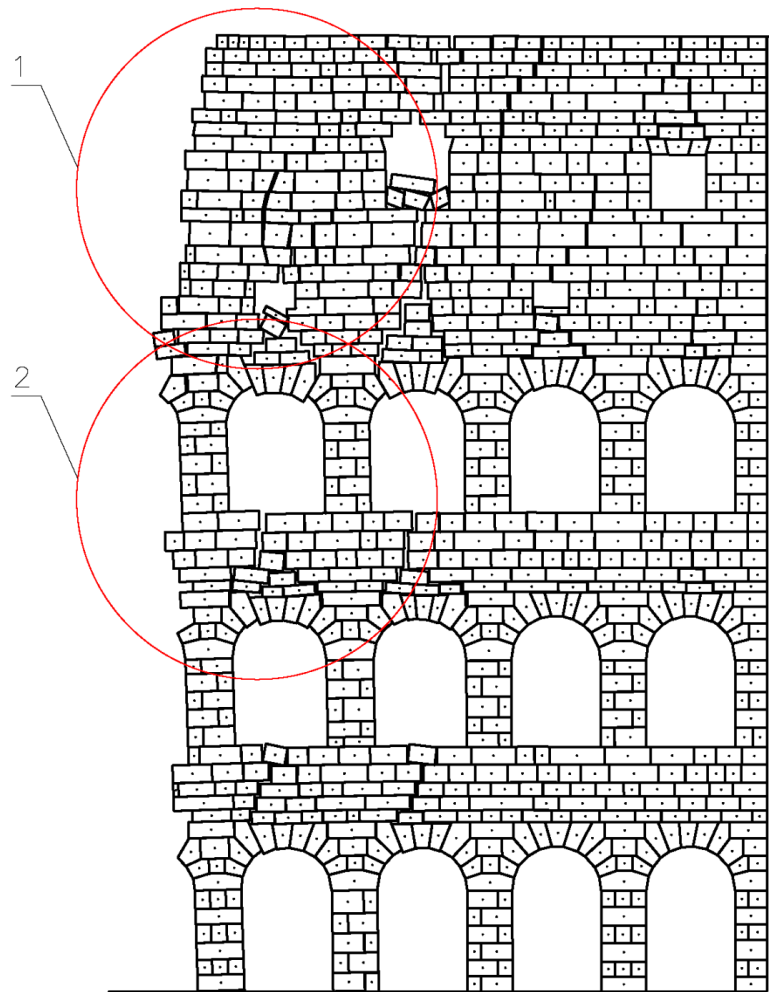


**Figure 4.25** Failure pattern based on pulse analysis



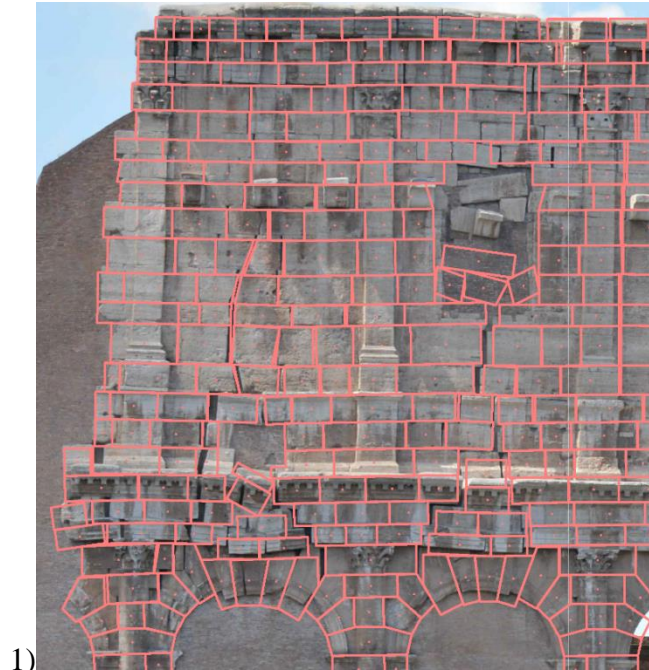


**Figure 4.26 Matching of the existing and pulse-by failure patterns**

Zoom 1 showed in details how the model was able to capture opening of 2 vertical cracks prolonging to the mid of the arches, following by partial failure of 4 voussoirs of each arch. Additionally, the failure of the voussoirs of the top opening in the model differs with their partial failure in the real structure. The phenomena can be explained by 2dimentiality of the numerical solution that is not able to represent precisely the intersection between different layers of the wall. On the other side, zoom 2 illustrates perfect matching of the failure pattern between arches of different level and continuous propagation of the vertical crack.

#### 4.5.4 Damage investigation

Based on the historical survey it was noted that before the 19<sup>th</sup> century intervention on the south-east end of the external wall of the Colosseum the respective structure stayed in its unchanged condition at least during 18<sup>th</sup> century. Also based on the picture survey the second model in UDEC has been created containing infill arches. From the other side, based on the historical data the list with the most severe earthquakes happened on the area around Rome with 150 km radius is shown in the Table 4.5.

**Table 4.5 List of the earthquakes during 1700-1810** (Guidoboni et al. 2007)

Date	Epicenter	Intensity	Location towards Rome	Intensity in Rome
14.01.1703	Appennino Umbro-Reatino	11	north-east	7
02.02.1703	Aquilano	10	north-east	7
12.05.1730	Valnerina	9	north-east	6
26.08.1806	Colli Albani	8	south-east	5-6

According to the list of significant earthquakes that took place during 18<sup>th</sup> century in Rome it is notable that the intensity of the last one in 1806 was lower than others, but only the last one endangered the south-east edge of the external wall, why? It may be several explanations. First of all, ‘fatigue’ of the structure after all preceding events as well as influence of the earthquake epicenter location that was on the south-east. However, it can be also additional reason such as lack of the arches infilling that more probable was removed before the last earthquake following the start of the Colosseum interventions and led to additional weekend of the structure. Thereby, it can be assumed that the filling in of the arches with bricks played a consolidation role for the structure and that is also confirmed by the numerical results based on pushover and pulse analysis (Figure 4.27).

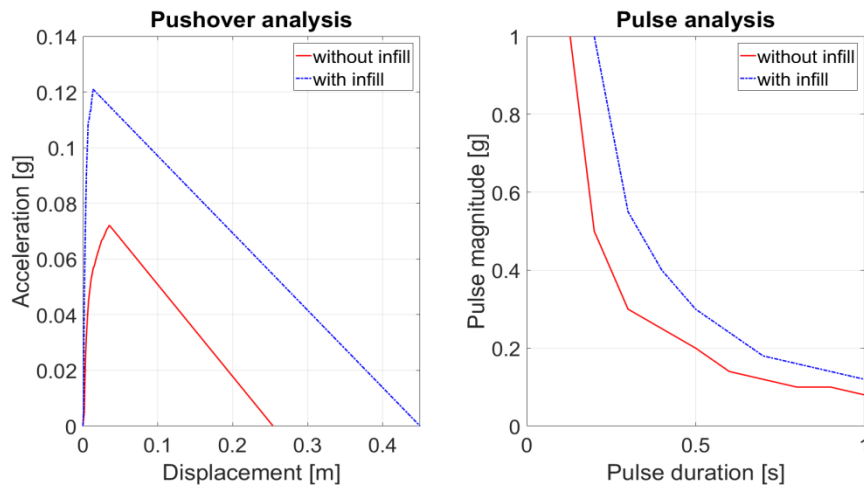


**Figure 4.27 Pushover curves and pulse failure domains of the models without infill and with infill of the second level arches**

The results above demonstrate significant influence of the arch infilling on the structural resistant of the external wall. There were almost 100% increase in both strength and displacement capacity according to pushover analyses, which was also confirmed by essential shift of the failure envelope based on pulse analysis. The obtained results supported the investigated theory, which stated that at the beginning of 19<sup>th</sup> century the brick infill of the arches was removed, that led to weakened of the structure and its partial collapse during the first happened earthquake, even with smaller intensity than the many preceding ones.

Moreover, the failure mechanism of the model with infilled arches (Figure 4.28) corresponded to the past damage pattern observed in the illustration from 1700 (Figure 4.8). Both damage were mainly governed by a vertical crack widening along the mid of the external arches.

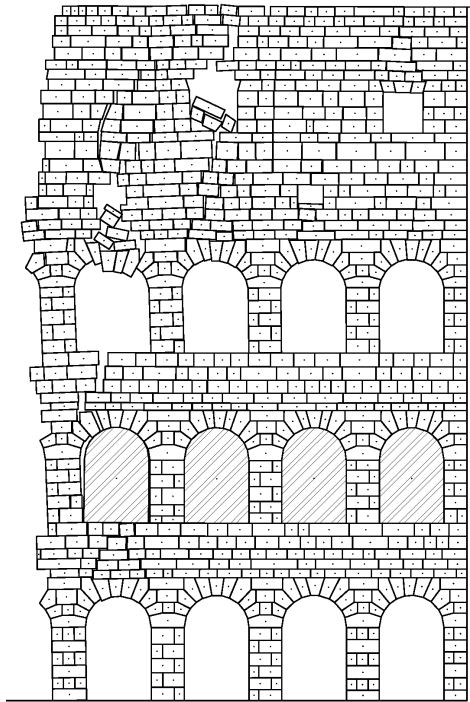


Figure 4.28 Failure mechanism with infill of the arches second level

#### 4.6 Summary

The present chapter contains research performed on the Colosseum focusing mainly on the south-east edge of the external wall. The curiosity of the study was in investigation of the past damage and evaluation the effective earthquake that caused the need on executing the restoration campaign in 1807, which was successfully realized by Stern.

The investigation started with the geometrical and structural survey of the entire monument. Then the extended research on past damage and restorations of the Colosseum was accomplished concentrating on the south-east wall and its restoration at the beginning of the 19<sup>th</sup> century. Concluding the survey by an overview of the researches recently published on the Colosseum by Croci, Funicello and Como and their existing theories on its damage causes. The theories are mainly based on seismicity of the area, which affect could have been amplified by geological specify of the valley and on the manmade influence, when the monument was used as a quarry for the building materials.

The numerical analysis of the investigated part of the Colosseum confirmed the seismic nature of its damage. The essential matching of the failure mechanisms between the real structure and DEM model was obtained based on pulse analysis.

Additionally, the analysis on a slightly modified model was performed representing the state of the structure with some infilled arches, an existence of which was identified based on historical survey. The investigated hypothesis stated that right before the 19<sup>th</sup> century restoration the infields were removed that led to weaken of the structure and its partial collapse during the first happened earthquake. The quasistatic and dynamic analysis demonstrated significant increase of the seismic capacity of the modified model, thereby, provided a support to a proposed hypothesis.

## **5 Seismic assessment of the Claudio Aqueduct**

### **5.1 Introduction**

The Claudio Aqueduct is a great example of the archaeological site, which is represented by construction from the Roman time partly remaining until now. Sometimes extra walls (arcades) were built to get the right level for the conduit, which was only done for a height less than 2 meter. To get the aqueduct on a higher position, a series of arches was built. The rest of the Claudio Aqueduct in Rome is one of the best known examples of this kind of arcade substructures. The cause that brought the monument to its partial collapse is not known for sure, but the most probable reason could be the lack of maintenance, material's degradation in time and as a result increased vulnerability to seismic actions. There is always a high interest in studying and preservation of the Roman aqueducts which represent an example of not only cultural but also 'engineering' heritage of the ancient world. In this connection exist several ongoing contemporary projects that aim to collect and connect all publications on ancient aqueducts (Passchier et al. 2017), (Schram 2017).

In the present chapter, the seismic assessment of arcades of the Claudio Aqueduct was carried out by reproducing the effective shape and position of the stone blocks that formed the aqueduct and using a numerical analysis strategy based on the DEM. Applicability of the approach was detected by simulation of expected failure mode under seismic action, performing pushover (Mordanova, de Felice, and Genoese 2017) and pulse analysis, implemented in the software UDEC. Sensitivity analyses on the mechanical parameters was also undertaken to verify their influence on the overall response. Several configurations of the model were elaborated in order to better understand the effect of existing damage and the increase in seismic capacity of the aqueduct after potential retrofitting.

### **5.2 Historical survey**

The Claudio Aqueduct is one of the longest and the most important aqueduct in Rome. Its construction was begun in 38 A.D. and completed in 52 A.D. by Emperor Claudius. At that time the aqueduct was about 68.5 km long (Figure 5.1), with the total daily flow rate of 184 m<sup>3</sup>.

About 58 km were constructed in the mountain sites with underground galleries and bridges, while the latter 10.5 km entering in Rome were made over substructures and arcades. With two water channels, 'Aqua Claudia' that placed directly over the arches and 'Anio Novus', which was erected after the Claudio water conduct and placed just above it.



**Figure 5.1** The route of the Aqua Claudia (in red) (adapted form (Droysen 1886))

It was sourced by several springs in the Anio Valley, near Agosta and originally there were two springs, the Caeruleus and Curtius, which were later supplemented with the Albulinus one. From the sources the Claudio aqueduct descended along the right bank of the river Anio, mostly underground and slightly uphill from the Marcia aqueduct, another ancient water supplier of Rome sourcing little bit uphill from the same area (Schram 2012). On its route the Claudio aqueduct several times crossed the bank of the Anio over bridges, some remains of which have been incorporated in a modern road bridge. Following the bank of the Anio the Aqua Claudia was accompanied by parallel aqueducts, such as the Marcia and Anio Novus, and lately even united with the last one on the final kilometers of the route. The Claudio aqueduct rose above the ground near Capannelle and continued its way on a long series of high arches. After about 10 kilometres on substructures the Claudio aqueduct entered Rome and passing through Porta Maggiore reached its 'castellum', a distribution basin. The last one was located on the Esquiline Hill, near

the temple to Minerva Medici and was destroyed by fire in 1880 when it was being used as a hay barn. (Schram 2017)

The arches of the Claudio Aqueduct were built with the construction technique called '*opus quadratum*'. They are composed of rectangular block made by cut volcanic stones, having different heights and position in alternate layers or by headers or by stretchers. The Anio Novus addition was made with '*opus reticulatum*', consisted of cubes from 7 to 8 cm on the side, which were fairly uniform and embedded into concrete. This technique, in fact, was more convenient for constructing water channels since its higher moisture resistance than the earlier ones (Lugli 1957). Depending on the construction site, peperino, red tuff and travertine stones were utilized (Figure 5.2).



**Figure 5.2** Upper channel - Anio Novus, made with '*opus testaceum*' mixed with '*opus laterazium*'; low channel and arcades of Aqueduct Claudio made with '*opus quadratum*'

The '*opus latericium*' along the aqueduct was mainly used as a reinforcing material for arches, channels and, in some cases, also for pylons. In particular, among the consolidation works made with this technique, inscriptions on the Porta Praenestina indicate that Vespasian and Titus between 75 and 80 AD for the channel of Anio Novus. Furthermore, the retrofitting works have been continued by Hadrian between 125 and 138 AD for channels of Anio Novus and Aqua Claudia together with the restoration of the Neronian arches of Claudia, from the Esquiline to the Palatine, by Antonini between 195 and 203 AD.





**Figure 5.3 Example of the ancient retrofitting brick works**

During the first consolidation works by Flvians the techniques such as '*opus reticulatum*' and '*opus latericium*' were used together by alternating; while with Adriano, in addition to the use of '*opus mixtum*', there was also '*opus latericium*' made with triangular bricks with regular layers in the supporting walls (Figure 5.3).

### **5.3 DE model**

#### **5.3.1 Model geometry**

The part under investigation was made of arches with constant radius of 6 m over pillars with cross section from 3.0 to 3.5 m and heights from 6 to 16 m. Two water channels with sections 1.3 x 2.4 m were directly above the arches. The geometry of the model comprised the last two arches of the aqueduct, with three pillars for a length of about 25 m, a height of about 16 m and a thickness of about 3 m (Figure 5.4).

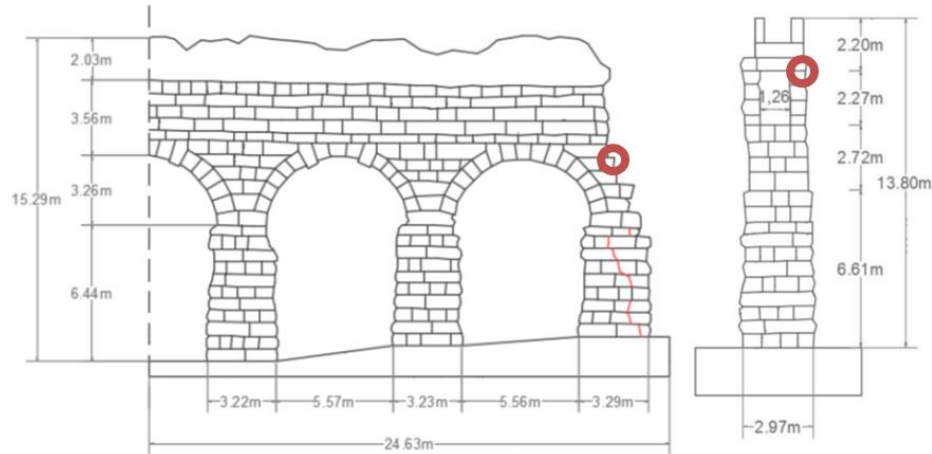


**Figure 5.4 Geometry of the model and control points**

The transversal section of the aqueduct was analyzed using two models (Figure 5.5) representing its actual state which contained reinforcement made of stainless AISI 316F steel rods with 30 mm diameter placed just below and above the water channel; and its initial state before reinforcement in order to investigate the improve of its seismic performance under current condition.

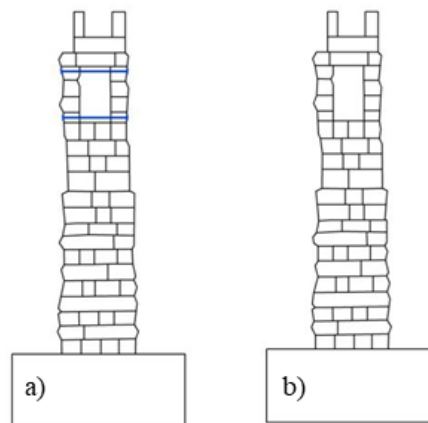


**Figure 5.5 Models of a) actual and b) initial states of transversal section**

The longitudinal section was also modeled under various conditions considering two longitudinal models reproducing the facades, which have slightly different masonry and damage patterns. For its current state several configurations of model were assigned depending on representation of the top channel. Three models are shown in the Figure 5.6 and contain simplified or well-defined upper channel blocks or an

absence of the upper channel. That was done in order to investigate the influence of the upper water channel on the seismic performance of the system.

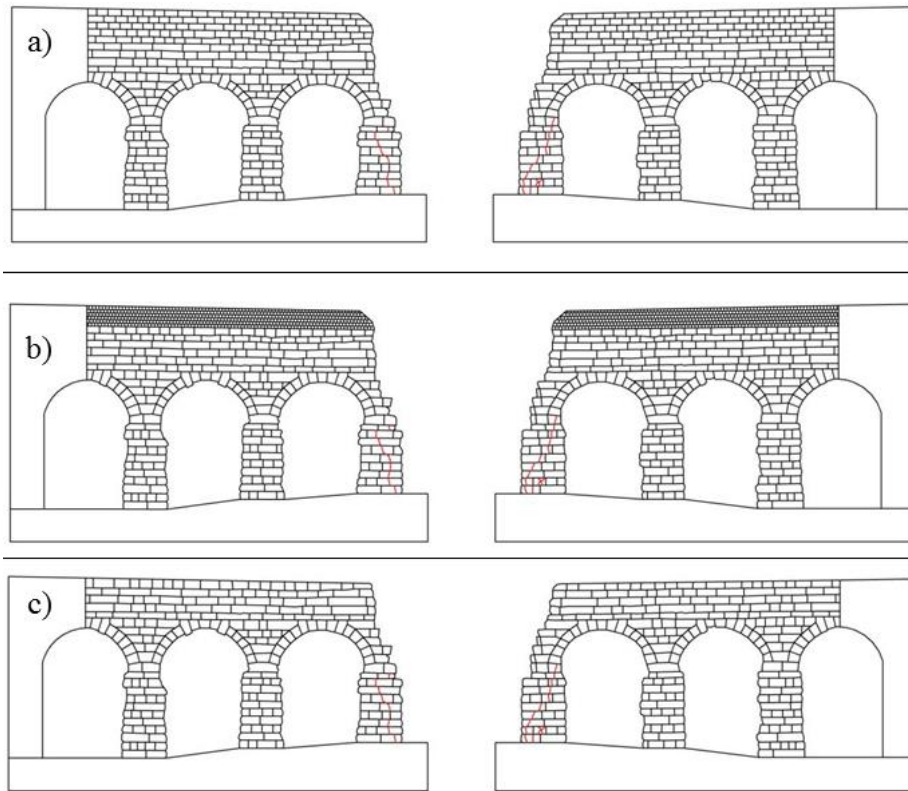


**Figure 5.6 Models of actual state of longitudinal section depending on upper channel representation: a) simplified, b) well-defined, c) without**

To make the analysis more complete potential reinforcing solutions of the longitudinal section were modeled with strengthening of the most vulnerable part according to analysis of the actual state. Thus, it was chosen to reproduce maximum and minimum reinforcement by inserting 2 or 8 steel bars in the base of the last pillar. Moreover, a model of an 'ideal' state of the section was also created in order to investigate the influence of the exciting cracks of the structural behavior and capacity (Figure 5.7).

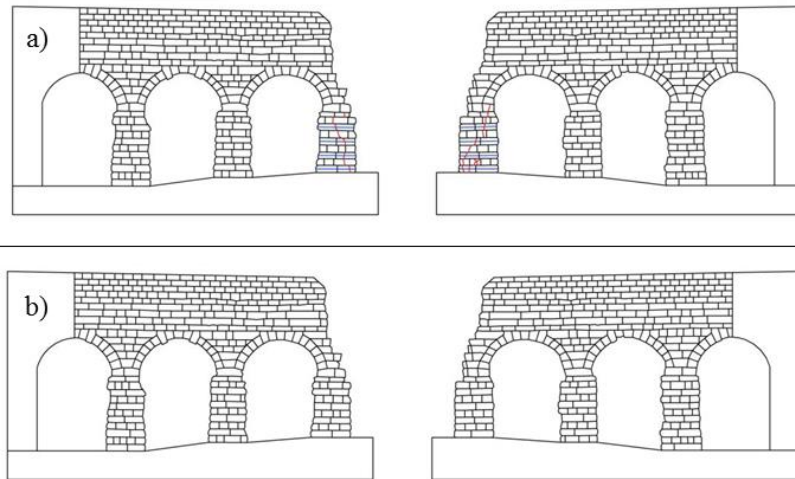


Figure 5.7 Models of a) reinforced and b) ideal states of longitudinal section

### 5.3.2 Material properties

After the geometry was obtained, the mechanical properties of the joints and the blocks were defined taking into account the effective depth of the macro-element. Only a few constitutive parameters were required to define the behavior of the joints, which were characterized by Coulomb friction angle, normal and shear stiffness, while the joint cohesion and tensile strength were neglected, since the analyzed structure was made of dry masonry.

Legend	Out-of-plane model				In-plane model			
	$t$ [m]	$\rho \cdot t$ [kg/m <sup>2</sup> ]	$K_n \cdot t$ [GPa·m]	$K_s \cdot t$ [GPa·m]	$t$ [m]	$\rho \cdot t$ [kg/m <sup>2</sup> ]	$K_n \cdot t$ [GPa·m]	$K_s \cdot t$ [GPa·m]
	3.34	6412.8	5.07	2.13	3.05	5856	4.41	1.85
	2.3	4416	3.33	1.4	2.83	5433.6	4.54	1.91
	2.75	5280	3.35	1.41	2.5	4800	3.85	1.62
	4.15	7968	4.69	1.97	1.45	2707.2	2.21	0.93
	3.78	7257.6	3.53	1.48	2.7	5184	3.78	1.59
	3.2	6400	1.21	0.51	2.06	4120	1.05	0.48
	0.93	1860	0.47	0.2				

Figure 5.8 Properties of the blocks/joints implemented in the model depending on effective thickness

According to laboratory test's investigation, the density of tuff blocks was 1920 kg/m<sup>3</sup>, its modulus of elasticity 2800 MPa, and the friction angle 30°. As the model is plane, the effective thickness  $t$  of masonry was considered, as showed in the Figure 5.8, for assigning the density  $\rho$  of the

discrete elements as well as the normal  $K_n$  and shear  $K_s$  stiffnesses of the joints.

Sensitivity analyses on friction angle (from 25° to 35°) and modulus of elasticity (from 1.5 to 5.6 GPa) were undertaken in order to verify the sensibility of the UDEC model.

### **5.3.3 Boundary condition and loading**

The numerical analyses were carried out in the transverse and longitudinal sections of the aqueduct, at its actual state and after potential reinforcement.

The ground in the model was implemented by base block, which is not a part of the structure but used exclusively for representing the bonding ground condition. In red, the control point using in the subsequent analyzes are highlighted (Figure 5.4).

All the analyses were carried out in two stages: first, each model was brought to equilibrium under gravity force; and then, an external load was applied representing seismic action. Depending on the type of approach the loading procedure is following:

- for quasistatic approach - increasing horizontal acceleration at the centroids of each block;
- for pulse approach - horizontal acceleration at centroids of each block during short period of time;

## **5.4 Quasistatic analysis**

In this section the results of the pushover analysis under out-of-plane and in-plane seismic loading are carried out. The expected collapse mechanisms were detected and used for providing information on potential strengthening solutions.

### **5.4.1 Out-of-plane loading**

The analysis on the out-of-plane behavior was performed on the transversal section of the aqueduct by applying the horizontal load in two directions on two states of the structure. The results demonstrated that at the initial state of the upper part of the aqueduct with water channel was the most vulnerable part (Figure 5.9a). Thanks to its past reinforcement currently a collapse mechanism did no longer activate the water channel but becomes a global overturning failure around a hinge located at the base of the structure (Figure 5.9b). An increase in strength of 25% and in

displacement of about 100% was obtained with the realized strengthening design (Figure 5.9c).

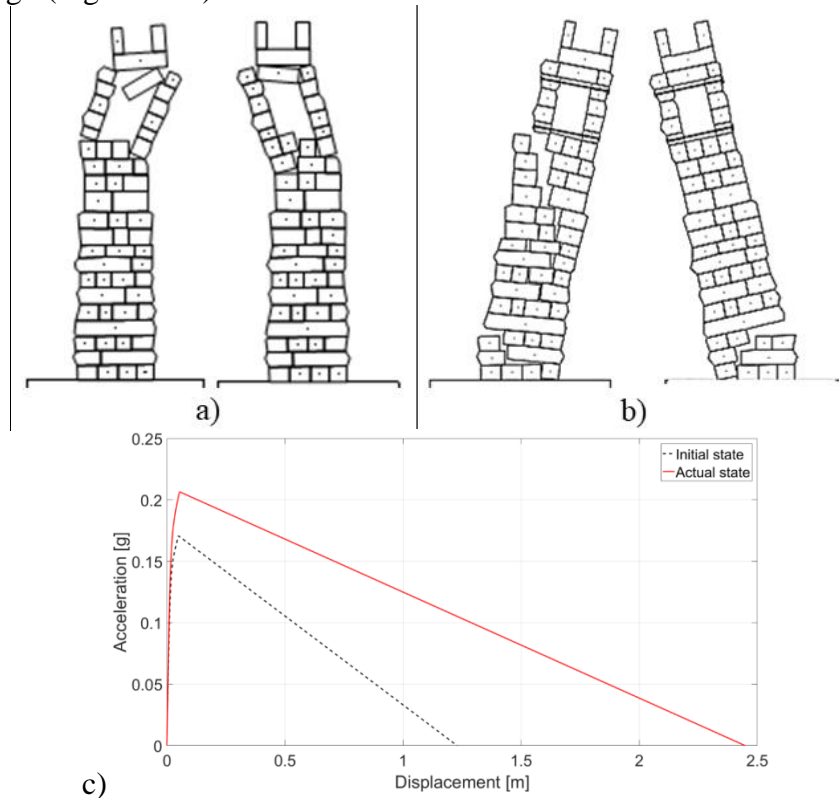


**Figure 5.9** Collapse mechanisms of a) initial and b) actual states of the transversal section and their c) capacity curves

## 5.4.2 In-plane loading

### 5.4.2.1 Actual state

Actual state of the longitudinal section of the aqueduct was described by several model's configuration, as was mentioned earlier, without upper channel or with its simplified and well-defined representation. The resulting failure mechanisms were similar for all the models, with a crack opening in an extreme pillar along the actual damage pattern (Figure 5.10). The only slight difference contained in failure modes of facade sides that was governed by their different existing crack pattern.

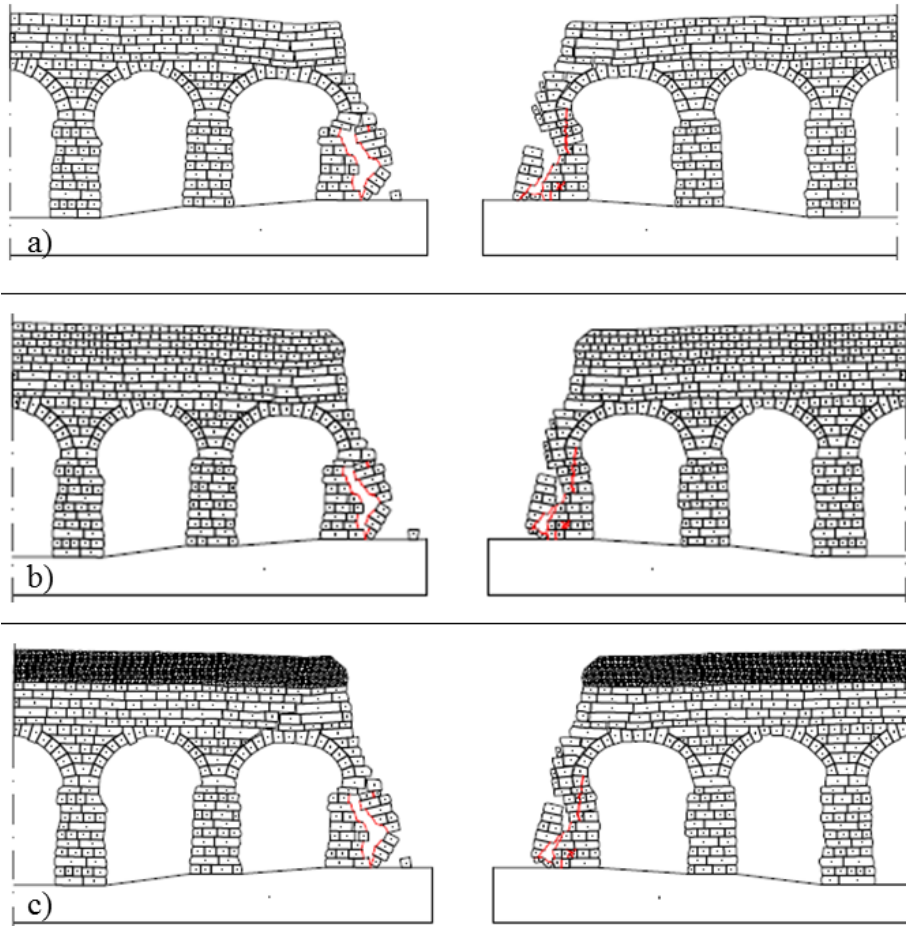


**Figure 5.10** Collapse mechanisms of actual state a) without, b) with simplified and c) with well-defined upper channel of the aqueduct

Thus, as a result, the mean value between the two leaves was taken in order to derive the in-plane capacity curve, as shown in Figure 5.11. This hypothesis could slightly underestimate the effective capacity, since the interlocking among the blocks of the two leaves was only partially taken into account. Models with upper channel independently of its representation demonstrated similar results with 0.14g of maximum acceleration and 0.45m of ultimate displacement. In contrary, the model without top channel provided higher results with 0.18g and 0.7m.

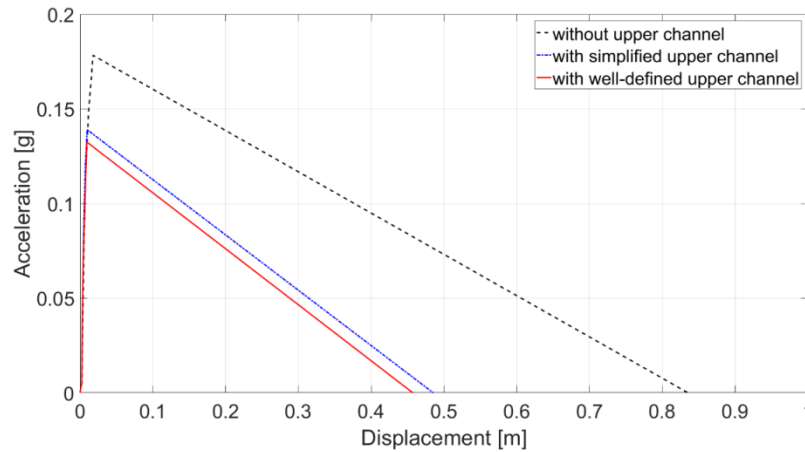


**Figure 5.11 Capacity curves of various in-plane models of actual state**

It can be stated that the existence or not of the top channel in the longitudinal model did not influence much on failure mode but effected considerably the in-plane seismic capacity of the aqueduct.

#### **5.4.2.2 Reinforced state**

The analyses on the longitudinal section of the aqueduct were repeated after its retrofitting and result in form of failure modes are shown in the Figure 5.12. It is notable that with the reinforcement of the extreme pillar a failure mechanism was now governed by global behavior of the system involving all the pillars and arches (Figure 5.12b,c). Interesting, that the structure in its '*ideal*' configuration demonstrated similar behavior with failure mechanism in both arches (Figure 5.12a).



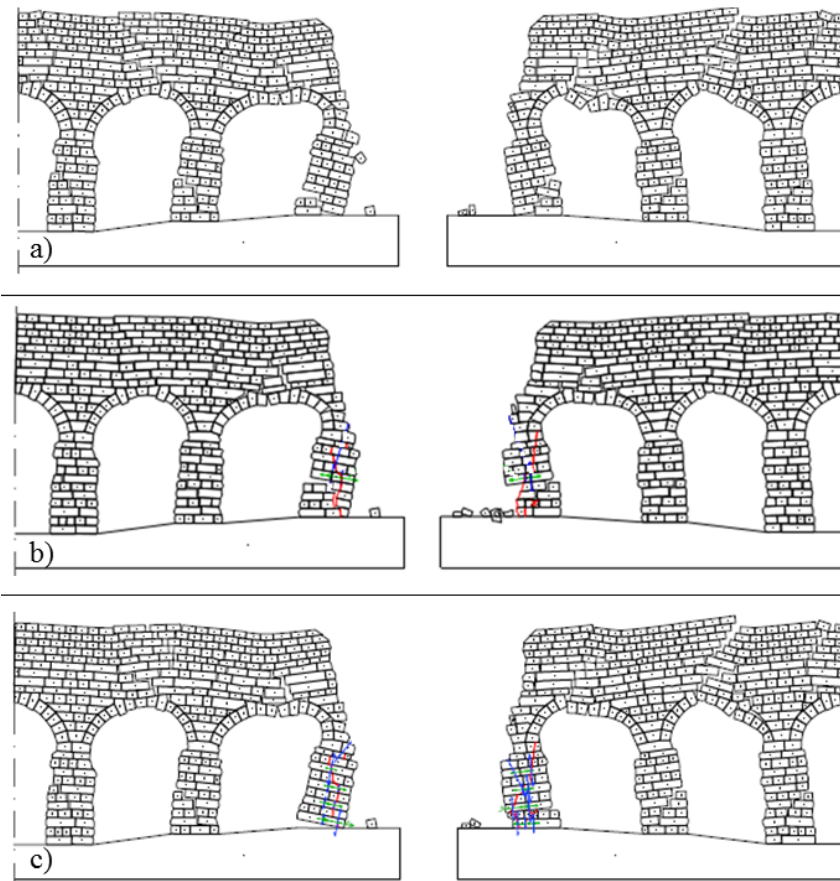


**Figure 5.12** Collapse mechanisms of a) ideal state of the structure and after its reinforcing with b) 2 and b) 8 steel bars

Results on in-plane stability of the aqueduct demonstrated a dramatic increase of its seismic capacity based on pushover analysis (Figure 5.13). In general, a substantial increase of about 80% in strength and 140% in displacement was reached with respect to the actual state that provides to the aqueduct strength similar to that corresponding to an “*ideal*” state. Following the results it can be concluded that retrofitting containing minimum proposed reinforcement was an essential measure for providing sufficient in-plane seismic capacity of the investigated part of the aqueduct.

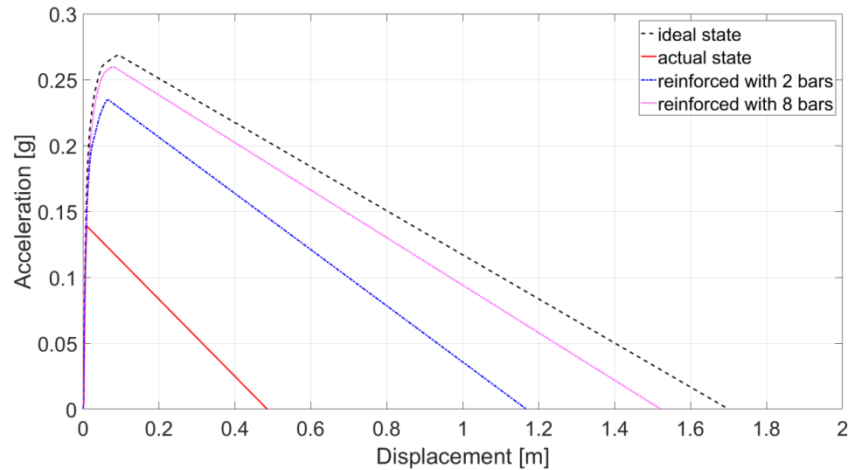


**Figure 5.13 Capacity curves of various in-plane models of reinforced state of the aqueduct**

### 5.4.3 Sensitivity analysis

The results of sensitivity analysis on the model constitutive parameters are illustrated in Figure 5.14. A strong dependence of the pushover curve on the friction angle was obtained, while the latter was almost not influenced by variation on the joint stiffness. This result can be generalized for quasi-static analysis, provided the contacts stiffness was not too underestimated, to allow for geometric nonlinearities to take place and drive the solution.

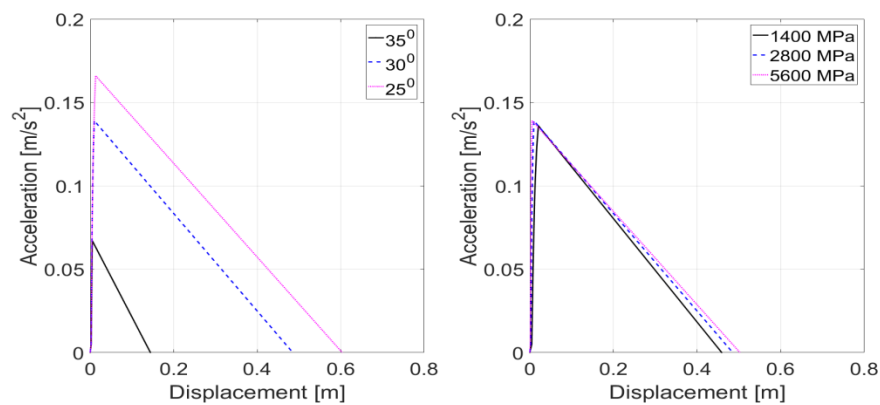


**Figure 5.14 Sensitivity analysis on a) friction angle and b) effective modulus of elasticity**

## 5.5 Dynamic analysis

Dynamic analysis was presented with pulse based approach on the both transversal and longitudinal sections. For out-of-plane loading both states of the transversal model was chosen, while for in-plane loading a model without upper channel was used as essential for providing sufficient results and required less computational time. The pulse load to all models was applied from left to right direction.

### 5.5.1 Out-of-plane loading

The pulse analysis on the out-of-plane loading of the Aqueduct Claudio demonstrated similar results with push-over procedure in case of failure mechanism but differed significantly in case of capacity values.

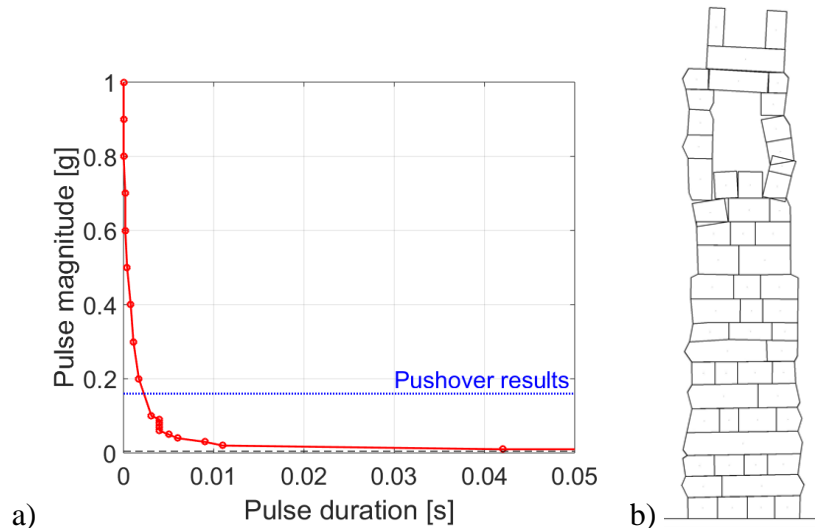


**Figure 5.15 Results of out-of-plane pulse loading of the aqueduct initial state in form of a) failure domain and b) failure mechanism**

Figure 5.15a shows the failure domain obtained for the initial state of the structure. The structure was only stable under pulse load below 0.05g with highly low value of response equal to 5 mm. The following analysis with increasing value of load and signal duration all brought structure to the collapse. The failure mechanism was governed by collapse of the upper water channel, as it was the most valuable part also according to pushover analysis. However, starting from 0.1g and higher the transversal model exhibited brittle collapse with the top response in range from 5 to 10 mm (Figure 5.15b) that are significantly lower than pushover results. The difference between the results might be account by brittle character

of failure under pulse analysis due to instantaneous feature of the load as well as damping effect. This is the issue for a future research.

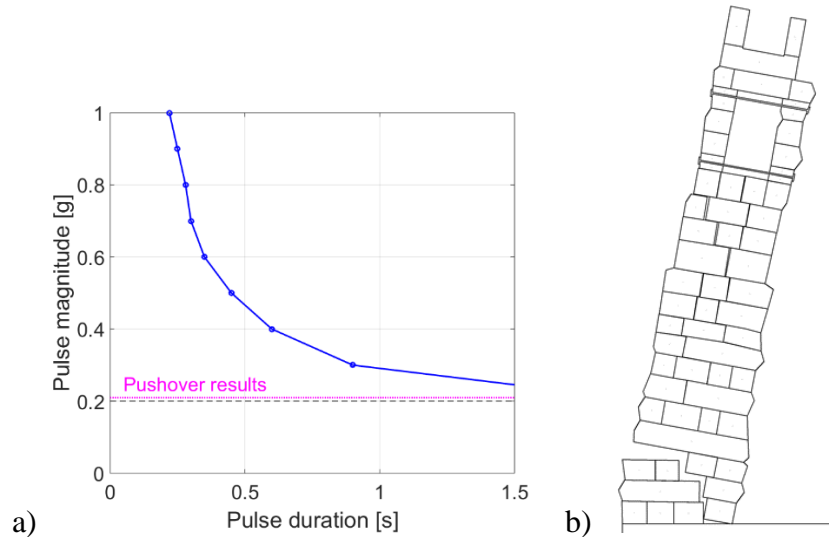


**Figure 5.16 Results of out-of-plane pulse loading of the aqueduct actual state in form of a) failure domain and b) failure mechanism**

The failure domain of the reinforced state of the monument subjected to the out-of-plane pulse loading is represented in Figure 5.16a. Like in the case of the initial state the magnitude required to cause the collapse of the structure increased with decreasing of the pulse duration. There is a threshold equal to 0.2g, below which the structure did not collapse that agreed with the pushover results of 0.21g. The ultimate displacement of the top part during the analysis was about 1.2 m, which preceded the global failure mechanism of the structure. Collapse of the structure at all pulse magnitude was governed by global overturning of the system around base that also confirmed the earlier results obtained by quasistatic analysis.

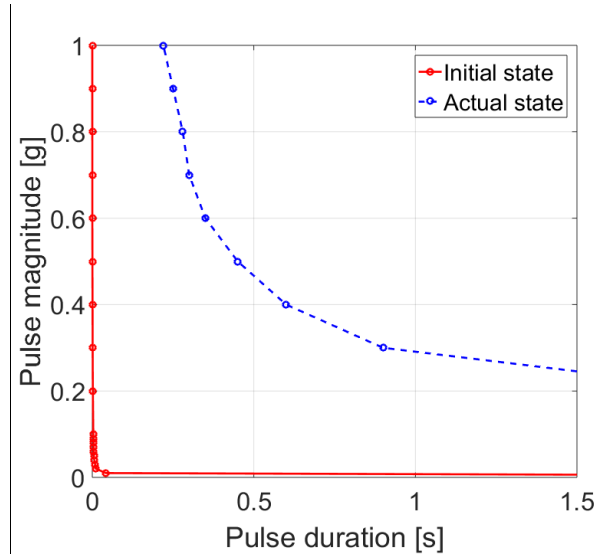


**Figure 5.17 Failure domains of transversal section subjected to step pulse**

The seismic effect of the realized strengthening of the out-of-plane section of the aqueduct was considerable in comparison with the pulse based analysis. Figure 5.17 demonstrates both failure domains and it is notable that reinforcement of the upper channel with steel bars increased significantly possible pulse duration. That was obtained thanks to providing more global behavior to the structure that also improved actual out-of-plane seismic stability of the aqueduct.

### 5.5.2 In-plane loading

The results on pulse in-plane loading of actual state are shown in Figure 5.18 in the form of failure domain. The magnitude required to cause the collapse decreased with increasing pulse durations, continuously approaching the acceleration value necessary to initiate the motion, which was in 10% range with quasistatic result. In the region below 0.16g, the response of the structure did not exhibit any significant damage. The region between 0.16g and the curve corresponded to conditions of recovery, whereby the structure survived indefinitely. Finally, pulses in the region above the curve led to failure, which in this case was governed by collapse of the last pillar. The maximum displacement of the control point right before the failure was equal to 0.4 m that was 2 times lower than one obtained from quasistatic analysis.

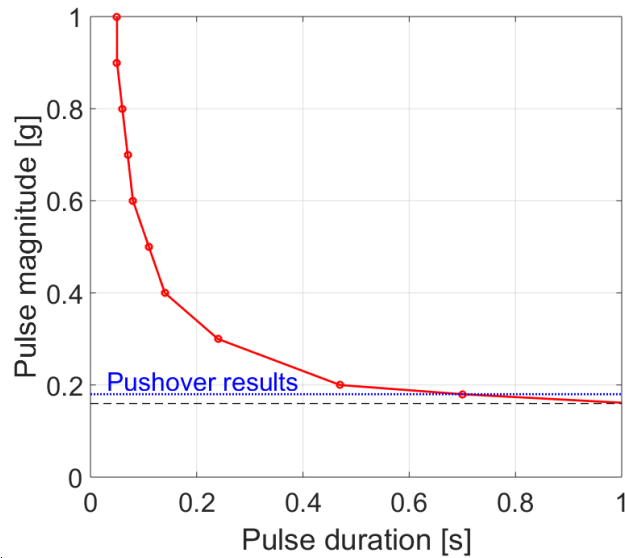


**Figure 5.18 Failure domain of in-plane pulse loading of the aqueduct actual state**

Similarly, failure domain obtained for reinforced state under pulse in-plane loading is displayed in the Figure 5.19. The minimum acceleration value necessary to initiate the motion was 0.2g, which was in 10% range with quasistatic result. In the region below 0.2g, the response of the structure did not exhibit any significant damage, while in the region between 0.2g and the curve the structure survived indefinitely. Lastly, pulses in the region above the curve led to structural failure that corresponds to the maximum displacement of the control point equal to 1 m, similar value as obtained from quasistatic analysis.

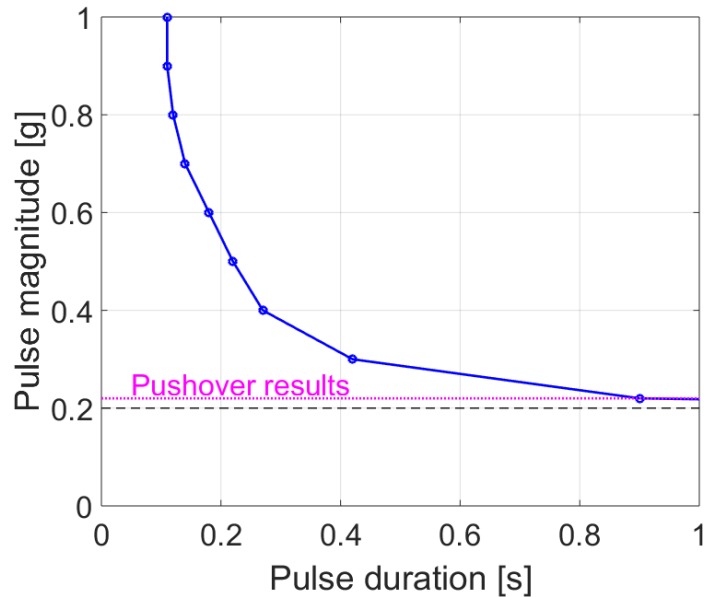
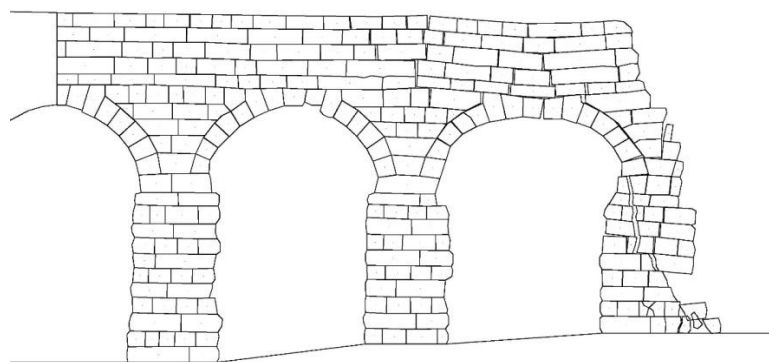


**Figure 5.19 Failure domain of in-plane pulse loading of the reinforced state**

The results of in-plane pulse loading in form of failure modes are presented in the Figure 5.20. The failure of the actual state was mainly governed by mechanism in the last arch of the section and widening of an existing crack in the extreme pillar. After strengthening of the last pillar, the failure became more global and formed in all elements of the investigated section: in form of diagonal cracks in the pillars and mechanisms in the arches. The value of the ultimate displacement also increased after reinforcing from 0.4m to 1m, respectively.



a)

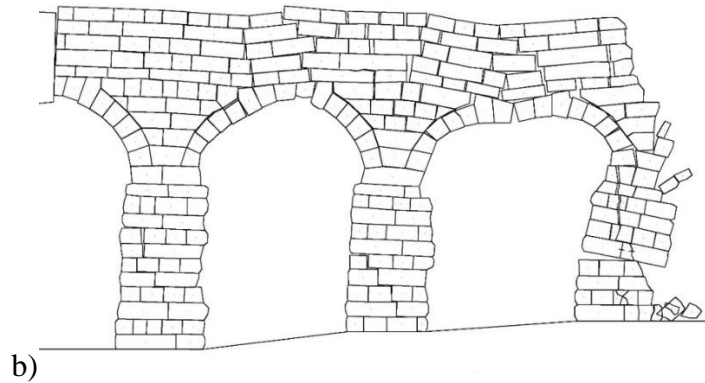


**Figure 5.20 Failure mechanisms under in-plane pulse loading of (a) actual and (b) reinforced states of the aqueduct**

The result failure domain of both states of longitudinal section is presented in the Figure 5.21. It is notable that reinforcing of the last pillar with 2 steel bars provided reasonable enlargement of the seismic capacities based on step pulse analysis. The safe domain shifted after reinforcement mainly due to rise of the possible pulse durations, for example for magnitudes above 0.4g the durations doubled due to increase of the minimum bearing acceleration.

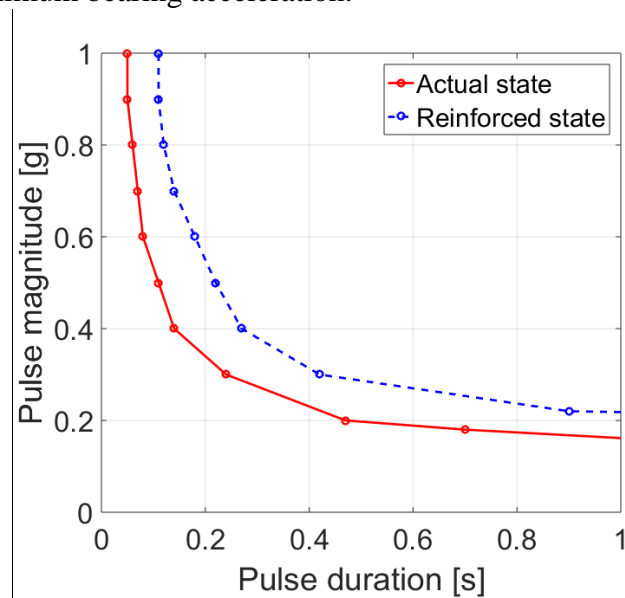


**Figure 5.21 Failure domains of longitudinal section subjected to step pulse**



## **5.6 Summary**

In the present chapter the mechanical behavior of the ending stone masonry arcades of the Claudio Aqueduct was modeled through the DEM in order to investigate the seismic capacity, to detect the expected failure mechanism, to identify the influence of the existing damage and, finally, to propose and diagnosis effective strengthening solutions.

The out-of-plane and in-plane analyses were performed by means of pushover and pulse approaches applied on, respective, transversal and longitudinal sections of the investigated aqueduct. Seismic capacities and failure mechanisms obtained by both approaches were in good agreements correspondingly for both actual and reinforced states of the sections. Exception was only the results of out-of-plane analysis obtained for the transversal section without reinforcement, which demonstrated highly brittle behavior with extremely low value of response ductility under pulse signal. In this case, the pulse and pushover results differ significantly in form of maximum values of acceleration and ultimate displacement that can be explained by instantaneous character of pulse signal and absence of viscous damping. This phenomenon should be studied in the future researches.

The actual state of damage of the stone blocks, that was surveyed and explicitly modeled, proved to strongly affect the failure mechanism and the resulting seismic capacity. Consequently, proposed potential retrofitting measures were intended to provide the structure with more homogeneity and increase its resistance to the seismic loads. In this connection, the characters of main failure mechanisms of the analyzed aqueduct sections transformed from local to more global after their reinforcements. Like for the transversal section it shifted from failure of the upper channel to global overturning around the base hinge, and for the longitudinal section the local failure governed in the last pillar altered to a global mechanism involving all the structural elements.

## 6 Seismic assessment of the Monastery of Beata Antonia

### 6.1 Introduction

The monastery of Beata Antonia is located in the city center of L'Aquila in Italy. The monument represents an example of the cultural heritage of XIV-XV centuries. During its long history the building of the monastery was modified several times and exposed to earthquakes frequent in that area. Moreover the last significant earthquake happened in 2009 with 6.3 Mw magnitudes and caused essential damage to the monument and its precious frescos (Figure 6.1). The church has serious cracks that affects the façade, with a situation close to the collapse, the hall and choir elements and the central nave (“Complesso Monumentale E Monastero Della Beata Antonia” 2017) (“Monastero Della Beata Antonia” 2010) (Figure 6.2).



**Figure 6.1** 15th century frescos in the Monastery of Beata Antonia

The chapter contains seismic assessment of the monastery by means of DE model using UDEC software. A 2D model was created representing the actual state of the monument in order to analyze the current safety level. The analyses were performed by means of several computational strategies including quasistatic and dynamic approaches. After installation

of potential interventions the analyses were repeated. Critical review of the modeling results is presented below.

## 6.2 *Historical survey*

The monastic complex was established in 1349 and initially it comprised a monastery and a hospital. The isolation of Beata Antonia, which was the actual monastery, preserved the historic architectural system presented by a rectangular form surrounded by four structures around a cloister. It contains two porticos of 14th-century, from the east and west, and the fifteenth-century sides with church and portico, from the south. (Figure 6.3) The last part will be studied in the present work.



**Figure 6.2** Current view on the Monastery of Beata Antonia

During its time, the complex was subjected to 2 major modifications: in the 1800s it was demolished an arches and the medieval bridge that united monastery to the building of the Conservatory of Music, formerly the hospital. While, in 1941 the northern wing of the cloister was demolished for the realization of the artery of Via Sallustio. Later on it was replaced in the 1960s by a multi-story building without any architectural character. The stone facade of the church dates back to the 14th century and is characterized by a simple portal, which lunette has a painting with S.Francesco, receiving stigmata. The architectural body of the church stretches along Sassa Street. The interior has a rectangular form with massive vaults resting on Renaissance capitals. The space of the church is divided by a partition wall into two distinct environments: the one reserved to the nuns and the other, the front, to the faithful. The chorus entirely frescoed and composed of 97 stalls, is a work of Milanese masters from 1516. (“Complezzo Conventuale Della Beata Antonia , l’Aquila” 2006)

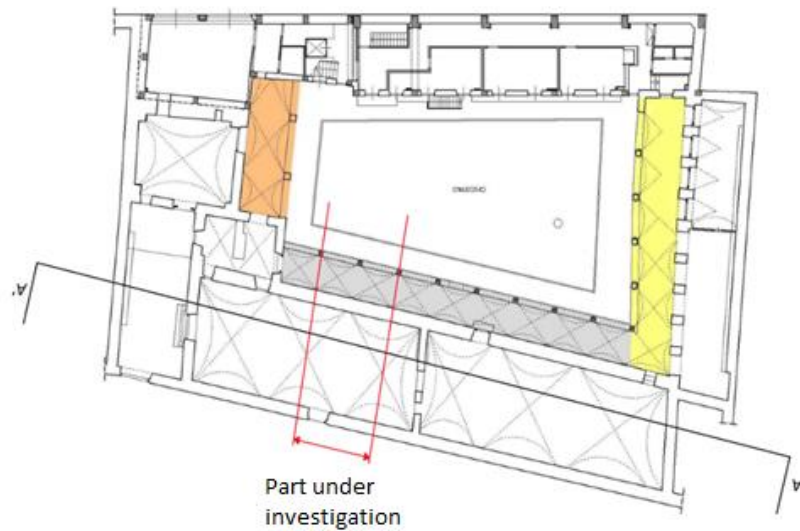


**Figure 6.3 Plan of the Monastery of Beata Antonia**

A current reuse project is intended to allocate the three historical wings of the complex to the headquarters of the Faculty of Religious Sciences, restoring and recapturing historic environment. The northern side, instead, is expected to be replaced with another well-built edifice in the urban context, which will host the L'Aquila Music Associations and also include a small auditorium for concerts. (“Monastero Della Beata Antonia” 2010)

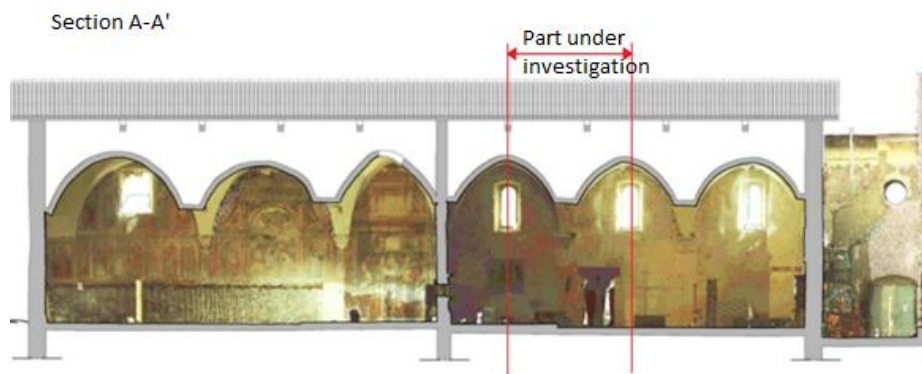


**Figure 6.4 Longitudinal cross-section of the Monastery of Beata Antonia**

## 6.3 DE model

### 6.3.1 Geometry and mechanical properties

The part under the investigation is the church of the monastery, which present the most valuable cultural part of the complex as well as the most vulnerable according to the last damage observation. The longitudinal cross-section (Figure 6.4) of the investigated part demonstrates an archy ceiling with the wooden roof construction.

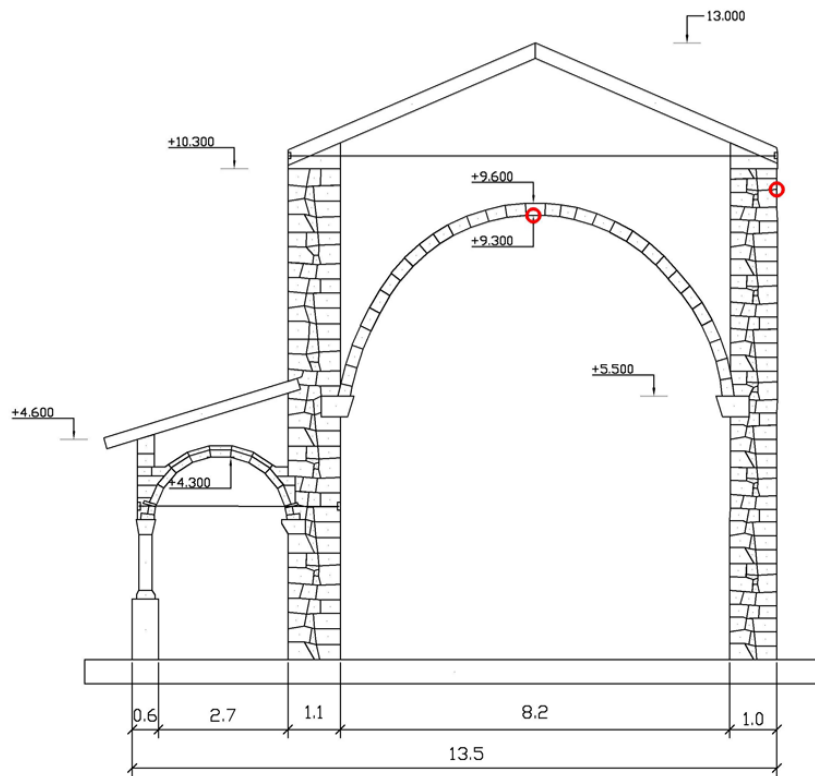


**Figure 6.5 Geometry of the model**

The model represents a transversal section of the 14th century structure, composed by a main building with stone walls maintained a vault and an attached portico (Figure 6.5). The section is about 13 meters high and about 13.5 meters wide. The model consisted of about 300 rigid blocks representing the real masonry pattern. Two main control points for the

analysis have been chosen on the top of the wall and on the main arch keystone.

The mechanical parameters used in the model depend on the type of the material and an effective thickness as illustrated in the Figure 6.6. Cohesion and tensile strength parameters have only been attributed a range of variability, as they will be subsequently characterized by appropriate model validation.

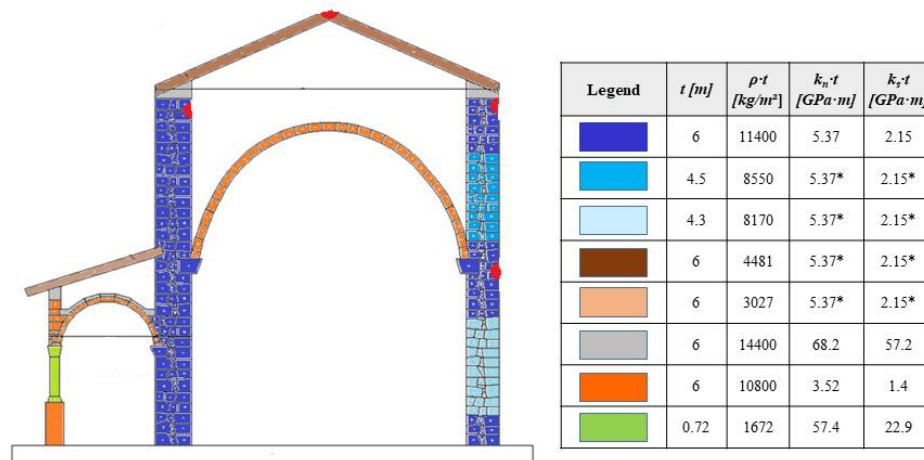


**Figure 6.6 Adopted mechanical properties for the blocks and joints**

- Irregular masonry (in three different shades of blue): walls both the exterior and the interior with thickness of 1 meter and double facing. The masonry pattern can be traced back to the main typical L'Aquila typology, with the average size of blocks of 15-25 cm in diameter. The mortar can be classified as the M4 - M5 class, the normal and shear stiffness of joints was equal to average value for all these blocks.
- Concrete elements (in grey): beside the roof beams underneath the main and secondary roofs, and the roof cover of the small arcade. To reproduce the curvature of the element it was necessary to divide it into blocks, to the corresponding joints high values of cohesion and tensile strength were assigned, in such a way as to simulate the continuous elastic behavior of the material.
- Brick elements (in orange): both vaults and below the column. The vault of the porch has a smaller thickness, since it made of a stretcher course, than the main one, where the arrangement is in a rowlock course.
- Stone elements (in green): column, the investigated section has an equivalent of two columns.

- Mixed materials (in two shadows of brown): roof structure and covering (roof beams, waterproofing, roof tiles, etc), which in model represented as heterogeneous material with various parameters for main and secondary roof, depending on their composition, with elastic joints in order to simulate the roof-wall connections.
- Metal elements (horizontal black lines): tie rods, which are represented by special structural UDEC build in elements, with only tensile strength and no compression.

### **6.3.2 Boundary conditions and loading**

The numerical analyses were carried out in the transverse section of the monastery, which was chosen as the most vulnerable part of the structure to the earthquake loading.

The ground in the model was implemented by base block, which is not a part of the building but used exclusively for representing the bonding ground condition. In red, the control point using in the subsequent analyzes are highlighted (Figure 6.5).

All the analyses were carried out in two stages: first, each model was brought to equilibrium under gravity force; and then, an external load was applied representing seismic action. Depending on the type of approach the loading procedure is following:

- for quasistatic approach - increasing horizontal acceleration at the centroids of each block;
- for pulse approach - horizontal acceleration at centroids of each block during short period of time;
- for seismic approach - velocity time history at all the nodes along the model base.

### **6.3.3 Validation of the model**

In order to validate the UDEC model, sensitivity analyzes on the cohesion and the tensile strength of the joints were conducted. The behavior of the joints as usually was described by Mohr-Coulomb criteria. The range of the values was about 10% for both tensile strength and cohesion. Based on current experience for historical dry-stone masonry, the value of the tensile strength for sensitivity analysis on cohesion was 0.1 MPa, while those of cohesion – 0. The validation of the model was performed by means of pushover analysis and results are reported the following:

---

- with values of tensile strength less than 0.1 MPa and any value of cohesion, the model of the monastery collapsed already under the action of gravity loads;

- for fixed value of tensile strength at 0.1 MPa and variable values of cohesion (from 0.1 to 0.3 MPa), as well as for fixed value of cohesion at 0 MPa and variable values of tensile strength (from 0.2 to 0.4 MPa), the model was stable under the gravity load, but with very scatter values of capacity parameters. In particular, with increasing of tensile strength the value of ultimate displacement  $u_d$  and maximum acceleration  $a_0$  increased, respectively, by almost 10% and 24% (in compare to the average values).

In conclusion, the value of tensile strength equal to 0.1 MPa and 0 MPa for cohesion was chosen to use for the joints in wall and arch elements. It was the lowest values for which the structure was able to support its weight and which represented the parameters of low-strength materials of historical irregular masonry.

#### **6.3.4 Retrofitting measures**

Based on the validation procedure of the model (and following seismic assessment of the actual state of the monument), the failure under horizontal load appeared firstly at the main arch. The several options of traditional arch retrofitting techniques were selected and analyzed by mean of seismic performance.

In order to improve the seismic resistance of the masonry section, the following intervention measures were applied and modeled separately (Figure 6.7):

- a) Tie rod: installation into the base of the main arch an additional metal tie rode to fasten the thrust, with the same properties as those already presented;

- b) Backfill of the main arch: addition of the bricks on the top of the main vault (mass density 1800 Kg / m<sup>3</sup>, modulus of elasticity 1500 MPa), with 50 cm of effective thickness, tensile strength of 0.2 MPa and cohesion of 0;

- c) Combined measure - backfill and extra tie rod of the main arch.



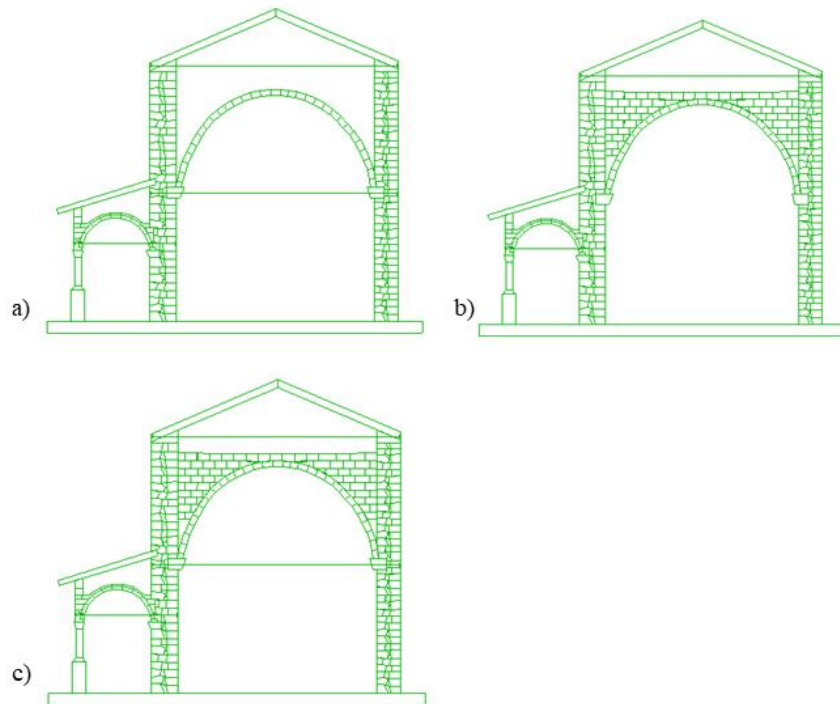


Figure 6.7 Models of the retrofitted states of the monastery

## 6.4 Quasistatic analysis

The quasistatic analysis was performed on the transversal section of the monastery of Beata Antonia. The results were obtained for the actual and retrofitted states of the monument, accompanied with their respective comparison. 2 different computational techniques were used for analyzing of the actual state, which main differences were discussed earlier in the Chapter 3.

### 6.4.1 Actual state

Push-over analysis on the current state of the monument was performed on the transversal section of the monastery based on 2 numerical procedures.

The capacity curves obtained by both pushover approaches showed in the Figure 6.8. The ascendant branches of the graphs practically coincided demonstrating similar results in terms of maximum acceleration level that was about 0.07g. The second parts of the pushover curves showed

similarity in the descending angle but significant difference in the end of the analysis. With the procedure#1 an ultimate displacement was obtained equal to 0.45 m, while with the procedure#2 the analysis was interrupted in the moment of collapse of the main arch.

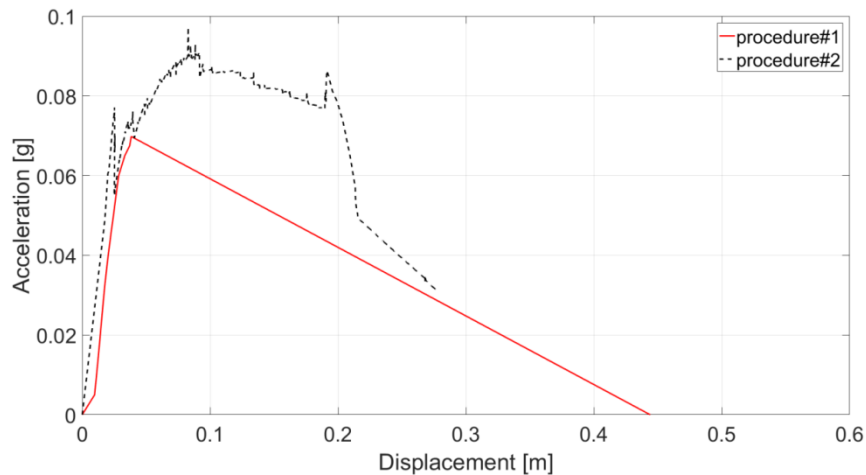


**Figure 6.8 Pushover curves obtained by 2 procedures**

Hereby, the failure mechanisms obtained by both procedures had similar characters (Figure 6.9). A collapse was formed locally with mechanism governed in the main arch, while the walls displayed an elastic-like displacement. Thus, from both approaches it is notable that the main arch was the most vulnerable element of the investigated system.

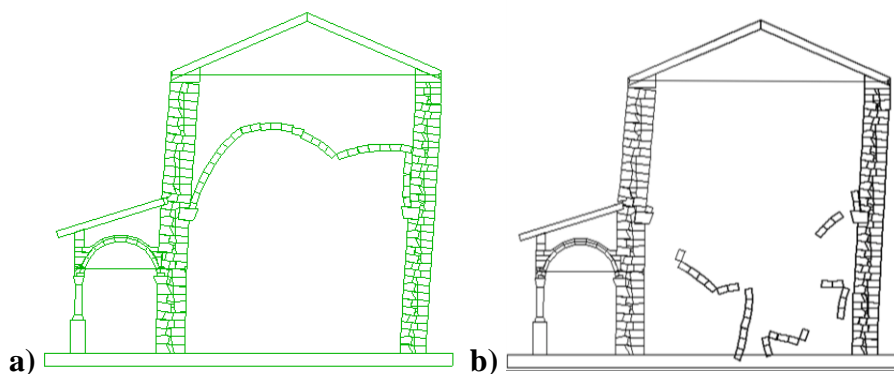


**Figure 6.9 Ultimate states obtained by different pushover techniques a) procedure#1 and b) procedure#2**

Finalizing the results obtained from the both procedures, it was chosen to use the procedure#1 for further analysis, as it demonstrated more stability during the calculations.

### 6.4.2 Retrofitted states

The quasistatic approach was used in order to identify the best intervention solution among proposed traditional techniques and to estimate their effectiveness in improving the structural seismic performance.

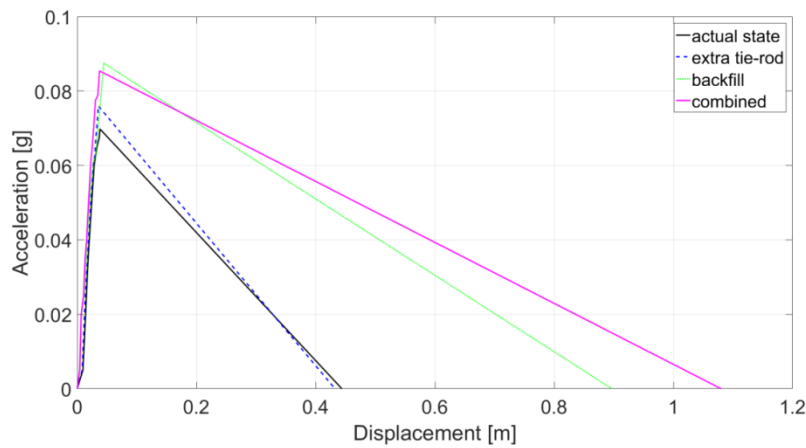


**Figure 6.10 Pushover results of the retrofitted states**

Figure 6.10 shows resultant pushover curves of the retrofitted models. It is notable that only insertion of the extra tie-rod in the main vault did not change significantly the structural capacity. Whereas separate installation of the backfilling on the top of the main vault has already improved the global capacity: maximum bearing acceleration became 0.85g and ultimate displacement 0.9 m. However, the best results were obtained with the combined retrofitting measure, which enhanced significantly both parameters in compare with the actual state: acceleration increased by 19% as only with backfilling measure and ultimate displacement almost tripled and became 1.1 m.

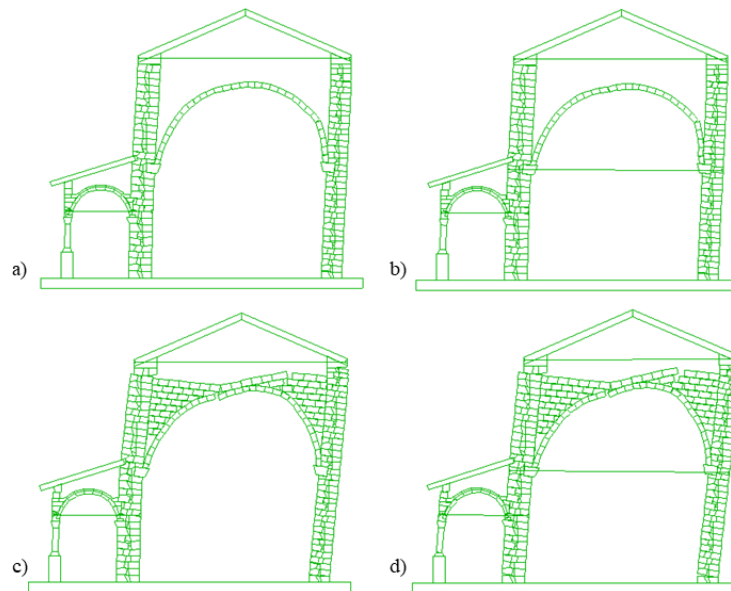


**Figure 6.11 Various ultimate states depending on the intervention a) actual state, b) extra tie-rod, c) backfill, d) combined**

The Figure 6.11 demonstrated the ultimate states of the structure depending on the retrofitting techniques. In compare with the actual state it is notable that intervention measures influenced the structure and its behavior in a different way, except insertion of an extra tie-rod, which repeated the failure mode as it was with local failure in the main arch. Instead, backfilling and combined interventions improved significantly the failure behavior, which became more global and involved not only the main vault but also external walls (Figure 6.11c,d). With the last two intervention techniques the structure demonstrated combined work of all the structural elements together that significantly improved seismic resistance of the entire system.

## **6.5 Dynamic analysis**

Dynamic analysis of the monastery was performed based on 2 approaches – step pulse signal and seismic excitation. The first part of results has been obtained based on model of actual state of the monument. While for the second part as a retrofitted model was chosen the best intervention option based on pushover analysis results that was combined measure -

backfilling and extra tie-rod of the main vault. Results of the dynamic analysis are presented below.

### 6.5.1 Pulse excitation

The step pulse analysis was performed by applying acceleration signal to centroids of each block. The parameters of the signal differed by range values of the acceleration, duration and direction of the load. The model was subjected to a range of step pulses with acceleration varying from the initial acceleration obtained in connection with the pushover results up to 0.6g. After applying of a signal the analysis was continued for about 3 second in order to assess the dynamic behavior of the system during and after application of the pulse. All the analysis was performed without implementation of an artificial damping. The load was employed horizontally in both directions, from left to right and vice versa, for the actual state analysis and only in one direction for the retrofitted state. In order to determine the pulse magnitude - duration failure domain for each pulse accelerations the analysis was repeated increasing by small steps the duration of the signal until collapse of the structure occurs. In this way, the safe – unsafe threshold of the acceleration magnitude was determined for each pulse durations.

#### 6.5.1.1 Actual state

The analysis on the actual state of the monastery was performed by applying pulse signal in both directions, as was stated before. The direction of the strongest signal of a possible earthquake was hard to predict precisely, thus the analysis was also performed in order to identify the influence of the load orientation.

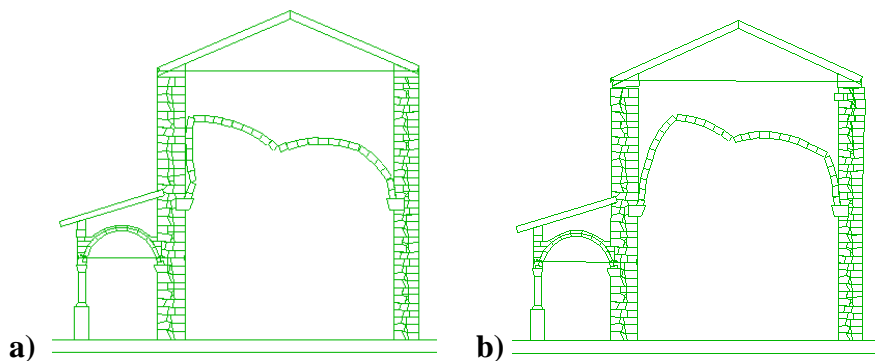
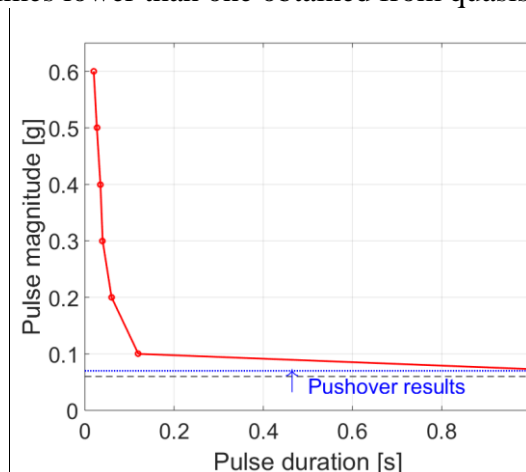


Figure 6.12 Failure mechanism of actual state depending on the pulse direction: a) from right to left and b) from left to right

A range of analysis was performed in both directions and influenced differently the structural response. As can be seen in the Figure 6.12 in both cases failure occurred by mechanism in the main arch with slight difference in the arch response. That difference can be explained by existence of the portico on the left part, which played role as a ‘restrain’ preventing evolution of the horizontal displacements. Thus, the loading from left to right governed considerably higher displacements and it was chosen as the definitive loading direction for pulse analysis of the monastery.

Results of the pulse analysis (left to right direction) on the actual state of the monastery are shown in the Figure 6.13 in the form of failure domain. The magnitude required to cause the structure collapse decreases with increasing of pulse durations, approaching asymptotically the magnitude necessary to initiate the motion, which was about 15% lower than obtained from pushover analysis. In the region below 0.06g, the response of the structure did not exhibit any damage, that the structure subjected to these pulses acted as a rigid body and simply followed the ground motion. The region between 0.06g and the curve corresponded to conditions of recovery, whereby the structure survived indefinitely. Finally, pulses in the region above the curve led to failure. Note that the monastery failure was defined here as the local collapse of the main vault. The maximum displacement of the wall control point at the failure was equal to 0.03 m, the value 10 times lower than one obtained from quasistatic analysis.



**Figure 6.13** Failure domain of the actual state of the structure subjected to step pulse

In Figure 6.14 it is displayed a distribution of velocity in the structure after a step pulse loading. As soon as structure staid only under gravity load, at first all the blocks were continuing moving in the load direction (Figure 6.14a). In few seconds velocity dissipated at major part of the blocks and remained only in the main arch. A mechanism created (Figure 6.14b,c) which further brought system to a failure.

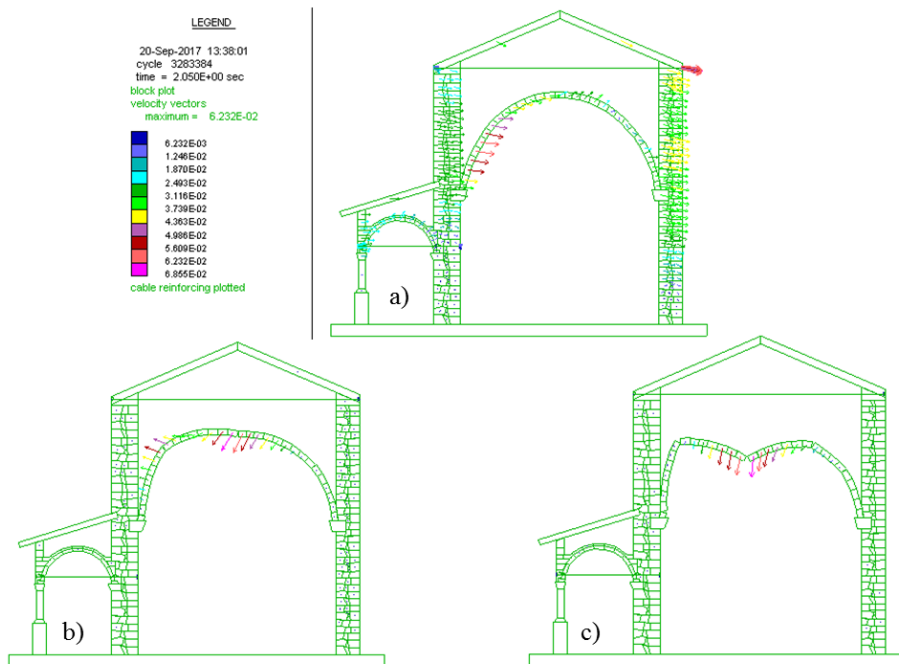


**Figure 6.14 Distribution of velocity and failure mode during applying pulse loading at actual state**

### 6.5.1.2 Retrofitted state

As was mentioned earlier a model of combined retrofitting was chosen for performing analysis under pulse signal.

In the Figure 6.15 demonstrates results of the pulse analysis on the retrofitted state of the monastery, which also represented in the form of failure domain. In the region below 0.12g, the response of the structure did not exhibit any damage that was about 25% higher than pushover analysis results. The region between 0.12g and the pulse curve corresponded to conditions of recovery, whereby the structure survived indefinitely with minor damage. Finally, pulses in the region above the

curve led the structure to collapse, which in retrofitted case was governed by global mechanism. The maximum displacement of the wall's control point was 0.7 m that 35% lower value than the one obtained from quasistatic analysis.

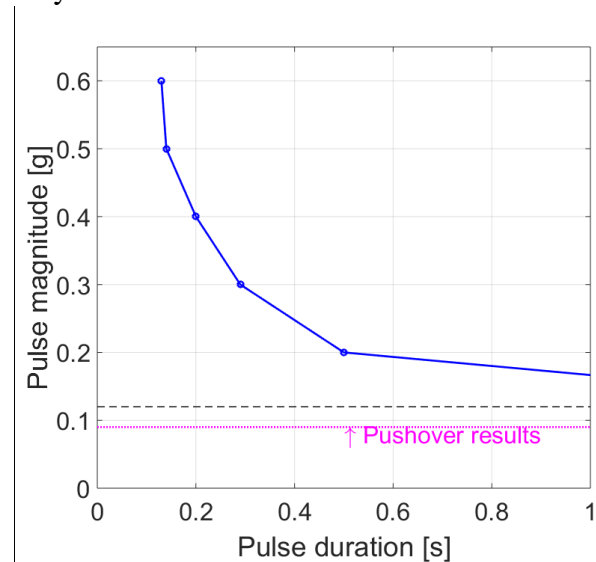


**Figure 6.15 Failure domain of retrofitted state of the monastery subjected to step pulse**

A distribution of velocity in the structure after a step pulse loading is displayed in Figure 6.16. As soon as structure staid only under gravity load, at first the blocks were continuing moving in the load direction especially on the upper part, where forces of inertia are higher (Figure 6.16a). In few seconds, when the structure was returning on its position, the velocity value decreased in major part of the blocks, except those placing on the top of the main arch (Figure 6.16b). The last snapshot demonstrates a failure of the structure governed by a collapse of blocks belonging to the main arch (Figure 6.16c).



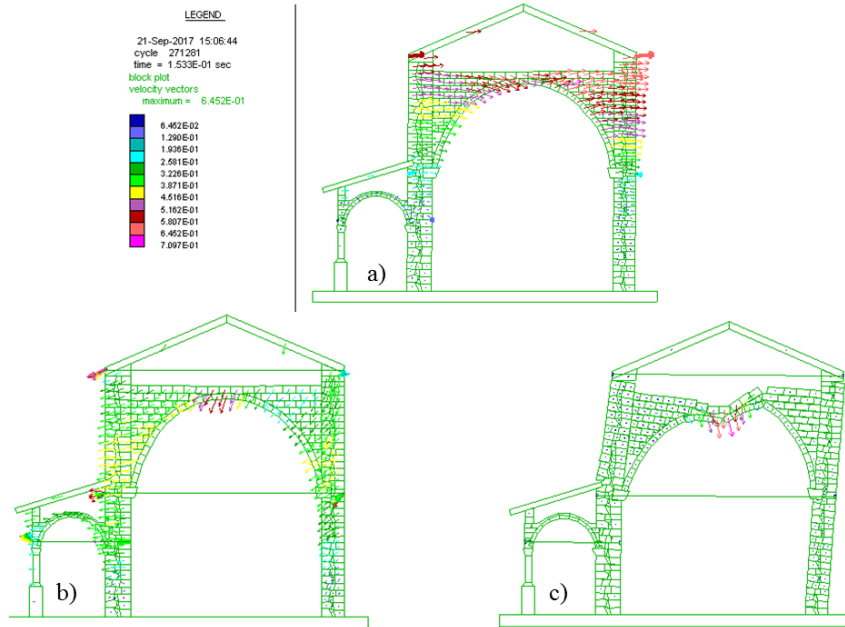


**Figure 6.16 Distribution of velocity and failure mode after applying pulse loading of the retrofitted model**

Finalizing the results of the pulse analysis obtained on the retrofitted model it is obvious that the seismic resistance of the structure improved considerably after combined intervention. In terms of failure domain the curve shifted significantly by rising of the pulse durations, which increased from 3 to 10 times (Figure 6.17). This phenomenon means enlargement of the safe threshold of the acceleration magnitude, after which the structure remained in stable condition.

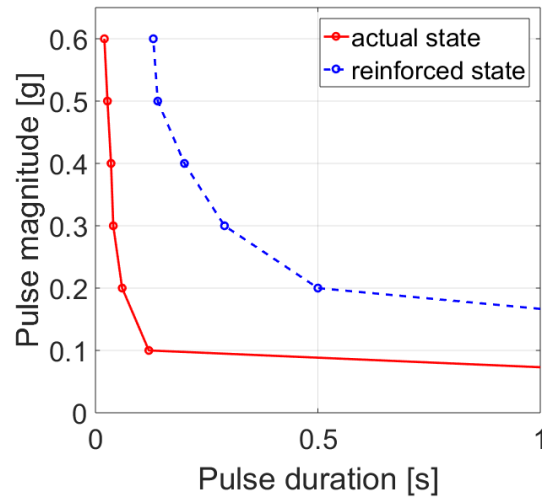


**Figure 6.17 Failure domain of both investigated states of the monastery subjected to step pulses**

From the Figure 6.18 it is notable an improvement of the retrofitted system also in case of failure mechanism. Local failure of the actual structure, governed by collapse in the main vault, changed to a global one after combined intervention. In this way, resistance of the retrofitted system increased by uniting its structural elements in the global behavior. The maximum horizontal displacement of the wall after retrofitting increased almost in 20 times in compare with its actual state.

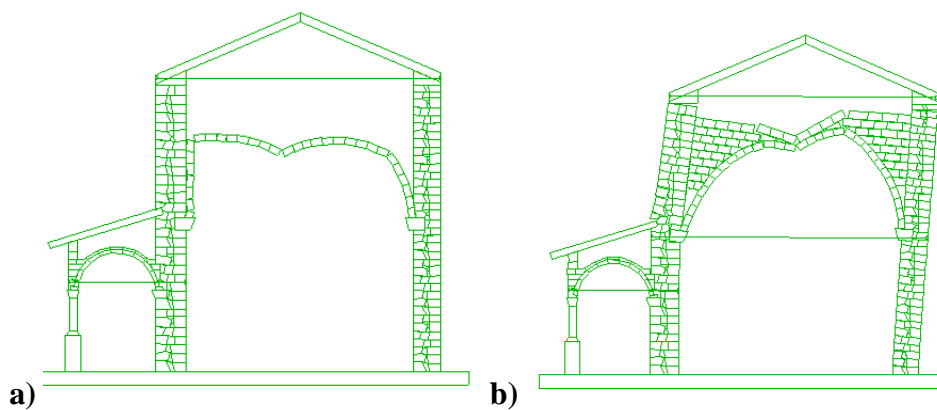


**Figure 6.18 Failure mechanisms of a) actual and b) retrofitted states of the monastery**

### 6.5.2 Seismic excitation

Dynamic analysis under seismic excitation was performed on the actual and retrofitted state of the monastery, similar with the pulse step analysis. Seismic signals were applied to the investigated models in both vertical and horizontal directions to investigate their influence in responses together with failure mechanisms.

Seismic signals recorded during 2009 L'Aquila earthquake with the main shock rated 6.3 on the momentum magnitude scale have been selected. The records differed by characteristics such as acceleration amplitude, predominant period, and frequency in order to investigate how they affect the stability of the monastery. Two stations in the radius of 10 km from the monastery were chosen for the analysis (Figure 6.19). The closest station to the epicenter and the monastery was IT.AQK, which located in L'Aquila city (B\* ground type, EC8) with the maximum recorded PGA 3.46 and 3.55 m/s<sup>2</sup>, respectively in horizontal and vertical orientations. The station with the strongest record in terms of PGA was MN.AQV (Aquila Castello) for B ground with PGA 6.44 and 4.86 m/s<sup>2</sup>, also for horizontal and vertical directions (Figure 6.20 and Figure 6.21).



**Figure 6.19 Location of the selected stations recorded L'Aquila earthquake 06.04.2009 ("ITACA 2.2 WG" 2017)**

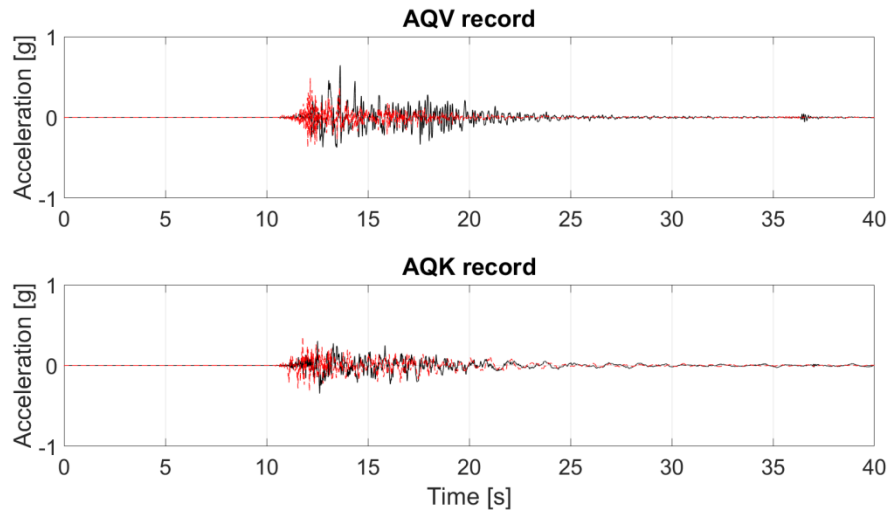


**Figure 6.20** Accelerations time histories for L'Aquila earthquake records (horizontal component – black solid line, vertical – red dashed line)

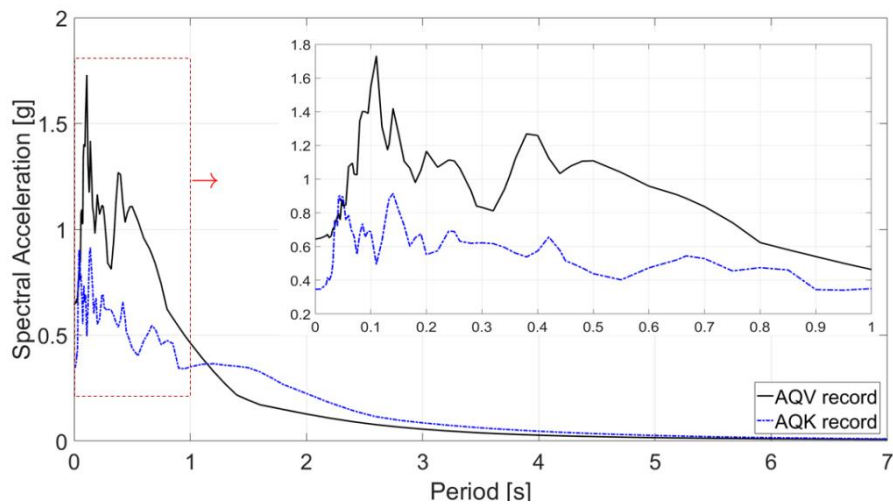


**Figure 6.21** Horizontal acceleration response spectrum for L'Aquila earthquake records

The signals were applied to the base block of the model in form of time history velocities, displayed in the Figure 6.22. The records were cut and a part with the highest amplitude duration 10 sec for each signal was used

for analysis. The implemented signals consisted of horizontal component, corresponded to the out-of-plane loading of the structure; and a vertical component to study its additional influence on the seismic response.

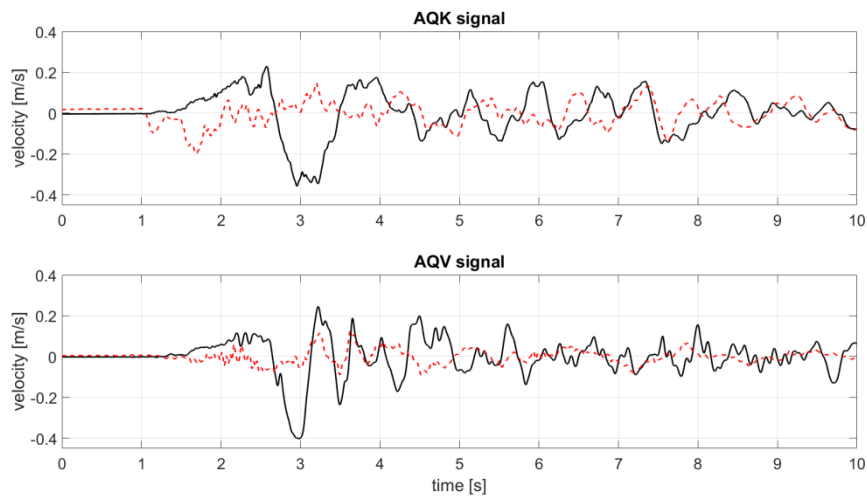


**Figure 6.22** Velocity time histories applied to the model (horizontal component – solid line, vertical component – dashed line)

### 6.5.2.1 *Actual state*

The seismic analysis on the transversal section of the monastery was performed in order to assess its seismic response and failure mechanisms. The results of the analysis are presented below.

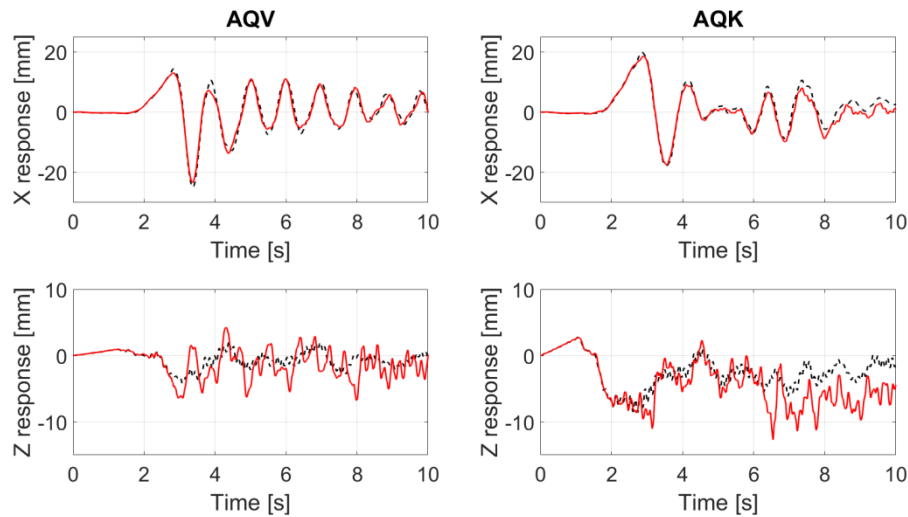


**Figure 6.23 Responses of actual state of the model under 15% AQV and 12.5% AQK records (control points: top wall – solid line, arch keystone – dashed line)**

Maximum responses of several control points preceded a failure of the structure are shown in Figure 6.23. The responses in X direction under AQV signal demonstrated more sinusoidal character for both walls and arch, while the AQK responses were less smooth. However both signals had an pulse like behavior (“ITACA 2.2 WG” 2017) and responses of both control points coincided perfectly. The responses in Z direction were significantly low then the X one whereas the level of both signals were in the same magnitude for X and Z orientation. The maximum values of responses under 15% of AQV and 12.5% of AQK stayed in the same range and were about 20-25 mm for the X axis and 6-10 mm for Z.

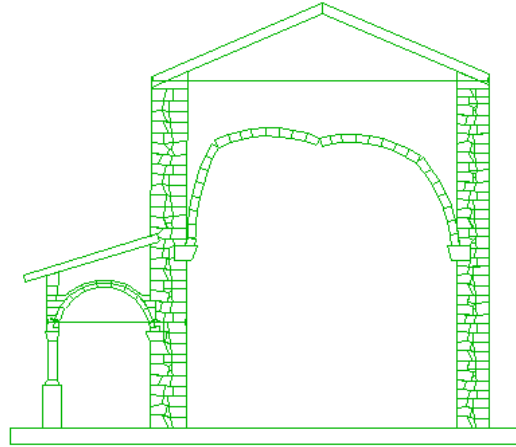


**Figure 6.24 Failure mechanism in the main vault under 15% AQK record**

The failure of the actual state of the monastery occurred by local mechanism governed in the main vault, without any visible damage in the other part of the structure that is demonstrated in the Figure 6.24.

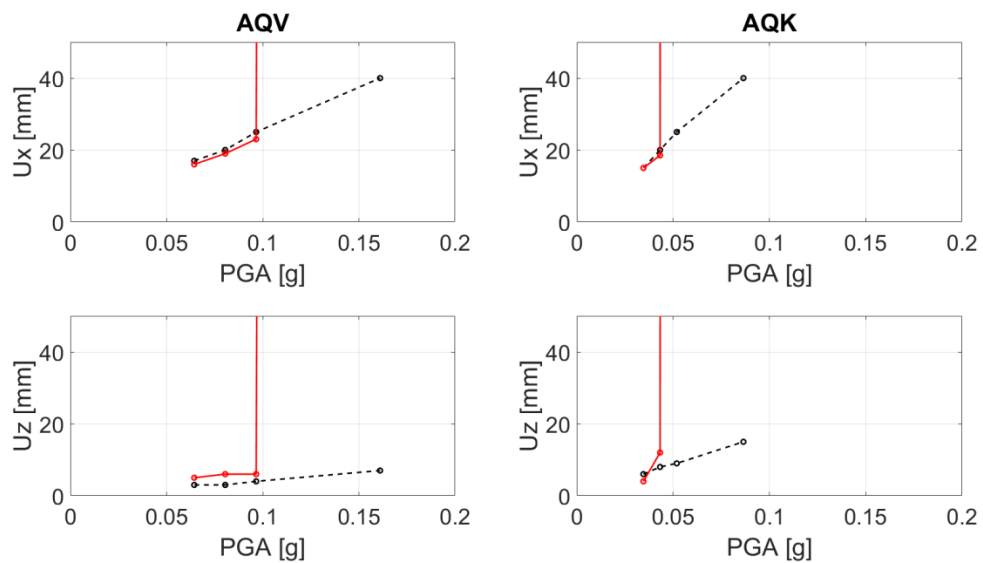


**Figure 6.25 Maximum responses of the actual structure under scaled L'Aquila earthquake records (control points: top wall – dashed line, arch keystone – solid line)**

The graphs Figure 6.25 displayed that there were certain level of PGA values where collapse of the main vault occurred, while the walls remained standing. Below this values all the responses increased linearly as the PGA increased, with exception on the arch response, which collapsed suddenly under 0.05g of AQK record and 0.16g of AQV record. The wall demonstrated different response behavior under various signals, as it was smoother under AQV instead of rapid grows of the x-response under AQK signal. However, the actual state of the monastery demonstrated very brittle behavior under seismic signals, especially its main vault, which failure was the first.

### 6.5.2.2 Retrofitted state

The dynamic analysis on the monastery's section was repeated after application of the combined retrofitting in order to assess improvement of the seismic response and collect failure modes.

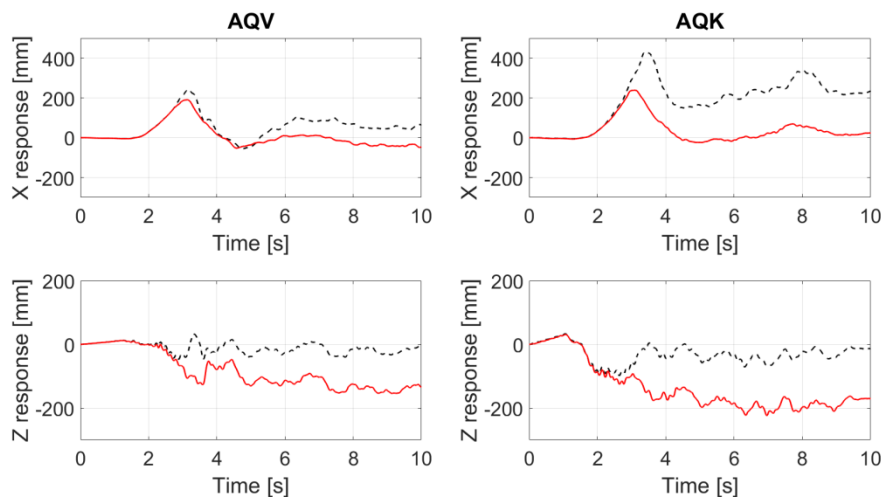


**Figure 6.26 Responses of the wall and arch of retrofitted system under 200% AQV and 150% AQK scaled earthquake records (control points: top wall – dashed line, arch keystone – solid line)**

From the graphs Figure 6.26 it is clearly seen that the responses of the left and the right external walls differed significantly in x-axis direction. Due to asymmetry of the monastery structure, the left wall 'confined' with the porticos, thus its horizontal response was considerably low in compare with the other side. The response of the key stone under 100% AQK record was in maximum range of 100 mm in y-axis direction. It is notable



that in the 2<sup>nd</sup> second the arch shifted and stayed stable in this position until the end of the analysis.

The graph of the responses of the top wall and the arch keystone on both x and z directions are shown in the Figure 6.26 and represent the responses preceded a failure. It is noticeable that the wall and the arch responses coincided at the beginning of the signals and after a pick load at 2 sec differed significantly. It is also notable high residual displacements of both wall and arch structural elements of about 0.2 m in X and Z directions, respectively. The maximum horizontal response of the arch keystone was the same for both signals, while value of the wall response under 150% AQK record was doubled in compare to 200% AQV signal and equaled to 400 and 200 mm, respectively.

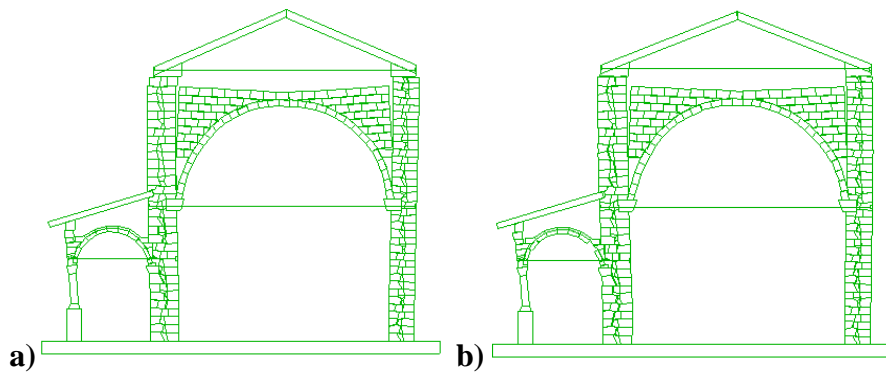


**Figure 6.27 States of the retrofitted structure after a) 150% of AQK signal and b) 200% of AQV signal**

The state of the structure after it was explored to the 150% of AQK signal demonstrated significant buckling of the external walls and the arch, with their residual displacement, as was mentioned earlier (Figure 6.27a). Next increase of the applied signal caused partial structural collapse. The failure of the retrofitted arch of the monastery appeared on the 3<sup>rd</sup> second of the 175% scaled AQK signal, while the external walls withstood this loading suffering severe damage with partial failure due to disaggregation.

The last state of the structure after 200% of AQV record demonstrated severe damage in all the structural elements, including tilting of the column with disaggregation of the external wall, both of the left part and separation of the backfilling from the right wall together with some sliding of the entire roof part. However, there was not significant damage

or displacement on the main vault. (Figure 6.27b) Consequently increasing of the signal up to 225% brought structure to collapse mainly due to disaggregation of the walls. In this connection, noticeable that AQK and AQV signals caused collapse of the monument in two different failure modes.

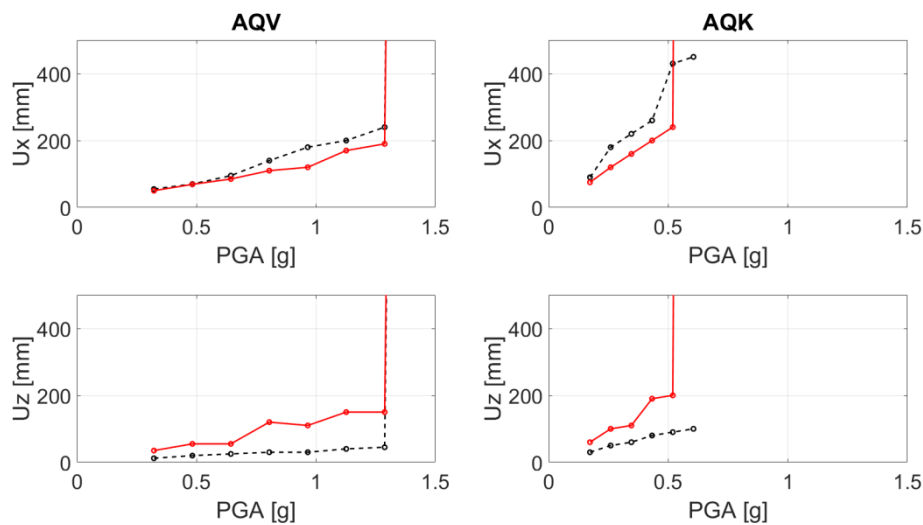


**Figure 6.28** Maximum responses of the retrofitted structure under scaled L'Aquila earthquake records (control points: top wall – dashed line, arch keystone – solid line)

Two seismic records of L'Aquila earthquake were applied to the model with combined retrofitting scaled if needed up to a specific level of seismic intensity in order to cause collapse. The influence of the acceleration level and pulse period in the seismic response was investigated. Figure 6.28 shows that the maximum displacement of the wall and main vault in both directions increased as the PGA increased. After certain PGA values collapse occurred or in the main vault (0.6g of AQK signal) or in all the structure (1.4g of AQV signal). Larger displacements especially in X direction were formed under AQK record, which has two predominant periods 0.05 and 0.14 s, while under AQV record with 0.1 s predominant period they were twice less at the prefailure loadings. In this connection, it can be stated that out-of-plane response of the main vault was crucially affected by high-frequency earthquakes even after its retrofitting.

However, the total response of the monastery after its combined retrofitting improved significantly with increase in the maximum values of PGA and displacement in about 10 times. (Figure 6.29) It is also notable that the slope of the graphs before and after retrofitting remained constant. However, in general no significant influence of the seismic records in Z direction has been recorded on the structural response, even though both records had essential vertical component.

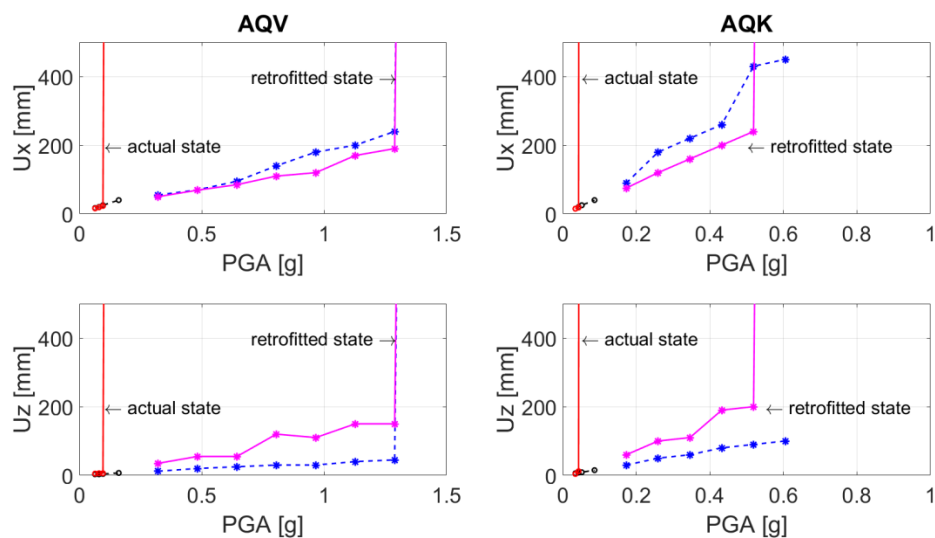


**Figure 6.29** Maximum responses of the actual and retrofitted states under scaled L'Aquila earthquake records (control points: top wall – dashed line, arch keystone – solid line)

## 6.6 Summary

The studied monastery of Beata Antonia locates in the city center of L'Aquila and represents an example of the 14<sup>th</sup> century architectural and cultural heritage. Its transversal section was investigated by means of DEM to assess the seismic behavior of its actual state and after potential retrofitting. The analyses were performed using quasistatic and dynamic approaches including pushover, step pulse and seismic analysis.

The current state of the structure presented high vulnerability to seismic actions because of the collapse in the main vault exhibited under minor horizontal loads. With retrofitting of the system contained insertion of an extra tie-rod and backfilling of the main vault the seismic response of the structure improved significantly in form of increasing maximum bearing

acceleration and ultimate displacement together with changing of the failure character to a more global.

The results of pushover and pulse analysis demonstrated good agreement in terms of maximum acceleration for both actual and retrofitted models and of maximum displacements mainly for retrofitted one. The ultimate displacement of actual state obtained by pushover analysis was considerably higher than by the pulse one, that can be connected with instantaneous nature of the pulse load or with damping influence that should be further studied.

For the seismic analysis the character and value of responses differed significantly between the signals, in spite of fact that both signals had pulse like character and were recorded during one earthquake event. Generally, it can be stated that out-of-plane response of the main vault of the structure was crucially affected by high-frequency earthquakes even after its retrofitting. While in general for performed dynamic analysis of the monastery, the trend was that with increasing of the magnitude of the dynamic input, either for pulse or seismic analysis, the failure mechanism of the structure changed from the brittle failure of the main vault to the global collapse of all the system involving also disaggregation of the external walls. The last phenomena appeared mainly for the retrofitted state of the monastery.

## 7 Concluding remarks

The overall objective of the dissertation was to establish applicability of Discrete Element Method for the assessment of the seismic behavior of architectural heritage structures. The understanding of the earthquake responses of historical buildings, either archeological structures or ancient monuments, is a prerequisite for rational preservation of heritage. Historical masonry structures cannot be correctly studied by existing guidelines developed for analyzing modern constructions essentially based on conventional methods of structural mechanics. Masonry is composed of two very different materials, i.e. the masonry units and a joining material, which often have already exhibited degradation due to long lifetime period or past external impacts. Masonry exhibits a heterogeneous behavior due to its discontinuous nature, its deformations and failure modes are strongly dependent on the joints. All of these points make DEM suitable for analysis of masonry structures subject to strong ground motions.

The code UDEC was used in this dissertation due to its advantages and capabilities provided by professional software, such as: the possibility of using rigid blocks and build-in constitutive laws for joints, output facilities (an extensive plotting facility is built directly into code), a powerful built-in programming language (FISH) that enables the definition of new variables and functions.

Based on the DEM formulation, automatic routines were developed and successfully integrated in the UDEC software in order to perform seismic assessment of architectural heritage masonry buildings. The first algorithm contained semi-automatic preprocessor for creating accurate block representation geometry, which is essential feature in DEM for reliable simulations. The second algorithm was developed for performing pushover analysis of masonry structures based on incremental application of horizontal acceleration to block centroids. The first part of the analysis proceeds until point of last static equilibrium, which defines maximum bearing acceleration, and the second part continues up to point of unstable equilibrium, which corresponds to ultimate displacement. In this connection, the results of pushover approach are represented in form of capacity curve. Another implemented routine aims at automatizing dynamic analysis based on step pulse excitation. The algorithm applied various pulse parameters to centroids of every block of the system combining the results in order to obtain the pulse amplitude – duration failure envelope of the structure. The last algorithm is used for seismic

analysis based on applying time histories signals to the model base simulating an effect of a real earthquake excitation.

All the aforementioned capabilities of the DEM were explored in the dissertation by referring to architectural heritage monuments. Application of the DEM was discussed on 3 case studies: the Colosseum and the Aqueduct Claudio in Rome and the monastery of Beata Antonia in L'Aquila. All the monuments located in Italy in seismic prone zone, thus their seismic assessment is an essential topic. The Colosseum and the Aqueduct Claudio were studied under pushover and pulse analysis, while the study of the monastery was performed using all three implemented analysis: pushover, pulse and seismic excitation, since there was a record of recent earthquake in L'Aquila.

Generally, pushover and pulse analysis demonstrated good agreement of the results in form of both maximum acceleration and ultimate displacement. Except some cases of brittle collapse under pulse analysis, due to sudden nature of the load or to the lack of damping that provide significantly lower values than the pushover ones. Interestingly, for seismic analysis, the character and value of the responses can change significantly between the signals, in spite of fact that both signals were recorded during one earthquake event. It can be stated that response of the investigated structure is strongly affected by the parameters of earthquake signals, such as frequency and amplitude.

The study of the Colosseum was mainly concentrated on the south-east part of the external wall, which in 1807 was restored by Stern. The research was focused on the causes that brought the monument to this restoration based on extensive historical survey and numerical simulations. The analysis performed with UDEC confirmed the seismic nature of the Colosseum structural damage and the inappropriate interventions preceding the earthquake of 1806, which endangered the monument even more. The results of this investigation reaffirm the capability of DEM as a tool for investigation of past events and damage causes.

Furthermore, the performed seismic analyses led to evaluate the potential reinforcement measures and assess their efficiency as shown in the two case studies: the Aqueduct Claudio and the monastery of Beata Antonia. These features of DEM can substantially contribute in designing of appropriate strengthening measures that is very important in case of heritage structures.

DEM is shown to be a powerful tool for safety assessment studies and design of retrofitting measures. However, in spite of all the advantages and benefits brought by this methodology, there are inherent shortcomings that need to be pointed out, such as:

- Time-consuming calculations due to the small time step required by the condition stability of explicit integration algorithm (time step was about  $10^{-5}$  sec during the analyses performed in the present work; for example, in case of monastery of Beata Antonia model consisting of about 300 blocks, the CPU time for pushover and pulse analysis was about 1 hour, while for time history analysis 3-4 hours due to use of model containing both rigid and deformable blocks);
- DE codes rely on point contacts and therefore a large number of contact points are required for a rigorous stress analysis across a joint.

Moreover, for future research connected with usage of DEM for seismic assessment of historical masonry, several features can be indicated such as:

- implementation of more elaborate constitutive models for joints representation in the DE codes to improve its performance in seismic analyses, by taking into consideration the complex post-peak behavior of masonry;
- further research on damping calibration in order to identify relation between damping and geometry non-linearity of the DE model;
- further improvement of mesh creator allowing the automatic generation of the vector files from raster images through edge detection;
- improvement of the pushover routine to make it less sensible for possible fractional failure of the masonry;
- improvement/implementation of more integrated routines for seismic assessment with less user's impacts.

---

## References

- Alexandris, A P., E Protopapa, and I Psycharis. 2004. "Collapse Mechanisms of Masonry Buildings Drived by the Distinct Element Method." In *13th World Conference on Earthquake Engineering*. Vancouver.
- Alexandris, A P., I. N. Psycharis, and E Protopapa. 2014. "The Collapse of the Ancient Temple of Zeus at Olimpia Revisted." In *2nd European Conference on Earthquake Engineering and Seismology*.
- Asteris, P. G., M. P. Chronopoulos, C. Z. Chrysostomou, H. Varum, V. Plevris, N. Kyriakides, and V. Silva. 2014. "Seismic Vulnerability Assessment of Historical Masonry Structural Systems." *Engineering Structures* 62–63: 118–34. doi:10.1016/j.engstruct.2014.01.031.
- Azevedo, J.J., G Sincaian, and J. V. Lemos. 2000. "Seismic Behavior of Blocky Masonry Structures." *Earthquake Spectra* 16 (2): 337–65. doi:10.1193/1.1586116.
- Bakeer, T. 2009. "Callapse Analysis of Masonry Structures under Earthquakes Actions." PhD thesis. Dresden university.
- Binda, L, G Cardani, A Saisi, and M R Valluzzi. 2006. "Vulnerability Analysis of the Historical Buildings in Seismic Area by a Multilevel Approach." *Asian Journal of Civil Engineering (Building and Housing)* 7 (4): 343–57.
- Bolt, B A. 1993. *Earthquakes*. Earth Science. W.H. Freeman.
- Bui, Q.-B., T.-T. Bui, and A. Limam. 2016. "Assessing the Seismic Performance of Rammed Earth Walls by Using Discrete Elements." *Cogent Engineering* 3 (1). doi:10.1080/23311916.2016.1200835.
- Bui, T.-T., and A. Limam. 2012. "Masonry Walls under Membrane or Bending Loading Cases: Experiments and Discrete Element Analysis." In *The Eleventh International Conference on Computational Structures Technology*, edited by B.H.V. Topping, Paper 119. Stirlingshire, Scotland: Civil-Comp Press.
- Cakti, E., O. Saygili, J. V. Lemos, and C. S. Oliveira. 2014. "A Parametric Study on Earthquake Behavior of Masonry Minarets." *Tenth U.S National Conference On Earthquake Engineering*. doi:10.4231/D3X34MS57.
- Cakti, E., O. Saygili, J. V. Lemos, and C. S. Oliveira. 2016. "Discrete Element Modeling of a Scaled Masonry Structure and Its Validation." *Engineering Structures* 126: 224–36. doi:10.1016/j.engstruct.2016.07.044.



- Cervera, M, M. Massanas, Pere Roca, and G. Arun. 2004. "Structural Analysis of Küçük Ayasofya Mosque in Istanbul." In *IV International Seminar on Structural Analysis of Historical Constructions: Possibilities of Numerical and Experimental Techniques*. Padova.
- Chopra, A K. 2012. *Dynamics of Structures: Theory and Applications to Earthquake Engineering*. 4th ed. Civil Engineering and Engineering Mechanics Series. Prentice Hall.
- Coarelli, F, and A Gabucci. 2001. *The Colosseum*. Getty Trust Publications. J. Paul Getty Museum.
- Coccia, S, M Como, M L Conforto, and U Ianniruberto. 2006. "Historical Static Analysis of the Coliseum." In *Second International Congress on Construction History*, 759–76. Cambridge UK.
- Como, M. 2013. "The Colosseum." In *Statics of Historic Masonry Constructions*, 38:927–37.
- "Complesso Conventuale Della Beata Antonia , l'Aquila." 2006. [www.abruzzo.beniculturali.it/](http://www.abruzzo.beniculturali.it/).
- "Complesso Monumentale E Monastero Della Beata Antonia." 2017. Scheda di valutazione e censimento dei danni. [http://151.12.58.154/mbac/pdf/terremoto/10\\_Beata\\_Antonia-Model.pdf](http://151.12.58.154/mbac/pdf/terremoto/10_Beata_Antonia-Model.pdf).
- Croci, G. 1990. *Studi E Ricerche Sul Colosseo*. Univ. degli studi La Sapienza.
- Croci, G. 1995. "The Colosseum: Safety Evaluation and Preliminary Criteria of Intervention." In *Structural Analysis of Historical Constructions*, edited by P. Roca, J.L. Gonzalez, A.R. Mari, and E. Onate, 154–65. Barcelona.
- Croci, G. 1998. *The Conservation and Structural Restoration of Architectural Heritage*. WIT press.
- Croci, G, and D. D'Ayala. 1989. "I Crolli E I Dissesti Del Colosseo: Le Ipotesi Di Effetti Sismici." *L'industria Delle Costruzioni* 23 (212): 78–87.
- Cundall, P.A. 1971. "A Computer Model for Simulating Progressive Large Scale Movements in Blocky Rock Systems." In *The Symposium of the International Society for Rock Mechanics*, 11–18. Nancy, France.
- Cundall, P.A. 1988. "Formulation of a Three-Dimensional Distinct Element Model Part I. A Scheme to Detect and Represent Contacts in a System Composed of Many Polyhedral Blocks." *Int. J. Rock*

- 
- Mech. Min. Sci. & Geomech.* 25 (3): 107–16.
- D'Ayala, D., and E. Speranza. 2003. "Definition of Collapse Mechanisms and Seismic Vulnerability of Historic Masonry Buildings." *Earthquake Spectra* 19 (3): 479–509. doi:10.1193/1.1599896.
- D'Ayala, D., and Sergio Lagomarsino. 2015. "Performance-Based Assessment of Cultural Heritage Assets: Outcomes of the European FP7 PERPETUATE Project." *Bulletin of Earthquake Engineering* 13 (1): 5–12. doi:10.1007/s10518-014-9710-1.
- Daudon, D., Y Sieffert, O Albarracín, L G Libardi, and G Navarta. 2014. "Adobe Construction Modeling by Discrete Element Method: First Methodological Steps." *Procedia Economics and Finance* 18 (September). Elsevier B.V.: 247–54. doi:10.1016/S2212-5671(14)00937-X.
- de Felice, G. 2011. "Out-of-Plane Seismic Capacity of Masonry Depending on Wall Section Morphology." *International Journal of Architectural Heritage* 5 (4–5): 466–82. doi:10.1080/15583058.2010.530339.
- de Felice, G., and R. Giannini. 2001. "Out-of-Plane Seismic Resistance of Masonry Walls." *Journal of Earthquake Engineering* 5 (2): 253–71. doi:10.1080/13632460109350394.
- de Felice, G, S De Santis, P. B. Lourenço, and N Mendes. 2016. "Methods and Challenges for the Seismic Assessment of Historic Masonry Structures." *International Journal of Architectural Heritage* 11 (1). Taylor & Francis: 1–18. doi:10.1080/15583058.2016.1238976.
- de Felice, G, Al Genoese, An Genoese, and B Lipo. 2015. "Seismic Assessment of Stone Masonry Historic Buildings Using Discrete Element Method." In *SECED 2015 Conference: Earthquake Risk and Engineering towards a Resilient World*, 227–33.
- de Felice, G, and A. Mauro. 2010. "On Overturning of the Façade in Churches with Single Nave: Some Case Studies from L'Aquila, Italy, 2009 Earthquake." *Advanced Materials Research* 133–134 (October): 807–12. doi:10.4028/www.scientific.net/AMR.133-134.807.
- De Lorenzis, L, M DeJong, and J Ochsendorf. 2007. "Failure of Masonry Arches under Impulse Base Motion." *Earthquake Engineering & Structural Dynamics* 36 (14): 2119–36. doi:10.1002/eqe.719.
- De Luca, D., ed. 1985. *Roma. Archeologia Nel Centro. L'area Archeologica Centrale*. Soprintendenza archeologia di Roma,

Ministeri per i beni culturali e ambientali.

- Dimitri, R., L. De Lorenzis, and G. Zavarise. 2011. "Numerical Study on the Dynamic Behavior of Masonry Columns and Arches on Buttresses with the Discrete Element Method." *Engineering Structures* 33 (12). Elsevier Ltd: 3172–88. doi:10.1016/j.engstruct.2011.08.018.
- Drej, A., and Carlos S. Oliveira. 2001. "The Seismic Behaviour of the 'Aquaduto Da Amoreira' in Elvas Using Distinct Element Modelling." In *Historical Constructions*, edited by P. B. Lourenço and Pere Roca, 903–11. Guimaraes.
- Droysen, G. 1886. *Allgemeiner Historischer Handatlas*. Velhagen & Klasing.
- Eurocode 8. 2005. *European Standard EN 1998-3:2005: Design of Structures for Earthquake Resistance - Part 3: Assessment and Retrofitting of Buildings*. Comité Européen de Normalisation, Brussels. Vol. 3.
- Frazzoni, L. 2016. "Il Colosseo. Biografia Di Un Capolavoro." *Archeo Monografie*, June.
- Funiciello, R, G Giordano, B Adanti, C Giampaolo, M Parotto, and L Balzerano. 2006. "Guida Ad Un Itinerario Geologico Attraverso La Città Di Roma." *Rome - the Imperial Fora: Archeological News & Related Studies*.
- Funiciello, R, L Lombardi, F Marra, and M Parotto. 1995. "Seismic Damage and Geological Heterogeneity in Rome's Colosseum Area: Are They Related?." *Annali Di Geofisica*.
- Funiciello, R, and A. Rovelli. 1998. "Terremoti E Monumenti a Roma." *Le Scienze*, May 1.
- Giampaolo, Ci, and L Aldega. 2013. "Il Travertino: La Pietra Di Roma." *Rendiconti Online Della Società Geologica Italiana* 27 (July): 98–109. doi:10.3301/ROL.2013.23.
- Giardini, D, G Gruenthal, K Shedlock, and P Zhang. 1999. "The Global Seismic Hazard Map." *Annali Di Geofisica* 42 (6): 1225–30. doi:10.1016/S0074-6142(03)80188-2.
- Giordano, A., E. Mele, and A. De Luca. 2002. "Modelling of Historical Masonry Structures: Comparison of Different Approaches through a Case Study." *Engineering Structures* 24 (8): 1057–69. doi:10.1016/S0141-0296(02)00033-0.
- Guidoboni, E., G. Ferrari, D. Mariotti, A. Comastri, G. Tarabusi, and G. Valensise. 2007. "CFTI - Med 4.0 (Catalogue of Strong Earthquakes

- in Italy 461 B.C. – 1997 and Mediterranean Area 760 B.C. – 1500).” *An Advanced Laboratory of Historical Seismology*. <http://storing.ingv.it/cfti4med/>.
- ICOMOS. 1964. “The Venice Charter.” In *11nd International Congress of Architects and Technicians of Historic Monuments*, 1–4.
- ICOMOS. 2003. “Recomendations for the Analysis, Conservation and Structural Restorations of Architectural Heritage.” In *International Scientific Committee for Analysis and Restoration of Structures of Architectural Heritage*, 1–37.
- Idris, J, M Al-Heib, and T Verdel. 2009. “Numerical Modelling of Masonry Joints Degradation in Built Tunnels.” *Tunnelling and Underground Space Technology* 24 (6). Elsevier Ltd: 617–26. doi:10.1016/j.tust.2009.05.002.
- “ITACA 2.2 WG.” 2017. *ITalian ACcelerometric Archive*. Istituto Nazionale di Geofisica e Vulcanologia. Dipartimento della Protezione Civile. <http://itaca.mi.ingv.it>.
- Italsca. 2011. “UDEC - Universal Distinct Element Code.” Italsca Consulting Group Inc.
- Jokilehto, J. 1986. “A History of Architectural Conservation.” The University of York.
- Komodromos, P, L Papaloizou, and P Polycarpou. 2008. “Simulation of the Response of Ancient Columns under Harmonic and Earthquake Excitations.” *Engineering Structures* 30 (8): 2154–64. doi:10.1016/j.engstruct.2007.11.004.
- Krawinkler, H, and G.D.P.K. Seneviratna. 1998. “Pros and Cons of a Pushover Analysis of Seismic Performance Evaluation.” *Engineering Structures* 20 (4–6): 452–64. doi:10.1016/S0141-0296(97)00092-8.
- Lemos, J. V. 1995. “Assessment of the Ultimate Load of a Masonry Arch Using Discrete Elements.” In *Computer Methods in Structural Masonry—3*, edited by J. Middleton and G. N. Pand, 294–302. Swansea: Books & Journals International.
- Lemos, J. V. 2007. “Discrete Element Modeling of Masonry Structures.” *International Journal of Architectural Heritage* 1 (2): 190–213. doi:10.1080/15583050601176868.
- Lemos, J. V., and A. Campos Costa. 2016. “Simulation of Shake Table Tests on Out-Of-Plane Masonry Buildings. Part (V): Discrete Element Approach.” *International Journal of Architectural Heritage* 11 (1): 1–8. doi:10.1080/15583058.2016.1237587.

- Lemos, J. V., A. C. Costa, and E. M. Bretas. 2011. "Assessment of the Seismic Capacity of Stone Masonry Walls with Block Models." *Computational Methods in Earthquake Engineering* Volume 21: 221–35. doi:10.1007/978-94-007-0053-6\_10.
- Lourenço, P. B. 1996. "Computational Strategies for Masonry Structures." PhD thesis. Delft University of Technology.
- Lourenço, P. B. 2002. "Computations on Historic Masonry Structures." *Prog. Struct. Engng Mater.*, no. 4: 301–19. doi:10.1002/pse.120.
- Luciani, R. 1990. *The Colosseum: Architecture, History, and Entertainment in the Flavian Amphitheatre, Ancient Rome's Most Famous Building*. Istituto geografico De Agostini.
- Lugli, G. 1957. *La Tecnica Edilizia Romana: Con Particolare Riguardo a Roma E Lazio*. La Tecnica Edilizia Romana: Con Particolare Riguardo a Roma E Lazio. Eredi Dott. G. Bardi.
- Magenes, G. 2000. "A Method for Pushover Analysis in Seismic Assessment of Masonry Buildings." *12th World Conference on Earthquake Engineering*, 1–8.
- Manziane, E. 1999. *The Colosseum (Amphitheatrum Flavium)*. Edizione Manziane.
- Meriggi, P., A. Mordanova, B. Pantò, S De Santis, and G de Felice. 2018. "Distinct Element Modelling of the out-of-Plane Seismic Behaviour of Masonry Walls." In *Structural Analysis of Historical Constructions*. submitted.
- "Monastero Della Beata Antonia." 2010. <http://www.culturaebeni.it/monumenti-adottare/lista-monumenti/4-monastero-beata-antonia.html>.
- Mordanova, A., G de Felice, and Al Genoese. 2017. "Seismic Assessment of the Claudio Aqueduct." In *3rd International Conference on Protection of Historical Constructions*. Lisbon.
- Mordanova, A., S De Santis, and G de Felice. 2016. "State-of-the-Art Review of out-of-Plane Strengthening of Masonry Walls with Mortar-Based Composites." In *Structural Analysis of Historical Constructions*, edited by B. Van Balen and B. Verstrynge, 337–43. Leuven: CRC Press. doi:10.1201/9781315616995-50.
- Moro, L, ed. 2007. *Guidelines for Evaluation and Mitigation of Seismic Risk to Cultural Heritage*. Arti Visive, Architettura E Urbanistica. Gangemi.
- Oliveira, D. V., G. Grecchi, A. McCall, J. Noh, E. Speer, and M. Tohidi. 2012. "Seismic Assessment of the Roman Temple of Evora,

- Portugal.” In *15th World Conference on Earthquake Engineerin*. Lisbon.
- Papantonopoulos, C., I. N. Psycharis, D. Y. Papastamatiou, J. V. Lemos, and H. P. Mouzakis. 2002. “Numerical Prediction of the Earthquake Response of Classical Columns Using the Distinct Element Method.” *Earthquake Engineering and Structural Dynamics* 31 (9): 1699–1717. doi:10.1002/eqe.185.
- Parker, J. H. 1876. *The Flavian Amphitheatre, Commonly Called the Colosseum at Rome: Its History & Substructures Compared with Other Amphitheatres*. Oxford: J. Parker & co.
- Passchier, C, G Sürmelihindi, D van Opstal, and W.D. Schram. 2017. “Roman Aqueduct Atlas Project ROMAQ.” <http://www.romaq.org/>.
- Penna, A. 2014. “Seismic Assessment of Existing and Strengthened Stone-Masonry Buildings: Critical Issues and Possible Strategies.” *Bulletin of Earthquake Engineering* 13 (4): 1051–71. doi:10.1007/s10518-014-9659-0.
- Pentecost, A. 2005. *Travertine*. Berlin/Heidelberg: Springer-Verlag. doi:10.1007/1-4020-3606-X.
- Pericolosità Sismica Di Riferimento per Il Territorio Nazionale*. 2006. Italy: <http://zonesismiche.mi.ingv.it/>.
- Pompeu, S, ed. 2010. *Guide for the Structural Rehabilitation of Heritage Buildings. CIB Publication 335*.
- Psycharis, I. N., J. V. Lemos, D. Y. Papastamatiou, C. Zambas, and C. Papantonopoulos. 2003. “Numerical Study of the Seismic Behaviour of a Part of the Parthenon Pronaos.” *Earthquake Engineering & Structural Dynamics* 32 (13): 2063–84. doi:10.1002/eqe.315.
- Rea, R, H-J Beste, and L C Lancaster. 2002. “Il Cantiere Del Colosseo.” *Mitteilungen Des Deutschen Archäologischen Instituts, Römische Abteilung* 109: 341–75.
- Rea, R, S Romano, and R S Valenzani. 2017. *Colosseo*. Electa. “Restauro Colosseo.” 2017. <http://restaurocolosseo.it>.
- Roberti, G.M., and O. Soina. 2001. “Discrete Element Analysis on the Sardinian ‘Nuraghe.’” In *Historical Constructions*, edited by P. B. Lourenço and Pere Roca, 719–28. Guimaraes.
- Roca, P, M Cervera, G Gariup, and L Pela’. 2010. “Structural Analysis of Masonry Historical Constructions. Classical and Advanced Approaches.” *Archives of Computational Methods in Engineering* 17 (3): 299–325. doi:10.1007/s11831-010-9046-1.
- Rosin, P.L., and E. Trucco. 2004. “The Amphitheatre Construction

- Problem.” *Incontro Internazionale Di Studi Rileggere L’Antico*, 1–10.
- Sarhosis, V., P. Asteris, T. Wang, W. Hu, and Y. Han. 2016. “On the Stability of Colonnade Structural Systems under Static and Dynamic Loading Conditions.” *Bulletin of Earthquake Engineering*, 1–22. doi:10.1007/s10518-016-9881-z.
- Sarhosis, V., K. Bagi, J. V. Lemos, and G. Milani, eds. 2016. *Computational Modeling of Masonry Structures Using the Discrete Element Method*. Advances in Civil and Industrial Engineering. IGI Global. doi:10.4018/978-1-5225-0231-9.
- Sarhosis, V, P.G. Asteris, A Mohebkah, J Xiao, and T Wang. 2016. “Three Dimensional Modelling of Ancient Colonnade Structural Systems Subjected to Harmonic and Seismic Loading.” *Structural Engineering and Mechanics* 60 (4): 633–53. doi:10.12989/sem.2016.60.4.633.
- Schram, W.D. 2012. “Dynamic Control Elements in Roman Aqueducts - a Reconnaissance Study.” In *15th International Conference on the History of Water Management and Hydraulic Engineering in the Mediterranean Region*, 229–46.
- Schram, W.D. 2017. “Roman Aqueducts.” <http://www.romanaqueducts.info>.
- Sinclairian, G. 2001. “Seismic Behaviour of Blocky Masonry Structures. A Discrete Element Method Approach.” PhD thesis, Instituto Superior Técnico, Universidade de Lisboa.
- Sinclairian, G, C S. Oliveira, and J. V. Lemos. 1998. “Assessment of the Seismic Behaviour of a Stone Masonry Aqueduct Using Discrete Elements.” In *11th European Conference on Earthquake Engineering*, edited by Bisch, Labe, and Pecker. Balkema.
- Soveja, L, M Budescu, and I Gosav. 2013. “Modelling Methods for Unreinforced Masonry Structures,” no. Lxiii.
- Stefanou, I, I Psycharis, and I O Georgopoulos. 2011. “Dynamic Response of Reinforced Masonry Columns in Classical Monuments.” *Construction and Building Materials* 25 (12). Elsevier Ltd: 4325–37. doi:10.1016/j.conbuildmat.2010.12.042.
- Uggeri, A. 1809. “Supplément. Édifices de La Décadence. Rome, 1806-1807.” *Journées Pittoresques Des Édifices de Rome Ancienne*.
- Uggeri, A. 1814. “Supplément. Partie I.” In *Journées Pittoresques Des Édifices de Rome Antique*. Rome: Bourlié, Francesco.
- Ulrich, T, C Negulescu, and A Ducellier. 2015. “Using the Discrete

- Element Method to Assess the Seismic Vulnerability of Aggregated Masonry Buildings.” *Bulletin of Earthquake Engineering* 13 (10). Springer Netherlands: 3135–50. doi:10.1007/s10518-015-9754-x.
- Valluzzi, M R, G Cardani, L Binda, and C Modena. 2004. “Seismic Vulnerability Methods for Masonry Buildings in Historical Centres: Validation and Application for Prediction Analyses and Intervention Proposals.” In *13th World Conference on Earthquake Engineering - WCEE*.
- Young, M. P., A. E. Schultz, and J. V. Lemos. 2015. “Seismic Analysis of the Panhellenic Sanctuary.” In *12th North American Masonry Conference*. Denver.